

**REGULATION OF MITOCHONDRIAL DIVISION BY
THE DRP1 RECEPTORS**

Thesis by

Oliver Calvin Losón

In Partial Fulfillment of the Requirements for the Degree of

Doctor of Philosophy

CALIFORNIA INSTITUTE OF TECHNOLOGY

Pasadena, California

2014

(Defended May 2, 2014)

© 2014

Oliver Calvin Losón

All Rights Reserved

ACKNOWLEDGMENTS

I am grateful for the mentorship and support of my advisor, Professor David Chan. He expected and only accepted the best from me, and for that I am a better scientist and person. I acknowledge my committee for the insightful discussion and guidance during my thesis work. I am especially thankful for the advice and knowledge shared by two committee members: Professor Doug Rees and Professor Shu-ou Shan.

I thank past and present members of the Chan lab, including Dr. Hsiuchen Chen, Dr. Zhiyin Song, Dr. Prashant Mishra, Dr. Nickie Chan, Dr. Huu Ngo, Dr. Anna Salazar, Dr. Anne Chomyn, Dr. Anh Pham, Dr. Chunshik Shin, Priscilla Lee Wah Tee, Harry Gristick, and Rebecca Rojansky, for useful discussions and collegial support.

I am grateful to Dr. Jens Kaiser for his mentorship and expert help in protein crystallography. I am also grateful to Raymond Liu and Shuxia Meng for their collaborative support.

I am thankful to the National Institutes of Health and the American Physiological Society for their fellowship funding during my training.

I am grateful for the love, support, and encouragement of my parents, brother, and family. The courage and work ethic that have helped them succeed are an example and inspiration to me.

I owe a great amount of thanks to my wife. Her love, support, encouragement, and friendship have been instrumental to my success and

perseverance. She gave me strength to overcome tough obstacles and celebrated my triumphs.

ABSTRACT

Mitochondria can remodel their membranes by fusing or dividing. These processes are required for the proper development and viability of multicellular organisms. At the cellular level, fusion is important for mitochondrial Ca^{2+} homeostasis, mitochondrial DNA maintenance, mitochondrial membrane potential, and respiration. Mitochondrial division, which is better known as fission, is important for apoptosis, mitophagy, and for the proper allocation of mitochondria to daughter cells during cellular division.

The functions of proteins involved in fission have been best characterized in the yeast model organism *Sarcccharomyces cerevisiae*. Mitochondrial fission in mammals has some similarities. In both systems, a cytosolic dynamin-like protein, called Dnm1 in yeast and Drp1 in mammals, must be recruited to the mitochondrial surface and polymerized to promote membrane division. Recruitment of yeast Dnm1 requires only one mitochondrial outer membrane protein, named Fis1. Fis1 is conserved in mammals, but its importance for Drp1 recruitment is minor. In mammals, three other receptor proteins—Mff, MiD49, and MiD51—play a major role in recruiting Drp1 to mitochondria. Why mammals require three additional receptors, and whether they function together or separately, are fundamental questions for understanding the mechanism of mitochondrial fission in mammals.

We have determined that Mff, MiD49, or MiD51 can function independently of one another to recruit Drp1 to mitochondria. Fis1 plays a minor role in Drp1 recruitment, suggesting that the emergence of these additional

receptors has replaced the system used by yeast. Additionally, we found that Fis1/Mff and the MiDs regulate Drp1 activity differentially. Fis1 and Mff promote constitutive mitochondrial fission, whereas the MiDs activate recruited Drp1 only during loss of respiration.

To better understand the function of the MiDs, we have determined the atomic structure of the cytoplasmic domain of MiD51, and performed a structure-function analysis of MiD49 based on its homology to MiD51. MiD51 adopts a nucleotidyl transferase fold, and binds ADP as a co-factor that is essential for its function. Both MiDs contain a loop segment that is not present in other nucleotidyl transferase proteins, and this loop is used to interact with Drp1 and to recruit it to mitochondria.

TABLE OF CONTENTS

	PAGE
Acknowledgements.....	iii
Abstract.....	v
List of Tables and Figures.....	ix
Chapter 1: Introduction	1
Mitochondrial Fusion and its Machinery.....	2
Mitochondrial Fission Machinery.....	6
Cellular State and Changes in Mitochondrial Shape.....	13
Physiological Roles for Fusion and Fission.....	15
Thesis Overview.....	24
References.....	28
Chapter 2: Fis1, Mff, MiD49, and MiD51 mediate Drp1 recruitment in mitochondrial fission	39
Abstract.....	40
Introduction.....	41
Results.....	44
Discussions.....	52
Experimental Procedures.....	54
Acknowledgments.....	61
Figure Legends.....	62
Figures.....	69
Supplementary Figure Legends.....	75
Supplementary Figures.....	78
References.....	82
Chapter 3: The mitochondrial fission receptor MiD51 requires ADP as a co-factor	85
Abstract.....	86
Introduction.....	87
Results.....	89
Discussions.....	99
Experimental Procedures.....	101
Acknowledgments.....	110
Figure Legends.....	111
Figures.....	116
Supplementary Figure Legends.....	123

	PAGE
Supplementary Figures.....	127
Supplementary Table.....	132
References.....	133
Chapter 4: Structure-function analysis of MiD49	138
Introduction.....	139
Results and Discussions.....	142
Experimental Procedures.....	148
Figure Legends.....	153
Figures.....	155
Tables.....	159
References.....	162
Chapter 5: Conclusions and Future Directions	166
Fis1 and Mammalian Fission.....	166
Differential Regulation of Fission by the MiDs.....	169
Are the Mammalian Fission Receptors Redundant?.....	170
The Role of Fission Receptors in Physiology.....	171
References.....	173

LIST OF TABLES AND FIGURES

CHAPTER 2: FIS1, MFF, MiD49 AND MiD51 MEDIATE DRP1 RECRUITMENT IN MITOCHONDRIAL FISSION

PRIMARY FIGURES	PAGE
Figure 2.1 Mitochondrial elongation in <i>Fis1</i> -null, <i>Mff</i> -null, and <i>Fis1/Mff</i> -null MEFs.....	69
Figure 2.2 Drp1 recruitment and assembly on mitochondria are affected in <i>Fis1</i> -null and <i>Mff</i> -null cells.....	70
Figure 2.3 Knockdown of MiD49 or MiD51 causes mitochondrial elongation and enhances the <i>Fis1</i> -null, <i>Mff</i> -null, and <i>Fis1/Mff</i> -null phenotypes.....	71
Figure 2.4 Over-expression of MiD49 or MiD51 causes enhanced phosphorylation of Drp1 on S637.....	72
Figure 2.5 Mitochondrial elongation and increased Drp1 S637-PO ₄ caused by MiD over-expression can be reversed by CCCP.....	73
Figure 2.6 MiD49 and MiD51 can restore CCCP-induced mitochondrial fragmentation in <i>Fis1/Mff</i> -null cells.....	74
SUPPLEMENTARY FIGURES	
Figure S2.1 Mitochondrial morphology in <i>Fis1</i> -null, <i>Mff</i> -null, and <i>Fis1/Mff</i> -null MEF cells.....	78
Figure S2.2 Rescue of <i>Fis1</i> -null and <i>Mff</i> -null cells.....	79
Figure S2.3 Mitochondrial elongation by a second set of MiD siRNAs.....	80
Figure S2.4 Mitochondrial elongation and increased Drp1 S637-PO ₄ caused by MiD overexpression can be reversed by CCCP or STS.....	81

CHAPTER 3: THE MITOCHONDRIAL FISSION RECEPTOR MiD51 REQUIRES ADP AS A CO-FACTOR

PRIMARY FIGURES	
Figure 3.1 The cytosolic region of MiD51 has a nucleotidyl transferase domain.....	116
Figure 3.2 MiD51 binds ADP with high affinity.....	117
Figure 3.3 MiD51 forms a dimer through electrostatic interactions.....	118
Figure 3.4 MiD51 uses a surface loop to bind Drp1.....	119

	PAGE
Figure 3.5 ADP binding and dimerization are required for the fission activity of MiD51.....	120
Figure 3.6 ADP promotes Drp1 oligomerization by MiD51.....	121
Figure 3.7 MiD51 and ADP promote Drp1 spiral assembly and GTP hydrolysis.....	122

SUPPLEMENTARY FIGURES

Figure S3.1 Related to Figure 3.1.....	127
Figure S3.2 Related to Figure 3.2.....	128
Figure S3.3 Related to Figure 3.3.....	129
Figure S3.4 Related to Figure 3.4.....	130
Figure S3.5 Related to Figure 3.5.....	131

SUPPLEMENTARY TABLE

Table S3.1 Data Collection and Refinement Statistics.....	132
--	------------

CHAPTER 4: STRUCTURE-FUNCTION ANALYSIS OF MiD49

FIGURES

Figure 4.1 Predicted structure of MiD49 Δ 1-124.....	155
Figure 4.2 Candidate surface entropy reduction residues.....	156
Figure 4.3 Piloting surface entropy reduction mutants.....	157
Figure 4.4 Drp1-binding motif on MiD49.....	158

TABLES

Table 4.1 MiD49 Δ 1-125 SER Mutants Piloting.....	159
Table 4.2 MiD49 Δ 1-125 R218A Crystallization Screen Hits....	160
Table 4.3 MiD49 Δ 1-125 R218A X-Ray Diffraction Data.....	161

CHAPTER 1

INTRODUCTION

The mitochondrion plays a pivotal role in the physiology of the cell. It is the major producer of energy and many of the molecules needed for the macromolecular assemblies of the cell. Mitochondria are dynamic organelles. They interact with other organelles to perform their function and to regulate cellular physiology, and they change their shape and size continuously. Mitochondrial morphology is primarily determined by the balance of two opposing processes called fusion and fission. Fusion merges the membranes of two separate mitochondria, and results in the unification and mixing of their compartments. Fission divides a single mitochondrion into two new mitochondria. The balance of these morphological forces determines the shape and length of mitochondria. Inhibition of fusion causes mitochondria to become fragmented because of unopposed fission. Conversely, inhibition of fission causes mitochondria to become extremely long and overly interconnected because of unopposed fusion. Over the last 20 years, a great deal has been learned about the molecular mechanisms by which mitochondria change their morphology. The importance of these processes for cellular and organismal physiology has also been studied in great detail.

Mitochondrial fusion and its machinery

Mitochondria have two separate membranes. The inner membrane creates an interior compartment called the matrix, and the outer membrane surrounds the inner entirely, creating a second compartment between the two called the inter-membrane space. The fusion of two mitochondria requires that the inner and outer membranes of one mitochondrion be fused with the respective membranes of another. Fusion must occur in steps, with the outer membranes fusing first, allowing the inner membranes to come into proximity for inner membrane fusion.

In mammals, fusion of the mitochondrial membranes is accomplished by three proteins. Outer membrane fusion requires the mitofusins Mfn1 and Mfn2 (Chen et al., 2003; Rojo et al., 2002), and inner membrane fusion requires OPA1 (Chen et al., 2005; Song et al., 2007). These proteins contain GTPase activity that is essential for their functions, and are part of the dynamin-like protein super family (Praefcke and McMahon, 2004). Both Mfns are anchored in the outer membrane by two transmembrane domains, with their N and C termini facing the cytosol. OPA1 is anchored in the inner membrane by a single transmembrane domain, with its C-terminus facing the inter-membrane space.

The mitofusins and outer membrane fusion

In vivo and *in vitro* studies have shown that the mitofusins are required on adjacent mitochondria for fusion to occur (Koshiba et al., 2004; Meeusen et al., 2004). Mfn1 and Mfn2 can form homo and hetero-oligomeric complexes capable

of mediating fusion (Chen et al., 2005; Chen et al., 2003). The mitofusins contain two 4,3 hydrophobic heptad repeat motifs (HR1 and HR2), and the second is used for this oligomerization. Structural studies demonstrated that an anti-parallel coiled-coil assembly formed by HR2 brings opposing mitochondrial membranes into close apposition—approximately 150 Å apart (Koshihara et al., 2004). Interestingly, this type of motif is also critical for membrane fusion mediated by the SNARE proteins and viral glycoproteins (Bonifacino and Glick, 2004; Eckert and Kim, 2001). Although important for mitochondrial fusion, HR2 alone is not sufficient for fusion, suggesting that conformational changes in the GTPase domain of the mitofusins may ultimately facilitate membrane fusion once the coiled-coil structure has brought opposing membranes into close proximity.

OPA1 and inner membrane fusion

Unlike the mitofusins, OPA1 exists as a complex mixture of isoforms. Differential RNA splicing and proteolytic processing produces a variety of long (transmembrane containing) and short (transmembrane devoid) forms of OPA1 (Chan, 2012; Delettre et al., 2001). Inner membrane fusion is lost in *OPA1*-null cells (Song et al., 2007), and re-expression of short forms of OPA1 are incapable of rescuing this defect, as well as long forms that cannot be processed to short form. Interestingly, re-expression of single long isoforms that can be processed can rescue inner membrane fusion, suggesting that both long and short forms of OPA1 are required for fusion (Song et al., 2007). *In vitro* experiments with a recombinant short form of human OPA1 demonstrated that the short form could

continue to interact with membranes in the absence of a transmembrane domain (Ban et al., 2010). The protein could also tubulate membranes, but was unable to cause membrane fusion. This *in vitro* study, together with the rescue experiments, supports a mechanism for inner membrane fusion where both long and short forms are necessary.

Paradoxically, other studies have shown that only the long form of OPA1, without processing, is necessary for fusion. Tondera et al. showed that under some cellular stress conditions, the long form of OPA1 was sufficient to mediate mitochondrial elongation (2009). Additionally, a recent article argues that normal inner membrane fusion is mediated by the long form of OPA1 alone and that the short form of OPA1 is important for fission (Anand et al., 2014). A new study from our laboratory presents data that clarifies a role for the short and long forms of OPA1 for fusion (Mishra et al., 2014). The data support a model where long forms of OPA1 act in trans across inner membranes and processing to short form destabilizes the trans oligomer, promoting membrane fusion. Future studies will be needed to help reconcile the discrepancies between these studies.

Full fusion occurs in a stepwise manner

Fusion of both mitochondrial membranes appears coordinated because of the rapid nature of inner membrane fusion following outer membrane fusion. Yet mitochondria do not always undergo complete fusion; that is, the outer membrane can fuse without the subsequent fusion of the inner membrane (Malka et al., 2005; Song et al., 2009; Twig et al., 2008). This observation supports a

stepwise and independent nature for outer and inner mitochondrial membrane fusion.

Mitochondrial fusion can be monitored by labeling mitochondria with different fluorescent proteins in separate cell lines and fusing these cell lines to allow the fluorescent mitochondria to interact. Subsequently, the mixing of the fluorescent signals among these mitochondria is assessed. This assay demonstrated the need for both the mitofusins and OPA1 to accomplish full fusion of mitochondria (Chen et al., 2003; Song et al., 2009). Experiments using photo-activatable GFP targeted to the outer membrane of mitochondria, which allows for monitoring outer membrane fusion of discrete mitochondria, showed that outer membrane fusion continues in the absence of inner membrane fusion, supporting the independent and stepwise nature of outer and inner membrane fusion. As anticipated, this study also demonstrated that inner membrane fusion cannot occur without outer membrane fusion (Song et al., 2009).

The development of an *in vitro* assay for mitochondrial fusion has been valuable for interrogating the mechanism of fusion and its regulation. The assay requires differentially fluorescent mitochondria and, like the cell based assay, mixing of fluorescence is assessed (Meeusen et al., 2004). The *in vitro* fusion assay was developed using purified yeast mitochondria, and demonstrated that in the absence of other cellular components, mitochondria could fuse. Furthermore, the stepwise nature of fusion was demonstrated with the use of mitochondria lacking the yeast mitofusin homolog Fzo1 or the OPA1 homolog Mgm1 (Meeusen et al., 2006; Meeusen et al., 2004). These *in vitro* results have

been recapitulated using mammalian mitochondria (Mishra et al., 2014). Together, the *in vitro* and cell biology experiments define full fusion as a stepwise process.

Mitochondrial fission machinery

During mitochondrial fission, the inner and outer membranes are divided. Two classes of proteins are necessary to execute fission. The first is a dynamin related protein called Drp1 that resides primarily in the cytosol. Members of the second class are integral outer membrane proteins that recruit Drp1 to the mitochondrial surface. Drp1 is believed to polymerize around the circumference of the mitochondrion, much like dynamin does on the neck of endocytic vesicles, but the exact mechanism is unclear. Mammalian mitochondrial fission requires four Drp1 receptors. Whether these receptors work in a coordinated pathway or independently is not known, nor is it understood why multiple receptors are necessary for Drp1 recruitment. Also enigmatic is how inner membrane division occurs and how it is coordinated with outer membrane division. Cell biological and *in vitro* studies have begun to elucidate the mechanism by which mitochondria divide. More recently, the interaction between mitochondria and the endoplasmic reticulum (ER) has been implicated in the fission mechanism.

A dynamin related protein is critical for fission

Drp1 is essential for mitochondrial fission provoked by virtually all cellular circumstances, like mitosis or stress. Inhibition of Drp1 function by RNA

interference (RNAi) or expression of a dominant negative allele causes severe elongation and interconnection of mitochondria, which can result in the formation of a perinuclear, collapsed mitochondrial mass (Lee et al., 2004; Smirnova et al., 2001). Genetically engineered mouse models carrying null alleles of Drp1 have confirmed these results, and demonstrate the importance of mitochondrial fission for development and the nervous system (Ishihara et al., 2009; Wakabayashi et al., 2009). These models also demonstrated that Drp1 is dispensable for mitochondrial fragmentation during pharmacologically induced apoptosis, suggesting that other mechanisms for mitochondrial division exist.

Drp1 and its yeast homolog Dnm1 can oligomerize *in vitro* into large, regular structures. Dnm1 forms a helical assembly resembling that of dynamin, but with a larger diameter (Hinshaw and Schmid, 1995; Ingeman et al., 2005). Interestingly, this diameter is similar to that of constriction sites found on yeast mitochondria *in vivo*. Drp1 can also form helical structures *in vitro* that are similar to those of Dnm1 (Koirala et al., 2013). These observations suggest that these structures may represent the minimal molecular unit for mitochondrial membrane division. Further support derives from the observation that Dnm1 can deform liposomes into tubules by polymerizing on their surface (Mears et al., 2011). This deformation is dynamic, as the addition of GTP causes Dnm1 polymers to further constrict the membranes, but not divide them. Dynamin behaves similarly, but makes membrane tubules of a smaller diameter (Chen et al., 2004; Stowell et al., 1999). Although such *in vitro* studies shed light on the mechanism for membrane

division, cell biological studies demonstrate that the mechanism is more complicated and requires other proteins.

Dynamin contains a pleckstrin homology (PH) domain that it uses to directly interact with lipids (Vallis et al., 1999). Dnm1 and Drp1 lack a PH domain and instead contain an uncharacterized B-insert region. The secondary structure of this region is predicted to be highly disordered, but has been proposed to function for lipid binding (Mears et al., 2011; Smirnova et al., 1998). In both the yeast and mammalian systems, outer mitochondrial membrane proteins are necessary for recruiting Dnm1 and Drp1 to the mitochondrial surface (see below), suggesting that although these dynamin related proteins retain some affinity for membranes, they are brought into the proximity of membranes primarily by their receptors.

Fission adaptors in the yeast system

Yeast mitochondria have a single Dnm1 receptor named Fis1 that is required for Dnm1 recruitment to mitochondria. Fission and Dnm1 recruitment also requires the cytosolic proteins Mdv1 and Caf4. A collection of cell biological and structural studies demonstrated that Fis1 interacts with the N-terminal portion of these proteins, and Dnm1 interacts with the C-terminal portion (Griffin et al., 2005; Koirala et al., 2010; Mozdy et al., 2000; Tieu and Nunnari, 2000; Tieu et al., 2002; Zhang et al., 2012). Thus, Mdv1 and Caf4 act as adaptors for the interaction between Fis1 and Dnm1.

In addition to functioning as an adaptor, Mdv1 stimulates the GTPase activity of Dnm1. Lackner et al. demonstrated that Mdv1 preferentially interacts with Dnm1 when bound to GTP (2009). Furthermore, the interaction with Mdv1 enhances the oligomerization of Dnm1, causing an increase in Dnm1 GTPase activity. Mdv1 even enhances the assembly of Dnm1 in the presence of liposomes, suggesting that a rate limiting step to formation of the Dnm1 fission apparatus might be nucleotide exchange. Similar observations have been reported for dynamin in the presence of membranes, but the need for an adaptor protein is not known to exist (Ferguson and De Camilli, 2012; Stowell et al., 1999). The importance of Dnm1 oligomerization for GTPase activity and fission is supported by the loss-of-function, dimeric mutant G385D (Ingerman et al., 2005; Sesaki and Jensen, 1999).

Fission adaptors in the mammalian system

The mammalian fission apparatus differs from that of yeast in a number of ways. Fis1 is conserved in mammals and it was initially shown to be important for fission, but later studies called its importance into question. In addition to these data, the relatively recent discoveries of three additional receptors on mammalian mitochondria with greater roles in Drp1 recruitment have heightened this skepticism. Unlike yeast, no cytosolic adaptors for Drp1 are known to exist in the mammalian system. The existence of additional Drp1 receptors, the minor role of Fis1, and lack of cytosolic adaptors suggest that the mammalian fission mechanism may be fundamentally different from that of yeast. Both Mdv1 and

Caf4 contain a WD40 domain that is critical for fission in the yeast system, but none of the mammalian Drp1 receptors have WD40 sequences; in fact, none of the receptors have any homology to Mdv1 or Caf4. Although we understand the mechanism of fission in yeast, the stark differences in mammals underscore how little is understood about mammalian fission. Key to understanding mammalian fission would be an understanding of the need for four receptors, and whether these receptors act in a coordinated or independent manner.

Early studies supported the assumption that Fis1 was also important for mammalian fission (Koch et al., 2005; Lee et al., 2004; Stojanovski et al., 2004; Yoon et al., 2003; Yu et al., 2005). Paradoxically, ablation of Fis1 did not affect Drp1 recruitment, but did cause mitochondrial elongation (Lee et al., 2004). A more recent study showed that knockdown of Fis1 in HeLa cells did not cause mitochondrial elongation, nor did targeted deletion of *Fis1* from human carcinoma HCT116 cells (Otera et al., 2010). One explanation for the discrepancy in the findings of these various studies could be their use of differing cell types. Because the mammalian fission mechanism contains several Drp1 receptors, it is possible that these receptors may have tissue or cell type specific function. Additional research is needed to clarify the role of Fis1 for mammalian fission.

Mff was discovered using an RNA interference screen with a *Drosophila melanogaster* cell culture model (Gandre-Babbe and van der Bliek, 2008). Like RNAi against *Drp1*, knockdown of Mff caused robust elongation of mitochondria. A subsequent study demonstrated the importance of Mff for Drp1 recruitment to

mitochondria (Otera et al., 2010). Mff and Drp1 can interact both *in vitro* and *in vivo*, but the interaction is weak and requires the use of a crosslinking reagent.

Two additional outer mitochondrial membrane proteins called MiD49 and MiD51 have been implicated in mammalian fission, but their role is unclear. Two recent studies draw conflicting conclusions about the function of MiD51, primarily from the results of their RNAi and overexpression experiments. One study found that mitochondrial morphology did not clearly change when either of the MiDs were knocked down alone, but did observe that mitochondria elongated significantly when they were knocked down together, suggesting that these proteins are functionally redundant (Palmer et al., 2011). In contrast, knockdown of MiD51 alone caused mitochondrial fragmentation in the other study (Zhao et al., 2011). Both groups found that overexpression of either MiD causes robust mitochondrial elongation (Liu et al., 2013; Palmer et al., 2011; Zhao et al., 2011). The reports agree that this occurs because fission is inhibited, yet they disagree about the nature of this inhibition. The former study argues that this inhibition is an indirect effect of protein overexpression, causing Drp1 to become sequestered and non-functional. The latter study argues that this is precisely the function of the MiDs. It is clear that the MiDs regulate Drp1 function and fission, but their precise role remains to be determined.

The endoplasmic reticulum and mitochondrial fission

Mitochondria interact with the ER at junctions called contact sites. These sites are tight, with a small gap of only 10 – 30 nm between the membranes of

these organelles (Csordas et al., 2006; Friedman et al., 2011). Contact sites between mitochondria and ER are critical for Ca^{2+} homeostasis, lipid biosynthesis, biogenesis of mitochondria, and organelle trafficking (Rowland and Voeltz, 2012). A synthetic biology screen in yeast discovered a protein complex called ERMES (ER-mitochondria encounter structure) that is important for mediating this inter-organelle interaction (Kornmann et al., 2009). Recent research has demonstrated that mitochondrial fission events correlate with ER-mitochondria contact sites.

High resolution fluorescence imaging and electron microscopy revealed that ER tubules wrap around constriction sites on mitochondria (Friedman et al., 2011). Mff and Drp1 both localize to these constriction sites, and real time imaging demonstrated that these sites are correlated with mitochondrial fission. A subsequent study demonstrated that actin polymerization occurs at these sites and is regulated by an isoform of formin protein (INF2) that is targeted to mitochondria. Together, these findings suggest that ER apposition to mitochondria may facilitate constriction site formation and would function upstream of the fission apparatus. Interestingly, mitochondrial constrictions have been documented in fission defective cells (Labrousse et al., 1999; Legesse-Miller et al., 2003), arguing that constriction and fission are separate processes. Furthermore, the diameter of a Dnm1/Drp1 assembly is most similar to that of constrictions, suggesting that a mitochondrion must first be constricted before this assembly can be formed (Ingerman et al., 2005; Mears et al., 2011). The

ERMES complex is also present at ER-mitochondria constriction sites, and its presence correlates with mitochondrial fission in yeast (Murley et al., 2013).

Whether an ERMES-like complex exists in mammals is not known, nor whether or not such a complex is important for fission. How Drp1 and Mff are recruited to mitochondrial constriction sites and how actin polymers could influence mitochondrial constriction are not understood. Knowledge about a mammalian ERMES complex and mechanism for mitochondrial constriction would be valuable in understanding the synergy between the mitochondrial fission apparatus and this inter-organellar interaction.

Changes in cellular state can affect mitochondrial morphology

Mitochondria are important to the function and health of virtually all cell types. Though differing cell types demand similar roles of their mitochondria, the structure and distribution of mitochondria varies substantially between them (Pham et al., 2012). Often, mitochondrial structure and distribution is precisely engineered for the function of a cell. For example, mitochondria of skeletal muscle cells are positioned between and along myofibrils to supply the contractile machinery with ATP and help in regulating cytosolic Ca^{2+} transients (Brini et al., 1997; Eisner et al., 2013; Ogata and Yamasaki, 1997; Rudolf et al., 2004). In neurons, mitochondria often adopt a smaller and ovoid shape, which helps with their transport to the distal ends of neural processes (Sheng and Cai, 2012). This distribution is critical for the formation of dendritic spines, which are key structures for neural connectivity and synaptic plasticity (Li et al., 2004).

Changes in the state of the cell can have profound effects on mitochondrial morphology. The length and interconnectivity of mitochondria change throughout the cell cycle of cultured cells (Margineantu et al., 2002). Taguchi and colleagues discovered that the fragmentation of mitochondria during mitosis is caused by an enhancement of mitochondrial fission, and is directly regulated by mitosis promoting factor (MPF; a complex of cyclin B and Cdk1) (2007). MPF is critical for promoting entrance into the mitotic and meiotic phases of the cell cycle, and promotes fission by phosphorylating Drp1 at serine 616. A later study showed that fragmentation of the mitochondrial network is critical for insuring proper allocation of mitochondria to daughter cells and continued cell viability (Kashatus et al., 2011). Interestingly, changes in mitochondrial morphology during the cell cycle have also been shown to influence the progression of the cell from G₁ to S phase, suggesting that mitochondrial morphology can regulate the cell cycle (Mitra et al., 2009).

Mitochondrial morphology is also sensitive to several types of cellular stress. Nutrient starvation, UV irradiation, and inhibition of RNA transcription or protein translation cause mitochondria to become hyperfused. This hyperfused state stimulates enhanced production of ATP, presumably to help the cell withstand and adapt to the stress (Tondera et al., 2009). During nutrient starvation, fission is inhibited and causes mitochondrial fusion to become unopposed (Gomes et al., 2011; Rambold et al., 2011). Drp1 becomes dephosphorylated at serine 616 and phosphorylated at serine 637, and together these modifications inhibit Drp1 activity, causing mitochondria to elongate and to

become overly interconnected (Chang and Blackstone, 2007; Cribbs and Strack, 2007; Taguchi et al., 2007). Nutrient starvation activates autophagy to degrade cellular components for recycling. These studies suggest that elongation of mitochondria prevents mitochondria from being recycled, protecting the major metabolic hub of the cell.

Mitochondria will robustly fragment when cells are treated with proton ionophores such as carbonyl cyanide m-chlorophenyl hydrazine (CCCP) or valinomycin. These agents depolarize the inner mitochondrial membrane by destroying the proton gradient generated by the electron transport chain. Loss of membrane potential causes long forms of OPA1 to be proteolytically processed to short forms by the ATP-independent peptidase OMA1 (Duvezin-Caubet et al., 2006; Ehses et al., 2009; Head et al., 2009; Ishihara et al., 2006). The short form of OPA1 is not capable of mediating fusion without long form (Mishra et al., 2014; Song et al., 2007). Furthermore, Drp1 becomes activated through dephosphorylation of serine 637 by calcineurin, causing enhanced localization to mitochondria and enhanced fission (Cereghetti et al., 2008). Thus, fragmentation occurs both by inhibition of inner membrane fusion and activation of fission.

Physiological roles for fusion and fission

The balance between fusion and fission is critical for determining the size, shape, and distribution of mitochondria. Why mitochondria are dynamic and what physiological roles dynamics plays are questions that the field has focused on more recently. The creation of fusion and fission mutant mouse models has been

key in addressing these questions. Hereditary human diseases caused by mutations in dynamics genes have also given clues as to the physiological importance of mitochondrial dynamics.

Fusion dysfunction and human disease

Charcot-Marie-Tooth type 2A (CMT2A) is caused by heterozygous mutations of the *Mfn2* gene (Zuchner et al., 2004). Patients have weakness, muscle atrophy, and sensory loss in the distal parts of their limbs because of peripheral axonal neuropathy. A transgenic mouse model of CMT2A argues that neurodegeneration of motor neurons is partially responsible for the myopathies and weakness characteristic of this disease (Detmer et al., 2008). Heterozygous mutations of *OPA1* cause autosomal dominant optic atrophy (Alexander et al., 2000; Delettre et al., 2000). This disease is characterized by loss of vision because of optic nerve atrophy. A subset of CMT2A and DOA patients have overlapping pathological presentations. CMT2A patients can have vision loss due to optic nerve atrophy, and DOA patients can have peripheral myopathies and neuropathies. Such similarities between these diseases suggest that fusion in general serves a critical role in the physiology and/or development of the nervous system and muscles.

Fusion promotes homogenization of mitochondria and protects their function

Mutant mice carrying null alleles of *Mfn1* or *Mfn2* die at midgestation (Chen et al., 2003). The Mfns are required for placental development and function, and thus *Mfn1*-null or *Mfn2*-null placentas are incapable of supporting fetal development. Conditional null alleles of *Mfn1* and *Mfn2* enabled the circumvention of this embryonic lethality by targeting the null allele only to the embryo. *Mfn2*-null mice survived to birth, but showed severe abnormalities and died within three weeks (Chen et al., 2007). Remarkably, *Mfn1*-null embryos survive to birth and through adulthood, with no obvious phenotype. Genetic analyses of *Mfn1*-null and *Mfn2*-null allelic series demonstrated that the Mfns have partially redundant roles in placental function and embryonic development, but each has discrete functions too. Further analysis of the *Mfn2*-null mice showed that massive Purkinje cell degeneration in the cerebellum is responsible for the movement abnormalities seen in these pups. Electron transport chain dysfunctions and loss of mtDNA nucleoids in Purkinje cells were determined to be causal for the degeneration.

A subsequent study used the conditional *Mfn1* and *Mfn2* alleles to ablate these genes specifically in skeletal muscle (Chen et al., 2010). Double *Mfn*-null mice are severely runted, have decreased muscle mass, and die by 6-8 weeks of age. In contrast, single null alleles of either *Mfn* did not significantly affect the animals, suggesting that the *Mfns* are functionally redundant in skeletal muscle. Ultrastructural analysis of double *Mfn*-null muscle fibers revealed a massive

expansion and accumulation of mitochondria in the subsarcolemmal space, similar to that observed in ragged-red fibers of mitochondrial myopathies caused by mtDNA mutations (DiMauro and Schon, 2003). Further analysis revealed that double *Mfn*-null fibers have respiratory dysfunction, reduced mtDNA levels, and increased mutation and deletion frequencies in their mtDNA. Similar abnormalities were found in *OPA1*-null mouse embryonic fibroblasts (MEFs).

The study of the *Mfn* mutant mice and *OPA1*-null MEFs have been critical to understanding the role of fusion for development, the physiology of neurons, and cells in general. Key findings from these studies are that content mixing and homogenization of the mitochondrial network are compromised by loss of fusion, and result in loss of respiration and mtDNA stability. An obvious question that follows is why does loss of fusion produce such abnormalities? Firstly, it is important to note that the vast majority of proteins in mitochondria are encoded by the nuclear genome and produced outside the mitochondria. Secondly, these proteins are translocated into mitochondria in a stochastic manner. Therefore, the distribution of these proteins across the mitochondrial population would become heterogeneous without content mixing. This could produce the *Mfn*-null and *OPA1*-null phenotypes noted above because of inadequate distribution of proteins involved in respiration, mtDNA replication, and stability. In fact, functional heterogeneity among mitochondria occurs in fusion deficient cell lines, supporting this logic (Chen et al., 2005; Chen et al., 2007; Chen et al., 2010). Additionally, fusion ameliorates factors that cause dysfunction, like mtDNA mutations, by diluting their effect across the entire network. For example, most

pathogenic mtDNA mutations are recessive and do not affect respiration even when they exist as 60-90% of total mtDNA content, because fusion promotes complementation with normal mtDNA genomes (Chomyn, 1998; Rossignol et al., 2003).

Removal of dysfunctional mitochondria

Mitochondrial full fusion is selective and requires both mitochondria be functional (Mishra et al., 2014; Twig et al., 2008; Youle and Narendra, 2011). Mitochondria that become dysfunctional often lose their membrane potential, causing robust processing of OPA1 and inhibition of inner membrane fusion and content mixing (Ehdes et al., 2009; Head et al., 2009; Ishihara et al., 2006). Loss of membrane potential has been shown to correlate with an inability to mediate full fusion *in vivo* and *in vitro* (Meeusen et al., 2004; Twig et al., 2008). In this way, fusion can be regulated by mitochondrial function and allows for the segregation of dysfunctional mitochondria.

Dysfunctional mitochondria are degraded by a specialized autophagy pathway called mitophagy. The serine/threonine kinase PINK1 and the E3 ubiquitin ligase Parkin are important players in this pathway (Jin et al., 2010; Narendra et al., 2008). PINK1 accumulates in the outer membrane during loss of membrane potential and recruits Parkin to mitochondria. In conjunction with the proteasomal system, Parkin/PINK1 help degrade a broad array of outer membrane proteins to facilitate mitophagy, and the Mfns are amongst the first proteins to be degraded (Chan et al., 2011; Tanaka et al., 2010). Mfn

degradation helps to insure that dysfunctional mitochondria remain isolated, and that the functional integrity of the network is not compromised. In addition to removal of mitochondria that lose membrane potential, Parkin/PINK1 mediated mitophagy has been shown to promote the removal of mitochondria carrying pathogenic mtDNA genomes (Suen et al., 2010). The Parkin/PINK1 system is thought to engage the autophagic machinery through the ubiquitination of outer membrane proteins. Ubiquitination is important for p62 recruitment, which interacts with LC3 and allows formation of the autophagosome around damaged mitochondria (Geisler et al., 2010). A recent study found that recruitment of LC3 to mitochondria during hypoxia-induced mitophagy occurs differentially and requires the integral outer membrane protein FUNDC1 (Liu et al., 2012).

In addition to the removal of damaged/dysfunctional mitochondria, mitophagy is also important for development. During erythrocyte maturation, mitochondria are cleared by autophagy (Schweers et al., 2007). The outer mitochondrial membrane protein Nix is necessary for this form of mitophagy, because it directly interacts with LC3 using its N-terminal WXXL motif (Novak et al., 2010). In addition to this developmental program, Nix helps facilitate mitophagy during mitochondrial membrane depolarization. It is unclear if Parkin/PINK1, FUNDC1, and Nix function in parallel or differential mitophagy pathways, but as these studies suggest, they may be used for degradation of mitochondria having differing dysfunctions, or during differing cellular circumstances.

Human disease and mouse models of fission dysfunction

There is only one documented case of a human mutation in a fission gene. This patient was a newborn who had multisystem abnormalities, including small head circumference, hypotonia, few spontaneous movements, optic atrophy, and poor feeding (Waterham et al., 2007). As a result, the patient died at 37 days. Fibroblasts from this patient have elongated mitochondria and peroxisomes. Causal for these abnormalities was a heterozygous mutation (A395D) in the middle domain of *Drp1*, which in dynamin-family proteins is involved in self-assembly. Biochemical and yeast two-hybrid analysis of this mutant suggest that this mutation disrupts higher-order assembly and GTP hydrolysis (Chang et al., 2010). As the mutation was heterozygous, it is likely that it acted in a dominant negative function, most likely by poisoning the formation and/or function of Drp1 oligomers.

Drp1 mutant mouse models have been developed to investigate the physiological roles of fission. These models were developed by independent laboratories and have similar abnormalities (Ishihara et al., 2009; Wakabayashi et al., 2009). Like the double *Mfn*-null mouse model, *Drp1*-null mice have developmental abnormalities and die at midgestation. Analysis of null embryos and MEF cell lines derived from them revealed that cell proliferation was not significantly altered, nor was respiration, mitochondrial membrane potential, or ATP production. An abnormally large amount of apoptotic cells were present in the formative brain but not in any other tissue, and live cell imaging of MEFs

revealed that mitochondria were not evenly distributed between daughter cells during mitosis. These phenotypes suggest that a disparity in mitochondrial inheritance, not function, may impact the development of the nervous system.

Both laboratories also created conditional null alleles for *Drp1* and selectively ablated expression in the nervous system. Embryos survived to birth, but died soon afterwards. These pups had a reduced forebrain and expanded subdural space and ventricles. They also had large amounts of apoptotic neural cells throughout the cortex, indicating that neurodegeneration occurs as a result of *Drp1* ablation. A cell culture model of primary cells from the forebrain revealed that *Drp1*-null cells were incapable of neurite outgrowth and synapse formation. These results agree with a previous study using a cell culture model of synaptogenesis where mitochondrial dynamics was perturbed (Li et al., 2004). Network formation is critical to neuronal survival and explains the neurodegeneration observed in *Drp1*-null neurons (Luo and O'Leary, 2005). Although these studies focused on the nervous system, fission is likely to also be important in other tissues, as *Drp1*-null embryos die sooner than their nervous system specific counterparts. It would be interesting to learn what the importance of fission is for the development of other tissues, given that the neuronal defect is caused by a cell-type specific defect. Additionally, the physiological importance of the Drp1 receptors would be valuable in understanding fission, but perhaps more importantly, in understanding the functional redundancies or specificities of each receptor.

Fission and apoptosis

Mitochondrial fission is associated with the initiation of apoptosis. Fragmentation of the mitochondrial network correlates in time with the release of pro-apoptotic, inter-membrane space proteins. Once in the cytosol, the released proteins activate caspase proteases and the “caspase cleavage cascade,” which is key in the dismantling of the cell for apoptosis (Salvesen and Dixit, 1997; Wang and Youle, 2009). Members of the Bcl-2 protein family are responsible for permeabilizing the outer mitochondrial membrane for release of these proteins, and have also been demonstrated to regulate mitochondrial dynamics directly. For example, overexpression of CED-9 or Bcl-x_L can induce mitochondrial fusion (Delivani et al., 2006), and Bax and Bak have been shown to regulate Mfn2 oligomerization and mitochondrial distribution, which are important for fusion (Karbowski et al., 2006).

In early studies, Drp1 activity was shown to be necessary for the release of some inter-membrane space, pro-apoptotic factors, and activation of apoptotic signaling pathways (Cassidy-Stone et al., 2008; Frank et al., 2001; Germain et al., 2005). Inhibition of Drp1 protected cells from apoptosis, as well as ablation of Fis1. Other studies showed that fission plays a minor role for progression of apoptosis (Breckenridge et al., 2008; Parone et al., 2006; Sheridan et al., 2008). Both *Drp1*-null mouse models have large amounts of apoptosis, especially in the nervous system, demonstrating that Drp1 is not necessary for apoptosis. Furthermore, *Drp1*-null MEFs were not resistant to treatments that activate

apoptosis, as had been previously described in other cell types where Drp1 had been inhibited. The mitochondria in *Drp1*-null MEFs fragmented and could release pro-apoptotic factors from the inter-membrane space; additionally, the caspase pathway was activated in a manner indistinguishable from wildtype cells. The *Drp1*-null mouse reported by Wakabayashi et al. had a significant reduction in a developmentally programmed apoptosis that occurs at the neural tube closing, supporting a role for Drp1 in apoptosis. Considering the various studies of apoptosis and the role of fission, it is possible that the discrepancies among these studies could be explained by their use of differing cell types. Surprisingly, the *Drp1*-null cells demonstrate that mitochondria can divide in the absence of Drp1 by a yet unknown mechanism. This too may also help explain why apoptosis can continue to occur in the absence of Drp1. Focused study of the mechanistic differences during apoptosis of these differing cell types may help reconcile the inconsistencies in observations of these studies.

Thesis overview

Although a great deal has been learned about mitochondrial fission using yeast as a model organism, the mammalian system differs substantially. The relatively recent discovery of new mitochondrial Drp1 receptors that are not present in yeast but are crucial in the mammalian system underscores this difference. Moreover, the role of Fis1 in mammals has become unclear because of conflicting data. The physiological importance of fission has been substantiated by both a clinical case and a fission deficient mouse model

(Ishihara et al., 2009; Wakabayashi et al., 2009; Waterham et al., 2007). Little mechanistic detail is known about fission. Using cell biological models and structural biology, we have begun to reveal these details.

Chapter 2: Drp1 recruitment for mitochondrial fission

It is unclear why mammalian mitochondrial fission requires more than one Drp1 receptor. Previous research has demonstrated definitive roles in fission for Mff, MiD49, and MiD51. Although Fis1 has been shown to be important, its role has become less clear because of recent research. Using *Fis1*-null, *Mff*-null and *Fis1/Mff*-null MEF cell lines in conjunction with RNAi against *MiD49* and *MiD51*, we show that each receptor acts independently to recruit Drp1 to mitochondria. We also demonstrate that MiD49 and MiD51 can activate fission when mitochondrial function is acutely perturbed, even in the absence of Fis1 and Mff. This study suggests that these receptors may act in separate, parallel pathways. Additionally, the MiDs may be important for selectively activating fission during mitochondrial stress.

Chapter 3: Structure-function analysis of MiD51

Beyond the GTPase activity of Drp1, few biochemical details are known about mitochondrial fission. Furthermore, how the mitochondrial receptors regulate Drp1 activity is poorly understood. To better understand how MiD51 regulates Drp1 activity, we determined the x-ray crystal structure for the cytosolic domain of MiD51. MiD51 contains a nucleotidyl transferase fold and uses a

variant set of residues to bind ADP. Our structure-function analysis revealed that MiD51 uses a surface loop to bind Drp1 independently of ADP binding. However, ADP binding is necessary for the activation of mitochondrial fission and Drp1 GTPase activity.

Chapter 4: Structure-function analysis of MiD49

When overexpressed, MiD49 and MiD51 both recruit Drp1 but paradoxically inhibit fission. Our structural and biochemical studies of MiD49 and MiD51 demonstrate that they have a divergent function. In order to better understand this divergence, we have worked to determine the atomic structure of MiD49. We tried to obtain protein crystals for the cytosolic domain of MiD49, but were unsuccessful. We created a predicted structure of MiD49 using the structure of MiD51 as a template in order to determine whether surface residues may cause high surface entropy and prevent crystal packing. We engineered several surface entropy reduction mutants, and one permitted the formation of protein crystals. The crystals have not diffracted with sufficient quality to determine the structure, and we are currently in the process of enhancing them.

The sequence conservation of the Drp1-binding loop segment of MiD51 is high in the homologous region of MiD49. Furthermore, our predicted structure of MiD49 has a loop segment that is very similar to that of the Drp1-binding loop in MiD51. To test the function of this segment for Drp1 recruitment, we made mutants and tested their ability to interact with Drp1 and to recruit Drp1 to

mitochondria of *Fis1/Mff*-null cells. As anticipated, homologous residues in MiD49 are important for Drp1 interaction and recruitment.

Chapter 5: Conclusions and future directions

Our work has begun to clarify the roles of the Drp1 receptors for mitochondrial fission. The knowledge gleaned from earlier studies of mitochondrial fission in yeast influenced the initial study of fission in mammals, but more recent work has demonstrated that the mechanism of fission between these organisms is substantially different. Here I will review the key findings from our work and propose differing roles for the various mammalian Drp1 receptors based on our findings and those of others. I will also propose areas of study that may help in understanding the mechanism of fission in mammals.

REFERENCES

- Alexander, C., Votruba, M., Pesch, U.E., Thiselton, D.L., Mayer, S., Moore, A., Rodriguez, M., Kellner, U., Leo-Kottler, B., Auburger, G., *et al.* (2000). OPA1, encoding a dynamin-related GTPase, is mutated in autosomal dominant optic atrophy linked to chromosome 3q28. *Nature genetics* 26, 211-215.
- Anand, R., Wai, T., Baker, M.J., Kladt, N., Schauss, A.C., Rugarli, E.I., and Langer, T. (2014). The i-AAA protease YME1L and OMA1 cleave OPA1 to balance mitochondrial fusion and fission. *The Journal of cell biology* *In press*.
- Ban, T., Heymann, J.A., Song, Z., Hinshaw, J.E., and Chan, D.C. (2010). OPA1 disease alleles causing dominant optic atrophy have defects in cardiolipin-stimulated GTP hydrolysis and membrane tubulation. *Human molecular genetics* 19, 2113-2122.
- Bonifacino, J.S., and Glick, B.S. (2004). The mechanisms of vesicle budding and fusion. *Cell* 116, 153-166.
- Breckenridge, D.G., Kang, B.H., Kokel, D., Mitani, S., Staehelin, L.A., and Xue, D. (2008). *Caenorhabditis elegans* drp-1 and fis-2 regulate distinct cell-death execution pathways downstream of ced-3 and independent of ced-9. *Molecular cell* 31, 586-597.
- Brini, M., De Giorgi, F., Murgia, M., Marsault, R., Massimino, M.L., Cantini, M., Rizzuto, R., and Pozzan, T. (1997). Subcellular analysis of Ca²⁺ homeostasis in primary cultures of skeletal muscle myotubes. *Molecular biology of the cell* 8, 129-143.
- Cassidy-Stone, A., Chipuk, J.E., Ingberman, E., Song, C., Yoo, C., Kuwana, T., Kurth, M.J., Shaw, J.T., Hinshaw, J.E., Green, D.R., *et al.* (2008). Chemical inhibition of the mitochondrial division dynamin reveals its role in Bax/Bak-dependent mitochondrial outer membrane permeabilization. *Developmental cell* 14, 193-204.
- Cereghetti, G.M., Stangherlin, A., Martins de Brito, O., Chang, C.R., Blackstone, C., Bernardi, P., and Scorrano, L. (2008). Dephosphorylation by calcineurin regulates translocation of Drp1 to mitochondria. *Proceedings of the National Academy of Sciences of the United States of America* 105, 15803-15808.

- Chan, D.C. (2012). Fusion and fission: interlinked processes critical for mitochondrial health. *Annual review of genetics* *46*, 265-287.
- Chan, N.C., Salazar, A.M., Pham, A.H., Sweredoski, M.J., Kolawa, N.J., Graham, R.L., Hess, S., and Chan, D.C. (2011). Broad activation of the ubiquitin-proteasome system by Parkin is critical for mitophagy. *Human molecular genetics* *20*, 1726-1737.
- Chang, C.R., and Blackstone, C. (2007). Cyclic AMP-dependent protein kinase phosphorylation of Drp1 regulates its GTPase activity and mitochondrial morphology. *The Journal of biological chemistry* *282*, 21583-21587.
- Chang, C.R., Manlandro, C.M., Arnoult, D., Stadler, J., Posey, A.E., Hill, R.B., and Blackstone, C. (2010). A lethal de novo mutation in the middle domain of the dynamin-related GTPase Drp1 impairs higher order assembly and mitochondrial division. *The Journal of biological chemistry* *285*, 32494-32503.
- Chen, H., Chomyn, A., and Chan, D.C. (2005). Disruption of fusion results in mitochondrial heterogeneity and dysfunction. *The Journal of biological chemistry* *280*, 26185-26192.
- Chen, H., Detmer, S.A., Ewald, A.J., Griffin, E.E., Fraser, S.E., and Chan, D.C. (2003). Mitofusins Mfn1 and Mfn2 coordinately regulate mitochondrial fusion and are essential for embryonic development. *The Journal of cell biology* *160*, 189-200.
- Chen, H., McCaffery, J.M., and Chan, D.C. (2007). Mitochondrial fusion protects against neurodegeneration in the cerebellum. *Cell* *130*, 548-562.
- Chen, H., Vermulst, M., Wang, Y.E., Chomyn, A., Prolla, T.A., McCaffery, J.M., and Chan, D.C. (2010). Mitochondrial fusion is required for mtDNA stability in skeletal muscle and tolerance of mtDNA mutations. *Cell* *141*, 280-289.
- Chen, Y.J., Zhang, P., Egelman, E.H., and Hinshaw, J.E. (2004). The stalk region of dynamin drives the constriction of dynamin tubes. *Nature structural & molecular biology* *11*, 574-575.
- Chomyn, A. (1998). The myoclonic epilepsy and ragged-red fiber mutation provides new insights into human mitochondrial function and genetics. *American journal of human genetics* *62*, 745-751.
- Cribbs, J.T., and Strack, S. (2007). Reversible phosphorylation of Drp1 by cyclic AMP-dependent protein kinase and calcineurin regulates mitochondrial fission and cell death. *EMBO reports* *8*, 939-944.

Csordas, G., Renken, C., Varnai, P., Walter, L., Weaver, D., Buttle, K.F., Balla, T., Mannella, C.A., and Hajnoczky, G. (2006). Structural and functional features and significance of the physical linkage between ER and mitochondria. *The Journal of cell biology* 174, 915-921.

Delettre, C., Griffoin, J.M., Kaplan, J., Dollfus, H., Lorenz, B., Faivre, L., Lenaers, G., Belenguer, P., and Hamel, C.P. (2001). Mutation spectrum and splicing variants in the OPA1 gene. *Human genetics* 109, 584-591.

Delettre, C., Lenaers, G., Griffoin, J.M., Gigarel, N., Lorenzo, C., Belenguer, P., Pelloquin, L., Grosgeorge, J., Turc-Carel, C., Perret, E., *et al.* (2000). Nuclear gene OPA1, encoding a mitochondrial dynamin-related protein, is mutated in dominant optic atrophy. *Nature genetics* 26, 207-210.

Delivani, P., Adrain, C., Taylor, R.C., Duriez, P.J., and Martin, S.J. (2006). Role for CED-9 and Egl-1 as regulators of mitochondrial fission and fusion dynamics. *Molecular cell* 21, 761-773.

Detmer, S.A., Vande Velde, C., Cleveland, D.W., and Chan, D.C. (2008). Hindlimb gait defects due to motor axon loss and reduced distal muscles in a transgenic mouse model of Charcot-Marie-Tooth type 2A. *Human molecular genetics* 17, 367-375.

DiMauro, S., and Schon, E.A. (2003). Mitochondrial respiratory-chain diseases. *The New England journal of medicine* 348, 2656-2668.

Duvezin-Caubet, S., Jagasia, R., Wagener, J., Hofmann, S., Trifunovic, A., Hansson, A., Chomyn, A., Bauer, M.F., Attardi, G., Larsson, N.G., *et al.* (2006). Proteolytic processing of OPA1 links mitochondrial dysfunction to alterations in mitochondrial morphology. *The Journal of biological chemistry* 281, 37972-37979.

Eckert, D.M., and Kim, P.S. (2001). Mechanisms of viral membrane fusion and its inhibition. *Annual review of biochemistry* 70, 777-810.

Ehse, S., Raschke, I., Mancuso, G., Bernacchia, A., Geimer, S., Tondera, D., Martinou, J.C., Westermann, B., Rugarli, E.I., and Langer, T. (2009). Regulation of OPA1 processing and mitochondrial fusion by m-AAA protease isoenzymes and OMA1. *The Journal of cell biology* 187, 1023-1036.

Eisner, V., Csordas, G., and Hajnoczky, G. (2013). Interactions between sarco-endoplasmic reticulum and mitochondria in cardiac and skeletal muscle - pivotal roles in Ca²⁺(+) and reactive oxygen species signaling. *Journal of cell science* 126, 2965-2978.

- Ferguson, S.M., and De Camilli, P. (2012). Dynamin, a membrane-remodelling GTPase. *Nature reviews Molecular cell biology* 13, 75-88.
- Frank, S., Gaume, B., Bergmann-Leitner, E.S., Leitner, W.W., Robert, E.G., Catez, F., Smith, C.L., and Youle, R.J. (2001). The role of dynamin-related protein 1, a mediator of mitochondrial fission, in apoptosis. *Developmental cell* 1, 515-525.
- Friedman, J.R., Lackner, L.L., West, M., DiBenedetto, J.R., Nunnari, J., and Voeltz, G.K. (2011). ER tubules mark sites of mitochondrial division. *Science* 334, 358-362.
- Gandre-Babbe, S., and van der Bliek, A.M. (2008). The novel tail-anchored membrane protein Mff controls mitochondrial and peroxisomal fission in mammalian cells. *Molecular biology of the cell* 19, 2402-2412.
- Geisler, S., Holmstrom, K.M., Skujat, D., Fiesel, F.C., Rothfuss, O.C., Kahle, P.J., and Springer, W. (2010). PINK1/Parkin-mediated mitophagy is dependent on VDAC1 and p62/SQSTM1. *Nature cell biology* 12, 119-U170.
- Germain, M., Mathai, J.P., McBride, H.M., and Shore, G.C. (2005). Endoplasmic reticulum BIK initiates DRP1-regulated remodelling of mitochondrial cristae during apoptosis. *The EMBO journal* 24, 1546-1556.
- Gomes, L.C., Di Benedetto, G., and Scorrano, L. (2011). During autophagy mitochondria elongate, are spared from degradation and sustain cell viability. *Nature cell biology* 13, 589-598.
- Griffin, E.E., Graumann, J., and Chan, D.C. (2005). The WD40 protein Caf4p is a component of the mitochondrial fission machinery and recruits Dnm1p to mitochondria. *The Journal of cell biology* 170, 237-248.
- Head, B., Griparic, L., Amiri, M., Gandre-Babbe, S., and van der Bliek, A.M. (2009). Inducible proteolytic inactivation of OPA1 mediated by the OMA1 protease in mammalian cells. *The Journal of cell biology* 187, 959-966.
- Hinshaw, J.E., and Schmid, S.L. (1995). Dynamin self-assembles into rings suggesting a mechanism for coated vesicle budding. *Nature* 374, 190-192.
- Ingerman, E., Perkins, E.M., Marino, M., Mears, J.A., McCaffery, J.M., Hinshaw, J.E., and Nunnari, J. (2005). Dnm1 forms spirals that are structurally tailored to fit mitochondria. *The Journal of cell biology* 170, 1021-1027.

Ishihara, N., Fujita, Y., Oka, T., and Mihara, K. (2006). Regulation of mitochondrial morphology through proteolytic cleavage of OPA1. *The EMBO journal* 25, 2966-2977.

Ishihara, N., Nomura, M., Jofuku, A., Kato, H., Suzuki, S.O., Masuda, K., Otera, H., Nakanishi, Y., Nonaka, I., Goto, Y., *et al.* (2009). Mitochondrial fission factor Drp1 is essential for embryonic development and synapse formation in mice. *Nature cell biology* 11, 958-966.

Jin, S.M., Lazarou, M., Wang, C.X., Kane, L.A., Narendra, D.P., and Youle, R.J. (2010). Mitochondrial membrane potential regulates PINK1 import and proteolytic destabilization by PARL. *Journal of Cell Biology* 191, 933-942.

Karbowski, M., Norris, K.L., Cleland, M.M., Jeong, S.Y., and Youle, R.J. (2006). Role of Bax and Bak in mitochondrial morphogenesis. *Nature* 443, 658-662.

Kashatus, D.F., Lim, K.H., Brady, D.C., Pershing, N.L., Cox, A.D., and Counter, C.M. (2011). RALA and RALBP1 regulate mitochondrial fission at mitosis. *Nature cell biology* 13, 1108-1115.

Koch, A., Yoon, Y., Bonekamp, N.A., McNiven, M.A., and Schrader, M. (2005). A role for Fis1 in both mitochondrial and peroxisomal fission in mammalian cells. *Molecular biology of the cell* 16, 5077-5086.

Koirala, S., Bui, H.T., Schubert, H.L., Eckert, D.M., Hill, C.P., Kay, M.S., and Shaw, J.M. (2010). Molecular architecture of a dynamin adaptor: implications for assembly of mitochondrial fission complexes. *The Journal of cell biology* 191, 1127-1139.

Koirala, S., Guo, Q., Kalia, R., Bui, H.T., Eckert, D.M., Frost, A., and Shaw, J.M. (2013). Interchangeable adaptors regulate mitochondrial dynamin assembly for membrane scission. *Proceedings of the National Academy of Sciences of the United States of America* 110, E1342-1351.

Kornmann, B., Currie, E., Collins, S.R., Schuldiner, M., Nunnari, J., Weissman, J.S., and Walter, P. (2009). An ER-mitochondria tethering complex revealed by a synthetic biology screen. *Science* 325, 477-481.

Koshiba, T., Detmer, S.A., Kaiser, J.T., Chen, H., McCaffery, J.M., and Chan, D.C. (2004). Structural basis of mitochondrial tethering by mitofusin complexes. *Science* 305, 858-862.

- Labrousse, A.M., Zappaterra, M.D., Rube, D.A., and van der Bliek, A.M. (1999). *C. elegans* dynamin-related protein DRP-1 controls severing of the mitochondrial outer membrane. *Molecular cell* 4, 815-826.
- Lackner, L.L., Horner, J.S., and Nunnari, J. (2009). Mechanistic analysis of a dynamin effector. *Science* 325, 874-877.
- Lee, Y.J., Jeong, S.Y., Karbowski, M., Smith, C.L., and Youle, R.J. (2004). Roles of the mammalian mitochondrial fission and fusion mediators Fis1, Drp1, and Opa1 in apoptosis. *Molecular biology of the cell* 15, 5001-5011.
- Legesse-Miller, A., Massol, R.H., and Kirchhausen, T. (2003). Constriction and Dnm1p recruitment are distinct processes in mitochondrial fission. *Molecular biology of the cell* 14, 1953-1963.
- Li, Z., Okamoto, K., Hayashi, Y., and Sheng, M. (2004). The importance of dendritic mitochondria in the morphogenesis and plasticity of spines and synapses. *Cell* 119, 873-887.
- Liu, L., Feng, D., Chen, G., Chen, M., Zheng, Q., Song, P., Ma, Q., Zhu, C., Wang, R., Qi, W., *et al.* (2012). Mitochondrial outer-membrane protein FUNDC1 mediates hypoxia-induced mitophagy in mammalian cells. *Nature cell biology* 14, 177-185.
- Liu, T., Yu, R., Jin, S.B., Han, L., Lendahl, U., Zhao, J., and Nister, M. (2013). The mitochondrial elongation factors MIEF1 and MIEF2 exert partially distinct functions in mitochondrial dynamics. *Experimental cell research* 319, 2893-2904.
- Luo, L.Q., and O'Leary, D.D.M. (2005). Axon retraction and degeneration in development and disease. *Annu Rev Neurosci* 28, 127-156.
- Malka, F., Guillery, O., Cifuentes-Diaz, C., Guillou, E., Belenguer, P., Lombes, A., and Rojo, M. (2005). Separate fusion of outer and inner mitochondrial membranes. *EMBO reports* 6, 853-859.
- Margineantu, D.H., Gregory Cox, W., Sundell, L., Sherwood, S.W., Beechem, J.M., and Capaldi, R.A. (2002). Cell cycle dependent morphology changes and associated mitochondrial DNA redistribution in mitochondria of human cell lines. *Mitochondrion* 1, 425-435.
- Mears, J.A., Lackner, L.L., Fang, S., Ingeman, E., Nunnari, J., and Hinshaw, J.E. (2011). Conformational changes in Dnm1 support a contractile mechanism for mitochondrial fission. *Nature structural & molecular biology* 18, 20-26.

- Meeusen, S., DeVay, R., Block, J., Cassidy-Stone, A., Wayson, S., McCaffery, J.M., and Nunnari, J. (2006). Mitochondrial inner-membrane fusion and crista maintenance requires the dynamin-related GTPase Mgm1. *Cell* 127, 383-395.
- Meeusen, S., McCaffery, J.M., and Nunnari, J. (2004). Mitochondrial fusion intermediates revealed in vitro. *Science* 305, 1747-1752.
- Mishra, P., Carelli, V., Manfredi, G., and Chan, D.C. (2014). Proteolytic cleavage of Opa1 stimulates mitochondrial inner membrane fusion and couples fusion to oxidative phosphorylation. *Cell Metabolism* *In press*.
- Mitra, K., Wunder, C., Roysam, B., Lin, G., and Lippincott-Schwartz, J. (2009). A hyperfused mitochondrial state achieved at G1-S regulates cyclin E buildup and entry into S phase. *Proceedings of the National Academy of Sciences of the United States of America* 106, 11960-11965.
- Mozdy, A.D., McCaffery, J.M., and Shaw, J.M. (2000). Dnm1p GTPase-mediated mitochondrial fission is a multi-step process requiring the novel integral membrane component Fis1p. *The Journal of cell biology* 151, 367-380.
- Murley, A., Lackner, L.L., Osman, C., West, M., Voeltz, G.K., Walter, P., and Nunnari, J. (2013). ER-associated mitochondrial division links the distribution of mitochondria and mitochondrial DNA in yeast. *eLife* 2, e00422.
- Narendra, D., Tanaka, A., Suen, D.F., and Youle, R.J. (2008). Parkin is recruited selectively to impaired mitochondria and promotes their autophagy. *Journal of Cell Biology* 183, 795-803.
- Novak, I., Kirkin, V., McEwan, D.G., Zhang, J., Wild, P., Rozenknop, A., Rogov, V., Lohr, F., Popovic, D., Occhipinti, A., *et al.* (2010). Nix is a selective autophagy receptor for mitochondrial clearance. *EMBO reports* 11, 45-51.
- Ogata, T., and Yamasaki, Y. (1997). Ultra-high-resolution scanning electron microscopy of mitochondria and sarcoplasmic reticulum arrangement in human red, white, and intermediate muscle fibers. *The Anatomical record* 248, 214-223.
- Otera, H., Wang, C., Cleland, M.M., Setoguchi, K., Yokota, S., Youle, R.J., and Mihara, K. (2010). Mff is an essential factor for mitochondrial recruitment of Drp1 during mitochondrial fission in mammalian cells. *The Journal of cell biology* 191, 1141-1158.
- Palmer, C.S., Osellame, L.D., Laine, D., Koutsopoulos, O.S., Frazier, A.E., and Ryan, M.T. (2011). MiD49 and MiD51, new components of the mitochondrial fission machinery. *EMBO reports* 12, 565-573.

- Parone, P.A., James, D.I., Da Cruz, S., Mattenberger, Y., Donze, O., Barja, F., and Martinou, J.C. (2006). Inhibiting the mitochondrial fission machinery does not prevent Bax/Bak-dependent apoptosis. *Molecular and cellular biology* 26, 7397-7408.
- Pham, A.H., McCaffery, J.M., and Chan, D.C. (2012). Mouse lines with photo-activatable mitochondria to study mitochondrial dynamics. *Genesis* 50, 833-843.
- Praefcke, G.J., and McMahon, H.T. (2004). The dynamin superfamily: universal membrane tubulation and fission molecules? *Nature reviews Molecular cell biology* 5, 133-147.
- Rambold, A.S., Kostecky, B., Elia, N., and Lippincott-Schwartz, J. (2011). Tubular network formation protects mitochondria from autophagosomal degradation during nutrient starvation. *Proceedings of the National Academy of Sciences of the United States of America* 108, 10190-10195.
- Rajo, M., Legros, F., Chateau, D., and Lombes, A. (2002). Membrane topology and mitochondrial targeting of mitofusins, ubiquitous mammalian homologs of the transmembrane GTPase Fzo. *Journal of cell science* 115, 1663-1674.
- Rossignol, R., Faustin, B., Rocher, C., Malgat, M., Mazat, J.P., and Letellier, T. (2003). Mitochondrial threshold effects. *The Biochemical journal* 370, 751-762.
- Rowland, A.A., and Voeltz, G.K. (2012). Endoplasmic reticulum-mitochondria contacts: function of the junction. *Nature reviews Molecular cell biology* 13, 607-625.
- Rudolf, R., Mongillo, M., Magalhaes, P.J., and Pozzan, T. (2004). In vivo monitoring of Ca²⁺ uptake into mitochondria of mouse skeletal muscle during contraction. *The Journal of cell biology* 166, 527-536.
- Salvesen, G.S., and Dixit, V.M. (1997). Caspases: intracellular signaling by proteolysis. *Cell* 91, 443-446.
- Schweers, R.L., Zhang, J., Randall, M.S., Loyd, M.R., Li, W., Dorsey, F.C., Kundu, M., Opferman, J.T., Cleveland, J.L., Miller, J.L., *et al.* (2007). NIX is required for programmed mitochondrial clearance during reticulocyte maturation. *Proceedings of the National Academy of Sciences of the United States of America* 104, 19500-19505.
- Sesaki, H., and Jensen, R.E. (1999). Division versus fusion: Dnm1p and Fzo1p antagonistically regulate mitochondrial shape. *The Journal of cell biology* 147, 699-706.

- Sheng, Z.H., and Cai, Q. (2012). Mitochondrial transport in neurons: impact on synaptic homeostasis and neurodegeneration. *Nature reviews Neuroscience* 13, 77-93.
- Sheridan, C., Delivani, P., Cullen, S.P., and Martin, S.J. (2008). Bax- or Bak-induced mitochondrial fission can be uncoupled from cytochrome C release. *Molecular cell* 31, 570-585.
- Smirnova, E., Griparic, L., Shurland, D.L., and van der Bliek, A.M. (2001). Dynamin-related protein Drp1 is required for mitochondrial division in mammalian cells. *Molecular biology of the cell* 12, 2245-2256.
- Smirnova, E., Shurland, D.L., Ryazantsev, S.N., and van der Bliek, A.M. (1998). A human dynamin-related protein controls the distribution of mitochondria. *The Journal of cell biology* 143, 351-358.
- Song, Z., Chen, H., Fiket, M., Alexander, C., and Chan, D.C. (2007). OPA1 processing controls mitochondrial fusion and is regulated by mRNA splicing, membrane potential, and Yme1L. *The Journal of cell biology* 178, 749-755.
- Song, Z., Ghochani, M., McCaffery, J.M., Frey, T.G., and Chan, D.C. (2009). Mitofusins and OPA1 mediate sequential steps in mitochondrial membrane fusion. *Molecular biology of the cell* 20, 3525-3532.
- Stojanovski, D., Koutsopoulos, O.S., Okamoto, K., and Ryan, M.T. (2004). Levels of human Fis1 at the mitochondrial outer membrane regulate mitochondrial morphology. *Journal of cell science* 117, 1201-1210.
- Stowell, M.H., Marks, B., Wigge, P., and McMahon, H.T. (1999). Nucleotide-dependent conformational changes in dynamin: evidence for a mechanochemical molecular spring. *Nature cell biology* 1, 27-32.
- Suen, D.F., Narendra, D.P., Tanaka, A., Manfredi, G., and Youle, R.J. (2010). Parkin overexpression selects against a deleterious mtDNA mutation in heteroplasmic cybrid cells. *Proceedings of the National Academy of Sciences of the United States of America* 107, 11835-11840.
- Taguchi, N., Ishihara, N., Jofuku, A., Oka, T., and Mihara, K. (2007). Mitotic phosphorylation of dynamin-related GTPase Drp1 participates in mitochondrial fission. *The Journal of biological chemistry* 282, 11521-11529.
- Tanaka, A., Cleland, M.M., Xu, S., Narendra, D.P., Suen, D.F., Karbowski, M., and Youle, R.J. (2010). Proteasome and p97 mediate mitophagy and

degradation of mitofusins induced by Parkin. *The Journal of cell biology* 191, 1367-1380.

Tieu, Q., and Nunnari, J. (2000). Mdv1p is a WD repeat protein that interacts with the dynamin-related GTPase, Dnm1p, to trigger mitochondrial division. *The Journal of cell biology* 151, 353-366.

Tieu, Q., Okreglak, V., Naylor, K., and Nunnari, J. (2002). The WD repeat protein, Mdv1p, functions as a molecular adaptor by interacting with Dnm1p and Fis1p during mitochondrial fission. *The Journal of cell biology* 158, 445-452.

Tondera, D., Grandemange, S., Jourdain, A., Karbowski, M., Mattenberger, Y., Herzig, S., Da Cruz, S., Clerc, P., Raschke, I., Merkwirth, C., *et al.* (2009). SLP-2 is required for stress-induced mitochondrial hyperfusion. *The EMBO journal* 28, 1589-1600.

Twig, G., Elorza, A., Molina, A.J., Mohamed, H., Wikstrom, J.D., Walzer, G., Stiles, L., Haigh, S.E., Katz, S., Las, G., *et al.* (2008). Fission and selective fusion govern mitochondrial segregation and elimination by autophagy. *The EMBO journal* 27, 433-446.

Vallis, Y., Wigge, P., Marks, B., Evans, P.R., and McMahon, H.T. (1999). Importance of the pleckstrin homology domain of dynamin in clathrin-mediated endocytosis. *Current biology : CB* 9, 257-260.

Wakabayashi, J., Zhang, Z., Wakabayashi, N., Tamura, Y., Fukaya, M., Kensler, T.W., Iijima, M., and Sesaki, H. (2009). The dynamin-related GTPase Drp1 is required for embryonic and brain development in mice. *The Journal of cell biology* 186, 805-816.

Wang, C.X., and Youle, R.J. (2009). The Role of Mitochondria in Apoptosis. *Annual review of genetics* 43, 95-118.

Waterham, H.R., Koster, J., van Roermund, C.W., Mooyer, P.A., Wanders, R.J., and Leonard, J.V. (2007). A lethal defect of mitochondrial and peroxisomal fission. *The New England journal of medicine* 356, 1736-1741.

Yoon, Y., Krueger, E.W., Oswald, B.J., and McNiven, M.A. (2003). The mitochondrial protein hFis1 regulates mitochondrial fission in mammalian cells through an interaction with the dynamin-like protein DLP1. *Molecular and cellular biology* 23, 5409-5420.

Youle, R.J., and Narendra, D.P. (2011). Mechanisms of mitophagy. *Nature reviews Molecular cell biology* 12, 9-14.

Yu, T., Fox, R.J., Burwell, L.S., and Yoon, Y. (2005). Regulation of mitochondrial fission and apoptosis by the mitochondrial outer membrane protein hFis1. *Journal of cell science* 118, 4141-4151.

Zhang, Y., Chan, N.C., Ngo, H.B., Gristick, H., and Chan, D.C. (2012). Crystal structure of mitochondrial fission complex reveals scaffolding function for mitochondrial division 1 (Mdv1) coiled coil. *The Journal of biological chemistry* 287, 9855-9861.

Zhao, J., Liu, T., Jin, S., Wang, X., Qu, M., Uhlen, P., Tomilin, N., Shupliakov, O., Lendahl, U., and Nister, M. (2011). Human MIEF1 recruits Drp1 to mitochondrial outer membranes and promotes mitochondrial fusion rather than fission. *The EMBO journal* 30, 2762-2778.

Zuchner, S., Mersiyanova, I.V., Muglia, M., Bissar-Tadmouri, N., Rochelle, J., Dadali, E.L., Zappia, M., Nelis, E., Patitucci, A., Senderek, J., *et al.* (2004). Mutations in the mitochondrial GTPase mitofusin 2 cause Charcot-Marie-Tooth neuropathy type 2A. *Nature genetics* 36, 449-451.

CHAPTER 2

Fis1, Mff, MiD49 and MiD51 mediate Drp1 recruitment in mitochondrial fission

Oliver C. Losón¹, Zhiyin Song^{1,3}, Hsiuchen Chen¹, and David C. Chan^{1,2}

¹From the Division of Biology and Biological Engineering

²Howard Hughes Medical Institute

California Institute of Technology

Pasadena, CA 91125

³present address:

College of Life Sciences

Wuhan University

Wuhan, Hubei, PR. China 430072

This chapter was published in *Molecular Biology of the Cell*.

ABSTRACT

Several mitochondrial outer membrane proteins—Fis1, Mff, MiD49, and MiD51—have been proposed to promote mitochondrial fission by recruiting the GTPase Drp1, but fundamental issues remain concerning their function. A recent study supported such a role for Mff, but not for Fis1. In addition, it is unclear whether MiD49 and MiD51 activate or inhibit fission, because their overexpression causes extensive mitochondrial elongation. It is also unknown whether these proteins can act in the absence of one another to mediate fission. Using *Fis1*-null, *Mff*-null, and *Fis1/Mff*-null cells, we show that both Fis1 and Mff have roles in mitochondrial fission. Moreover, immunofluorescence analysis of Drp1 suggests that Fis1 and Mff are important for the number and size of Drp1 puncta on mitochondria. Finally, we find that either MiD49 or MiD51 can mediate Drp1 recruitment and mitochondrial fission in the absence of Fis1 and Mff. These results demonstrate that multiple receptors can recruit Drp1 to mediate mitochondrial fission.

INTRODUCTION

The opposing processes of fusion and fission (division) regulate mitochondrial morphology and function (Chan, 2012; Westermann, 2010; Youle and van der Bliek, 2012). During mitochondrial fission, the dynamin-related GTPase Drp1 is recruited from the cytosol onto the mitochondrial outer membrane, where it assembles into puncta. These puncta consist of oligomeric Drp1 complexes that wrap around and constrict the mitochondrial tubule to mediate fission (Mears et al., 2011). This proposed mechanism is analogous to how dynamin pinches off endocytic vesicles at the plasma membrane (Ferguson and De Camilli, 2012; Schmid and Frolov, 2011). Because much of Drp1 resides in the cytosol, key mechanistic issues are how Drp1 is recruited to the mitochondrial surface and what factors influence its assembly.

In mammals, four integral membrane proteins of the mitochondrial outer membrane—Fis1, Mff, MiD49, and MiD51—have been proposed to act as receptors that recruit Drp1 to the mitochondrial surface. However, there is much uncertainty concerning the precise role of these candidates and their relationship to each other. Fis1 was the first proposed receptor, based on definitive genetic and biochemical data from the budding yeast *S. cerevisiae*. The yeast Drp1 ortholog, Dnm1, requires Fis1 to localize to mitochondria (Fekkes et al., 2000; Mozdy et al., 2000; Tieu and Nunnari, 2000). Fis1 physically interacts with Dnm1 via one of two molecular adaptors, Mdv1 or Caf4 (Cervený and Jensen, 2003; Griffin et al., 2005; Tieu et al., 2002).

In mammals, however, there are no apparent orthologs of Mdv1 or Caf4, and the evidence supporting a role for Fis1 in mitochondrial fission is mixed. Supporting a role in fission, overexpression of Fis1 in mammalian cells promotes fragmentation of mitochondria (Stojanovski et al., 2004; Yoon et al., 2003; Yu et al., 2005), and inhibition of Fis1 results in elongation (Gandre-Babbe and van der Bliiek, 2008; Koch et al., 2005; Lee et al., 2004; Stojanovski et al., 2004; Yoon et al., 2003). However, a recent study showed that deletion of the *Fis1* gene from human colorectal carcinoma HCT116 cells does not disrupt mitochondrial morphology or Drp1 recruitment to mitochondria, and suggested that mitochondrial defects from *Fis1* knockdown studies may be due to off-target effects (Otera et al., 2010). *Mff* is currently the strongest candidate for a Drp1 receptor. Knockdown of *Mff* results in mitochondrial elongation (Gandre-Babbe and van der Bliiek, 2008) and reduces the amount of Drp1 recruited to mitochondria (Otera et al., 2010).

MiD49 and MiD51 (also called MIEF1) have been proposed to be components of the mitochondrial fission machinery (Palmer et al., 2011), but there is conflicting evidence concerning their mechanism of action. One study showed that a double knockdown results in mitochondrial elongation and reduces recruitment of Drp1 to mitochondria, supporting a role in fission (Palmer et al., 2011). Paradoxically, over-expression of either MiD49 or MiD51 also causes mitochondrial elongation (Palmer et al., 2011; Zhao et al., 2011), and another study showed that knockdown of MiD51 causes mitochondrial fragmentation

(Zhao et al., 2011). These latter observations led to the alternative proposal that MiD51 inhibits mitochondrial fission (Zhao et al., 2011).

To clarify the role of these candidate Drp1 receptors, we studied their function in mouse embryonic fibroblasts (MEFs). Our results support their role in mitochondrial fission and indicate that each protein is capable of recruiting Drp1 and promoting mitochondrial fission.

RESULTS

Fis1 and Mff can function independently of one another to regulate mitochondrial fission in MEFs

Given the disputed role of Fis1 in mitochondrial fission (Otera et al., 2010), we sought to directly compare the roles of Fis1 and Mff by generating MEF cell lines with null alleles of Fis1, Mff, or both. These cells are completely deficient for the relevant proteins (Fig. S2.1A). Mitochondrial morphology was assessed by immunofluorescence against the mitochondrial marker Tom20 (Fig. 2.1A). Consistent with previous studies using *Mff* knockdown (Gandre-Babbe and van der Bliek, 2008; Otera et al., 2010), mitochondria in *Mff*-null cell lines are severely elongated and interconnected. In contrast, mitochondria in *Fis1*-null cell lines have more moderate elongation and interconnection (Fig. 2.1A). We used a morphology scoring assay in which each cell was categorized as having short tubules, long tubules, net-like mitochondria, or collapsed mitochondria. For both mutants, more cells were found to have long or net-like mitochondria relative to wildtype cells (Fig. 2.1B), but the phenotype of *Mff*-null cells is much more pronounced than that of *Fis1*-null cells. Two other independent pairs of wildtype and *Fis1*-null cell lines gave similar results (Fig. S2.1B). Interestingly, mitochondrial elongation is most severe in the *Fis1/Mff* double mutant and approaches that of *Drp1*-null cells, indicating that the phenotype of Mff loss is substantially enhanced by additional removal of Fis1.

These observations were confirmed with several independent methods. First, we used morphometric image analysis to evaluate mitochondrial

length/interconnectivity. We quantified the number of discrete mitochondria and the total mitochondrial area in the cell periphery, where individual mitochondria can be readily resolved. The ratio of these two values provided a quantitative measure of mitochondrial length/interconnectivity. Significant differences were found among the wildtype cells and each of the mutants (Fig. 2.1C). The phenotypic trend found with this approach agreed well with the manual morphological scoring.

We also used FRAP (fluorescence recovery after photobleaching) to further quantify these differences in mitochondrial morphology. A region of interest (ROI) containing multiple mitochondria with matrix-targeted Cox8-Dendra2 was photobleached, and the recovery of fluorescence over 10 seconds was monitored. Because of the short recovery time, the fluorescence recovery is dependent on the length and interconnectivity of the photobleached mitochondria, not on mitochondrial fusion. Each of the mutant cell lines demonstrated higher levels of recovery than wildtype cells, with *Fis1/Mff*-null cells having the highest level (Fig. 2.1D and E; Fig. S2.1C). The recovery properties of *Fis1*-null and *Mff*-null were intermediate, with *Mff*-null cells showing higher levels of recovery than *Fis1*-null cells. To corroborate the FRAP results, we used an independent approach to measure the diffusion of Cox8-Dendra2. After photoconverting Cox8-Dendra2 with a 405 nm laser in a region of interest, we quantified the area to which the photoconverted signal immediately spread. We found that *Fis1/Mff*-null cells have the largest diffusion value, followed by *Mff*-null, then *Fis1*-null, and lastly wildtype cells (Fig. S2.1D). Taken together, these

results demonstrate that both Fis1 and Mff regulate mitochondrial length and interconnectivity, with Mff playing the predominant role in MEFs.

Given that both Fis1 and Mff function to regulate mitochondrial morphology, we tested whether Fis1 and Mff could act independently of one another. When *Fis1*-null and *Mff*-null cells are transfected with Fis1 and Mff expression constructs, respectively, both show a robust rescue in mitochondrial morphology, as expected (Fig. 2.1F, G and S2.2). Interestingly, when Fis1 is expressed in *Mff*-null cells or Mff is expressed in *Fis1*-null cells, there is also a substantial, albeit less complete, rescue in mitochondrial morphology. These results demonstrate that Fis1 and Mff can act independently and partially replace each other to regulate mitochondrial morphology.

Mitochondrial fission is induced by a number of physiological situations (Chan, 2012; Westermann, 2010). To determine whether Fis1 or Mff might selectively mediate mitochondrial fission in one of these pathways, we challenged wildtype and mutant cells with CCCP (for mitochondrial membrane depolarization), staurosporine (STS) or etoposide (for apoptosis), 1% O₂ (for hypoxia) or 0.1% serum (Fig. 2.1H; Fig. S2.1E). After each challenge, *Fis1*-null cells showed mitochondrial shortening, but less than in wildtype cells. In contrast, *Mff*-null and *Fis1/Mff*-null cell lines were highly resistant to mitochondrial shortening after each of these treatments. We conclude that both Fis1 and Mff are important for mitochondrial fission under basal and induced conditions, with Mff playing a larger role in both cases.

Fis1 and Mff are important for recruitment of Drp1 to mitochondria. To determine whether the mutant cells are defective in recruiting Drp1, we used immunofluorescence to visualize Drp1 puncta on mitochondria *in vivo*. In wildtype cells, much of the Drp1 staining is diffuse in the cytosol, but a proportion can be found in punctate structures on mitochondria. This recruitment to mitochondria is reduced in cells with *Mff* knockdown (Otera et al., 2010). Our knockout cells have reduced numbers of mitochondrial Drp1 puncta, with *Fis1/Mff*-null cells having the greatest defect, followed by *Mff*-null cells, and then *Fis1*-null cells (Fig. 2.2A). We used image analysis to quantify the density (number of puncta/mitochondrial area) of Drp1 puncta on mitochondria (Fig. 2.2B). *Fis1*-null cells have a small but significant decrease in the density of mitochondrial Drp1 puncta. *Mff*-null and *Fis1/Mff*-null cells have more substantial decreases. Interestingly, the average total fluorescence per puncta (Fig. 2.2A and C) as well as the average size of puncta (Fig. S2.1F) also show substantial declines in the mutant cells. As expected, exogenous expression of Mff in *Mff*-null cells rescued mitochondrial morphology and restored mitochondrial Drp1 puncta (Fig. S2.2B and D). This rescue depended on the R1 region (containing an 11 residue repeat; R1) and the transmembrane domain, as previously shown (Gandre-Babbe and van der Bliek, 2008; Otera et al., 2010). The levels of Drp1 in purified mitochondrial fractions from *Mff*-null and *Fis1/Mff*-null cells were substantially lower than those from wildtype and *Fis1*-null cells (Fig. 2.2D). The levels from *Fis1*-null mitochondria were only slightly less than wildtype. These imaging and biochemical data

indicate that Fis1 and Mff facilitate Drp1 recruitment onto mitochondria, with Mff playing the predominant role.

The MiDs can mediate mitochondrial fission in the absence of Fis1 and Mff. MiD49 and MiD51 play important roles in controlling mitochondrial morphology, but it is unclear whether they positively (Palmer et al., 2011) or negatively regulate mitochondrial fission (Zhao et al., 2011). One study found that simultaneous knockdown of both *MiD49* and *MiD51* caused mitochondrial elongation (Palmer et al., 2011), whereas another study found that knockdown of *MiD51* caused mitochondrial fragmentation (Zhao et al., 2011). To examine this issue, we used siRNA to knockdown *MiD49* and *MiD51*. Knockdown of either gene causes a similar enhancement of mitochondrial length and interconnectivity (Fig. 2.3A and B; Fig. S2.3), suggesting that these proteins positively regulate mitochondrial fission. Simultaneous knockdown of *MiD49* and *MiD51* does not cause a more severe phenotype than knockdown of either gene alone. It was previously reported that knockdown of both genes is necessary to cause mitochondrial elongation (Palmer et al., 2011). Our observation that a single knockdown is sufficient may be due to a higher efficiency of knockdown. For both *MiD49* and *MiD51*, we identified multiple siRNAs that caused a similar elongation of mitochondria (Fig. S2.3B).

The mitochondrial phenotype of *Fis1/Mff*-null cells is not as severe as that of *Drp1*-null cells (Fig. 2.1A and B), suggesting that residual mitochondrial fission exists in these cells. We found that knockdown of either *MiD49* or *MiD51* enhances the mitochondrial connectivity of *Fis1/Mff*-null cells, as well as in *Fis1*-

null and *Mff*-null cells (Fig. 2.3C; Fig. S2.3B). Simultaneous knockdown of MiD49 and MiD51 again does not cause a more severe phenotype than knockdown of either gene alone.

If MiD49 and MiD51 are involved in mitochondrial fission, it is puzzling that over-expression of either protein leads to extreme mitochondrial elongation (Palmer et al., 2011; Zhao et al., 2011). We also found similar elongation of mitochondria when MiD49 or MiD51 is over-expressed (Fig. 2.5C). This effect is associated with enhanced Drp1 levels on mitochondria (Fig. 2.4C; Fig. S2.4C). We wondered whether these proteins might be recruiting an inactive form of Drp1. Phosphorylation of Drp1 at S637 has been shown to negatively regulate Drp1 function (Cereghetti et al., 2008; Chang and Blackstone, 2007; Cribbs and Strack, 2007). Drp1 is also phosphorylated at S616, and this modification has been shown to positively regulate Drp1 function during mitosis (Kashatus et al., 2011; Taguchi et al., 2007). Using phospho-specific Drp1 antibodies that detect phosphorylation on S616 or S637, we found that levels of Drp1 S637-PO₄, but not S616-PO₄, are significantly enhanced in cell lines constitutively over-expressing either MiD49 or MiD51 (Fig. 2.4A, B; Fig. S2.4A). We also found enhanced levels of Drp1 S637-PO₄, but not S616-PO₄, in the mitochondrial fractions of these cells (Fig. 2.4C, bottom panel). These results suggest that the MiDs may preferentially bind to the S637-PO₄ form of Drp1. To test this idea, we co-transfected 293T cells with Myc tagged forms of MiD49 or MiD51 in combination with wildtype Drp1, an S→A (phospho-null) mutant or an S→D (phosphomimetic) mutant of Drp1 at S616 or S637. Cells were treated with a

reversible crosslinker to capture the MiD-Drp1 interaction, and cell lysates were subjected to anti-myc immunoprecipitation. Wildtype Drp1 and Drp1^{S637D} were co-immunoprecipitated more efficiently than Drp1^{S637A} (Fig. 2.4D). This preference is specific for residue S637 and is not found for S616.

Dephosphorylation at S637 is activated by CCCP and STS (Cereghetti et al., 2008; Cribbs and Strack, 2007). Treatment of MiD over-expressing cells with CCCP caused a reduction in Drp1 S637-PO₄ levels (Fig. 2.5A) and further enhancement of Drp1 recruitment to mitochondria (Fig. S2.4C). In contrast, phosphorylation at S616 was not modulated during CCCP treatment in wildtype cells or cells constitutively over-expressing either MiD49 or MiD51 (Fig. 2.5B). Interestingly, mitochondria in cells over-expressing MiD49 or MiD51 showed rapid and robust shortening upon treatment with CCCP or STS (Fig. 2.5C and D; Fig. S2.4B). Thus, the mitochondrial elongation caused by MiD over-expression is associated with enhanced Drp1 S637-PO₄ levels, and can be reversed by treatments that cause dephosphorylation of Drp1 at this site.

With a method to activate the pro-fission mode of the MiDs, we investigated whether they are capable of mediating mitochondrial fission in the absence of Fis1 and Mff. Expression of either MiD protein partially rescues recruitment of Drp1 to the mitochondria of *Fis1/Mff*-null cells (Fig. 2.6A and B). In spite of this Drp1 recruitment, the mitochondria of *Fis1/Mff*-null cells expressing MiDs remain extremely elongated (Fig. 2.6A, C, D). As noted earlier, *Fis1/Mff*-null cells are highly resistant to CCCP-induced mitochondrial fragmentation (Fig. 2.1H). However, when these cells over-express MiD49 or MiD51 and are treated

with CCCP, their mitochondria undergo rapid shortening, in contrast to non-transfected cells or cells transfected with an empty vector (Fig. 2.6C and D). Taken together, our experiments demonstrate that, under certain cellular contexts, the MiDs can function in the absence of Fis1 and Mff to recruit Drp1 to mitochondria and mediate mitochondrial fission.

DISCUSSION

Our work clarifies several issues concerning the recruitment of Drp1 to mitochondria. Analysis of *Fis1*-null MEFs indicates a clear, though minor, role of Fis1 in Drp1 recruitment and mitochondrial fission. Consistent with previous results (Otera et al., 2010), its role appears to be substantially less important than that of Mff. It is possible that the relative importance of Fis1 versus Mff depends on the particular cell type. Cell type specificity may explain why we found a clear mitochondrial morphology defect in *Fis1*-null MEFs, versus a previous study of *Fis1*-null HCT116 cells (Otera et al., 2010). It is also possible that the relative importance of these proteins depends on which signaling pathway is activated, although we have not yet identified conditions that selectively promote Fis1-mediated fission (Fig. 2.1H).

Our results suggest that Fis1 and Mff, beyond merely recruiting Drp1, may have a role in promoting Drp1 assembly. In the absence of Fis1, Mff, or both, the remaining Drp1 puncta associated with mitochondria are notably smaller in size and intensity. In this regard, these Drp1 receptors may play a role similar to yeast Mdv1, which promotes self-assembly of Dnm1 (Lackner et al., 2009). Future biochemical studies will be needed to test this model.

Previous studies have yielded perplexing observations of MiD49 and MiD51 over-expression versus knockdown. In particular, it has been unclear why MiD over-expression causes mitochondrial elongation (Palmer et al., 2011; Zhao et al., 2011). We find that when these proteins are over-expressed, recruitment of Drp1 is enhanced, but there is also increased inhibitory phosphorylation of Drp1

on S637. With CCCP treatment, this phosphorylation is reduced, and mitochondrial fission ensues. We cannot rule out that additional mechanisms may also inhibit Drp1 function upon MiD over-expression. Our results suggest the potential for regulation, where the outcome of MiD activity depends on the physiological state of the cell. For example, we speculate that MiDs may recruit Drp1, but maintain it in an inactive state until a cellular signal triggers fission.

Finally, our results indicate that Fis1, Mff, MiD49, and MiD51 can each recruit Drp1 and promote mitochondrial fission. In particular, the MiDs are able to promote fission in the absence of both Fis1 and Mff. It remains possible that these proteins can also function together to mediate fission. Future studies will clarify whether these proteins preferentially operate in specific cell types or cellular circumstances.

EXPERIMENTAL PROCEDURES

Materials

Antibody sources: Drp1 (BD Biosciences), Drp1 S616-PO₄ and S637-PO₄ (Cell Signaling), superoxide dismutase 2 (SOD2; Abcam), β -tubulin (TUBB; Imgenext), Tom20 (Santa Cruz), MiD49 (also known as SMCR7; Protein Tech Group), MiD51 (also known as SMCR7L; Protein Tech Group), Actin (Millipore), Fis1 (Alexis Corps/Axxora), Mff (Sigma-Aldrich, and gift from A. van der Bliek, University of California, Los Angeles, CA), Myc (mouse monoclonal 9E10 from Covance, and rabbit polyclonal from Sigma-Aldrich). CCCP (Sigma-Aldrich) was used at 50 μ M. Staurosporine (Sigma-Aldrich) was used at 1 μ M. Etoposide (Sigma-Aldrich) was used at 100 μ M. Z-VAD-FMK (BD Biosciences) was used at 50 μ M. Cells were grown in LabTek chambered glass slides (Nunc) for fixed and live cell imaging.

Immunofluorescence and imaging

For immunofluorescence, cells were fixed in 4% formaldehyde for 10 min at 37°C, permeabilized with 0.1% Triton-X100 at room temperature, and incubated with antibodies in 5% fetal calf serum. For Drp1 immunofluorescence, cells were permeabilized in a low concentration digitonin buffer (0.001% digitonin, 20 mM HEPES, 150 mM NaCl, 2 mM MgCl₂, 2 mM EDTA, 320 mM sucrose, pH 7.4) for 1.5 min at 37°C, and then immediately fixed. Cells were then processed as described above.

Scoring of mitochondrial network morphology was performed blind to genotype and treatment. All quantification was done in triplicate and 100 cells were scored per experiment.

All fluorescence imaging was performed using a Plan-Apochromat 63X/1.4 oil objective on a Zeiss LSM 710 confocal microscope driven by Zen 2009 software (Carl Zeiss). Image cropping was performed using ImageJ software (rsbweb.nih.gov/ij/). Global adjustments to brightness and contrast were performed using Photoshop (Adobe). 488 nm and 561 nm lasers were used to excite unconverted and photo-converted Dendra2, respectively, and a 405 nm laser was used to photo-convert Dendra2. Live cell imaging was done on a stage-top heated platform maintained at 37°C.

FRAP and diffusion assays

Cells constitutively expressing matrix targeted Cox8-Dendra2 were used for both assays. For FRAP, mitochondria in a 13 x 2 μm region were photo-bleached using a 405 nm laser at 10% laser power. Imaging was performed in a 15 x 9 μm region. Bleaching was performed to about 10% of original fluorescence for all trials. For photo-conversion of Cox8-Dendra2, a 405 nm laser at 4% laser power was used to photo-convert mitochondria in a 13 x 2 μm region. After photo-conversion, a Z-stack was collected of the entire cell. The area of the signal was measured using ImageJ and normalized to the original photo-converted area of mitochondria in the 13 x 2 μm region.

Image analysis

All image analysis was performed using ImageJ software. For mitochondrial morphometric analysis, Z-stacks were collected from cells labeled with Tom20 and summed projections were generated. Analysis was limited to regions of interest in the periphery of cells, where individual mitochondria are readily resolved, and images were thresholded to select mitochondria. From the thresholded fluorescence, binary images were generated, and the total mitochondrial area and number of discrete mitochondria were measured. The morphometric ratio was generated by dividing the number of mitochondria over the total mitochondrial area.

Mitochondrial Drp1 puncta were analyzed in the periphery of cells by first creating a binary mask of the mitochondrial channel (Tom20 or Cox8-Dendra2) and using it to subtract all extra-mitochondrial Drp1 fluorescence. To select mitochondrial Drp1 puncta for analysis, mitochondrial Drp1 fluorescence was thresholded. The thresholding value was determined as the average threshold value needed to select mitochondrial Drp1 puncta in wildtype cells. To count mitochondrial puncta and measure their area, the thresholded image was converted to a binary image. To measure Drp1 puncta fluorescence, puncta identified by thresholding were analyzed for fluorescence intensities.

Generation of mutant MEFs

Mouse embryonic stem (ES) cell lines containing gene trap disruptions of Fis1 (line S9-7D1) and Mff (line AZ0438) were available at the Mutant Mouse

Regional Resource Centers. The ES cell lines were injected into blastocysts to generate mouse lines. From matings of heterozygous animals, we established MEF lines from mid-gestation embryos, as previously described (Chen et al., 2003). Western blot analysis of the *Fis1*-null, *Mff*-null, and *Fis1/Mff*-null cells confirmed complete loss of the relevant proteins (Fig. S2.1A).

Cell culture

Cell lines stably expressing Cox8-Dendra2, MiD49-Myc, and MiD51-Myc were generated via retroviral transduction. All cell lines were cultured in Dulbecco's modified Eagle's medium (DMEM) containing 10% FBS and supplemented with 100 U/mL penicillin, 100 μ g/mL streptomycin, and 2 mM glutamine.

For hypoxia experiments, cells were placed into a Billups-Rothenberg modular incubator chamber and the atmosphere was exchanged with 1% O₂/5% CO₂. O₂ levels were monitored using a Sperian Toxipro single gas detector. Cells were incubated at 37°C for 24 hours.

Cloning and RNAi

Fis1, *Mff* isoform 5, *MiD49*, *MiD51*, and *Drp1* variant 2 transcripts were amplified from a MEF cDNA library using PCR. *MiD49* and *MiD51* were cloned into the XhoI and BamHI sites of a pcDNA3.1(-) plasmid containing a C-terminal 4xMyc tag. *Fis1*, *Fis1* Δ TMD (transmembrane domain deleted), *Mff* isoform 5, *Mff* Δ R1 (amino acid repeat 1 [residues 20 – 31] deleted), *Mff* Δ TMD, and *Drp1*

variant 2 were cloned into the BamHI and XhoI sites of pcDNA3.1(+). The entire open reading frames were confirmed by DNA sequencing. For generation of retroviral vectors, MiD49/51-Myc, Mff, Mff Δ R1, and Mff Δ TMD sequences were cloned into the pQCXIP-Puromycin vector (Invitrogen). Cells transduced with these viral constructs were selected with 1 μ g/mL puromycin (Invitrogen) for 4 to 5 days.

Oligonucleotides for siRNAs were purchased from Integrated DNA Technologies. The *MiD49* siRNA oligonucleotides were based on the following sequences:

5'-ACACCTAAGTTCAGCACTATAGCAC-3' (*MiD49*siRNA #1)

5'-GCCATGCCTTGAAGATGTGAATAAA-3' (*MiD49*siRNA #2).

The *MiD51* siRNA oligonucleotides were based on the following sequences:

5'-AGATTCCAAATGTCCTAAATCACAG-3' (*MiD51*siRNA #1)

5'-GGAATAAGACAGTATTTAGGTTTCC-3' (*MiD51*siRNA #2).

Results presented in Fig. 2.3 were obtained with *MiD49* siRNA #1 and *MiD51* siRNA #1. Results presented in Fig. S2.3 were obtained with *MiD49* siRNA #2 and *MiD51* siRNA #2. Control siRNA was targeted against a non-coding sequence in the mouse genome:

5'-CGTTAATCGCGTATAATACGCGTAT-3'.

siRNA nucleotides and plasmids were transfected using Lipofectamine 2000 (Invitrogen). Cells transfected with plasmids were assessed 24 hours post transfection. Fis1 and Mff plasmids were co-transfected with either Cox8-TagRFP or Cox8-DsRed at a ratio of 5:1. MiD49/51-Myc positive cells were

visualized with an anti-Myc antibody. Transfection of siRNA oligonucleotides was performed when cells were plated, at 24 hours and 48 hours post plating. Mitochondrial morphology and protein levels were assessed at 72 hours.

Drp1 immunoprecipitation and cell fractionation

To assess levels of Drp1 S637-PO₄, Drp1 was immunoprecipitated (anti-DLP1; BD Biosciences) from 5 million cells lysed in IP buffer (1% Triton X100, 5% glycerol, 150 mM NaCl, 25 mM Tris-HCl, 1 mM EDTA, pH 7.4) supplemented with a protease inhibitor cocktail (HALT; Thermo-Pierce). The lysates were cleared with a 21,000 *g* spin at 4°C for 10 min. Immune complexes were captured with protein A/G agarose (Thermo-Pierce), and the beads were washed with IP buffer.

For cell fractionation, cells were collected by trypsinization and washed once with PBS. Cells were resuspended in 1.5 mL mitochondria isolation buffer (10 mM HEPES, 220 mM mannitol, 70 mM sucrose, 80 mM KCl, 1 mM EDTA, 2 mM Mg Acetate, pH 7.4) supplemented with a protease inhibitor cocktail, and lysed using a nitrogen bomb (Parr) at 250 psi for 10 min, followed by mechanical homogenization with a glass-glass dounce homogenizer. Lysates were centrifuged at 700 *g* three times for 10 min to obtain a postnuclear supernatant. The postnuclear supernatant was centrifuged at 10,000 *g* for 10 min to obtain a crude mitochondrial pellet. The resultant supernatant was centrifuged at 21,000 *g* for 30 min to obtain the cytosol fraction. To obtain purified mitochondria, the crude mitochondrial pellet was placed in a discontinuous Percoll gradient

consisting of 80, 52, and 26% Percoll diluted in mitochondria isolation buffer. Centrifugation was performed at 42,500 *g* for 45 mins. Purified mitochondria were recovered from the 52 and 26% Percoll interface.

Myc co-immunoprecipitation assay

MiD-Drp1 interactions were assessed by transfecting 293Ts with Myc-tagged MiD constructs and Drp1 mutant constructs. For mouse Drp1 variant 2, residues S579 and S600 correspond to human Drp1 residues S616 and S637. Human nomenclature is presented in Figure 2.4D for consistency. Cells were harvested by trypsinization 24 hours post transfection, and crosslinked with 250 μ M Dithiobis(succinimidylpropionate) (Thermo-Pierce) in PBS for 30 mins at room temperature. Crosslinker was quenched by adding Tris-HCl pH 7.5 to a final concentration of 150 mM, and incubating for an additional 10 mins. Cells were pelleted, the quenched crosslinker solution was removed, and pellets were solubilized in RIPA buffer (50 mM Tris-HCl pH 8.0, 150 mM NaCl, 0.1% SDS and 1% NP-40) supplemented with a protease inhibitor cocktail. Myc immunoprecipitation was performed with rabbit anti-Myc agarose beads (Sigma). Crosslink bonds were reversed by solubilizing samples in Laemmli buffer (50 mM Tris-HCl pH 6.8, 1% SDS, 5% glycerol, and 0.005% bromophenol blue) containing 10% β -mercaptoethanol and boiling for 5 mins.

ACKNOWLEDGEMENTS

This work was supported by the National Institutes of Health (GM062967). OCL was supported by a R. L. Kirschstein National Research Service Award (5F31GM089327). The *Drp1*-null cells were a generous gift from Katsuyoshi Mihara (Kyushu University).

FIGURE LEGENDS

Figure 2.1. Mitochondrial elongation in *Fis1*-null, *Mff*-null, and *Fis1/Mff*-null MEFs.

(A) Mitochondrial morphology in wildtype and mutant cells. Mitochondria were visualized by immunofluorescence against Tom20. Scale bar, 10 μm . Inset scale bar, 5 μm . (B) Scoring of mitochondrial network morphologies for the indicated cell lines. Each cell was scored into 1 of 4 morphological categories. Triple asterisks indicates $P < 0.001$, double asterisks indicates $P < 0.005$, and single asterisks indicates $P < 0.02$. (C) Morphometric analysis. Well-resolved mitochondria (Tom20) in the cell periphery were used for morphometric analysis. Total mitochondrial number and area were measured; the ratio of these two values was plotted as percent of wildtype. 20 ROIs from two independent experiments were analyzed. Error bars indicate SEM. Asterisks indicates $P < 0.0001$. (D) FRAP analysis. For each of the indicated cell lines, the graph shows the fluorescence recovery over 10 s after photobleaching. Fluorescence data were collected every 200 ms post-bleach. (E) Endpoint analysis of FRAP data. The fluorescence recovery \pm SEM at 10 s post-bleaching is shown. For (D) and (E), 20 FRAP trials were averaged. Double asterisks indicates $P < 0.001$, and single asterisks indicates $P < 0.01$. (F and G) *Fis1*-null (F) and *Mff*-null (G) cells were transiently transfected with expression constructs for *Fis1*, *Mff*, or an empty control vector. Cells were scored into 1 of 4 morphological categories. F, fragmented; <50, less than 50% of mitochondria are long tubules; >50, greater than 50% of mitochondria are long tubules; N, net-like. Double asterisks indicates

$P < 0.005$, and single asterisks indicates $P < 0.05$. Statistical testing was performed by combining the F and <50 classes, which represent cells with mostly short mitochondria. (H) Cells from the indicated cell lines were treated with either 50 μM CCCP for 1 hour, 100 μM etoposide for 5 hours, 1% O_2 for 24 hours, or 0.1% serum for 3 days. Histograms show the percent of cells with fragmented or mostly short tubular mitochondria. For panels C, E and H: WT, wildtype; FN, *Fis1*-null; MN, *Mff*-null; DN, *Double*-null. For panels B, F, G, and H, data are the averages \pm SEM from three independent experiments, with 100 cells scored per experiment. All statistical testing was performed with the Student's *t* test.

Figure 2.2. Drp1 recruitment and assembly on mitochondria are affected in *Fis1*-null and *Mff*-null cells.

(A) Drp1 puncta in the indicated cell lines. To improve visualization of mitochondrial Drp1, the cells were briefly treated with 0.001% digitonin prior to fixation to reduce the level of cytosolic Drp1. Mitochondria were highlighted by immunofluorescence against Tom20. Scale bar in left panels, 10 μm . Center and right panels are magnified images of the boxed regions. Scale bar, 5 μm . In the right panel, a mask corresponding to the mitochondrial channel was applied to the Drp1 channel to obtain only mitochondrial Drp1 fluorescence. The heat map reflects Drp1 fluorescence intensity (FI). (B) Density of mitochondrial Drp1 puncta. (C) Drp1 fluorescence per puncta. In B and C, the data are normalized to the wildtype control. Error bars indicate SEM. 25 ROIs were analyzed from 10-12 cells for each group. Asterisks indicates $P < 0.05$ and double asterisks indicates

$P < 0.005$. Statistical testing was performed with the Student's t test. (D) Drp1 recruitment to mitochondria. Cytosol and purified mitochondrial fractions were prepared from the indicated MEF cells, and analyzed by Western blotting for Drp1, Tom20 (mitochondrial marker), and β -tubulin (TUBB; cytosolic marker). The mitochondrial lanes were loaded with 30-fold more cell equivalents compared to the cytosolic lanes. Both short and long exposures for the Drp1 blot are presented. For panels C through D: WT, wildtype; FN, *Fis1*-null; MN, *Mff*-null; DN, *Double*-null.

Figure 2.3. Knockdown of *MiD49* or *MiD51* causes mitochondrial elongation and enhances the *Fis1*-null, *Mff*-null and *Fis1/Mff*-null phenotypes.

(A) Mitochondrial morphology in wildtype MEFs treated with control siRNA, siRNA against *MiD49*, siRNA against *MiD51* or both. Scale bar, 10 μ m. Insets are magnified images of the boxed regions. Scale bar, 5 μ m. Mitochondria were highlighted by expression of Cox8-DsRed. (B) Western blot of cell lysates containing single and double knockdown of the MiDs. SOD2 is a loading control. (C) Scoring of mitochondrial network morphologies for knockdown experiments in wildtype, *Fis1*-null, *Mff*-null, and *Fis1/Mff*-null cells. Data were obtained from three independent experiments, with 100 cells scored per experiment. Error bars indicate SEM. S, short; L, long; N, net-like; C, collapsed.

Figure 2.4. Over-expression of MiD49 or MiD51 causes enhanced phosphorylation of Drp1 on S637.

(A) Increased Drp1 S637-PO₄ in cells over-expressing MiD49 or MiD51. In the top panel, lysates from control HeLa cells or HeLa cells expressing MiD49-Myc or MiD51-Myc were analyzed by Western blotting for Drp1 and the Myc-tagged MiD. In the bottom panel, Drp1 was immunoprecipitated, and the levels of Drp1 S637-PO₄ were detected with a phosphospecific Drp1 antibody. Drp1 was used as a loading control for the immunoprecipitated samples. (B) Drp1 S616-PO₄ levels in cells over-expressing MiD49 or MiD51. Lysates from control HeLa cells or HeLa cells expressing MiD49-Myc or MiD51-Myc were analyzed by Western blotting for Drp1, Drp1 S616-PO₄ and the Myc-tagged MiD. Actin was used as a loading control. (C) Increased Drp1 S637-PO₄ recruitment to mitochondria in cells over-expressing MiD49 or MiD51. In the top panel, cytosol and crude mitochondrial fractions were prepared from the indicated HeLa cells and analyzed by Western blotting for Drp1, superoxide dismutase 2 (SOD2; mitochondrial), and β -tubulin (TUBB; cytosolic). The mitochondrial lanes were loaded with 20-fold more cell equivalents compared to the cytosolic lanes. In the bottom panel, the loading of mitochondrial fractions was normalized for the total Drp1 level. The relative levels of Drp1 S616-PO₄ and Drp1 S637-PO₄ on mitochondria were assessed by Western blotting with phosphospecific antibodies. In A, B, and C, densitometry was performed on the S616-PO₄ and Drp1 S637-PO₄ blots, and was normalized to the total Drp1 in each sample. Values are presented as proportions of wildtype. (D) Binding of MiD49 and

MiD51 to phospho-mutants of Drp1. 293T cells were co-transfected with Myc-tagged MiD and Drp1 mutants as indicated. Cells were treated with crosslinker and solubilized. The top panel shows expression of Drp1 and Myc-MiD in the lysates. In the bottom panel, anti-Myc immunoprecipitates were analyzed for Drp1. Note that this assay only detects transfected Drp1 (compare lanes 2 and 3 to 7 and 10). S, wildtype Drp1; A, phospho-null mutant; D, phosphomimetic mutant.

Figure 2.5. Mitochondrial elongation and increased Drp1 S637-PO₄ caused by MiD over-expression can be reversed by CCCP.

(A) Reduction of Drp1 S637-PO₄ levels in CCCP treated cells. In the left panel, lysates from control HeLa cells or HeLa cells expressing MiD49-Myc or MiD51-Myc were analyzed by Western blotting for Drp1. Cells were treated with DMSO (indicated by D) or CCCP (indicated by C). In the right panel, Drp1 S637-PO₄ was analyzed as in Fig. 2.4A. Both short and long exposures for the Drp1 S637-PO₄ blot are presented. (B) Drp1 S616-PO₄ levels do not change in CCCP treated cells. Lysates from control HeLa cells or HeLa cells expressing MiD49-Myc or MiD51-Myc were analyzed as in Fig. 2.4B. Cells were treated with DMSO (indicated by D) or CCCP (indicated by C). Densitometry was performed on the S616-PO₄ and Drp1 S637-PO₄ blots, and was normalized to the total Drp1 in each lane. Values are presented as ratios of the CCCP/DMSO values for each group. (C) CCCP reverses mitochondrial elongation in MiD over-expressing MEFs. Cells were transfected with MiD49-Myc or MiD51-Myc and subsequently

treated with vehicle (DMSO) or CCCP. MiD expressing cells were identified by Myc immunofluorescence, and mitochondria were visualized with Tom20 immunofluorescence. In the DMSO-treated samples, note that MiD-Myc expression causes mitochondrial elongation. In the CCCP-treated samples, note that MiD-Myc expressing cells have fragmented mitochondria. Scale bar, 10 μm .

(D) Scoring of mitochondrial network morphologies for MEFs transfected with MiD49-Myc, MiD51-Myc, or empty vector, and treated with DMSO or CCCP. The data are from three independent experiments, each with 100 cells scored. Error bars indicate SEM. S, short; L, long; N, net-like; C, collapsed.

Figure 2.6. MiD49 and MiD51 can restore CCCP-induced mitochondrial fragmentation in *Fis1/Mff*-null cells.

(A) Restoration of Drp1 puncta in *Fis1/Mff*-null cells. *Fis1/Mff*-null cells were transfected with MiD49-Myc, MiD51-Myc or empty vector. Cells were analyzed for MiD-Myc expression (anti-Myc), mitochondrial morphology (Cox8-Dendra2) and Drp1. Scale bar, 10 μm . Right column contains magnified images of the boxed regions. Scale bar, 5 μm . (B) Density of Drp1 puncta on mitochondria. 20 ROIs were analyzed in 8-10 cells per group. Data are normalized to wildtype cells. Error bars indicate SEM. Asterisks indicate $P < 0.001$. DM, *Fis1/Mff* double mutant. (C) Scoring of mitochondrial network morphologies for *Fis1/Mff*-null cells transfected with MiD49-Myc, MiD51-Myc, or empty vector, and treated with DMSO or CCCP. Data are from three independent experiments, each with 100 cells scored. Error bars indicate SEM. S, short; L, long; N, net-like; C, collapsed.

Double asterisks indicates $P = 0.002$, and single asterisks indicates $P = 0.02$. (D) Representative micrographs of *Fis1/Mff*-null cells transfected with MiD49-Myc or MiD51-Myc, and treated with DMSO or CCCP. MiD-Myc expressing cells were analyzed for mitochondrial morphology (Tom20). With CCCP treatment, note that the MiD-Myc transfected cells have fragmented mitochondria, whereas the non-transfected cells are resistant to CCCP-induced fragmentation. Scale bar, 10 μm . Statistical testing was performed with the Student's *t* test.

Figure 2.1

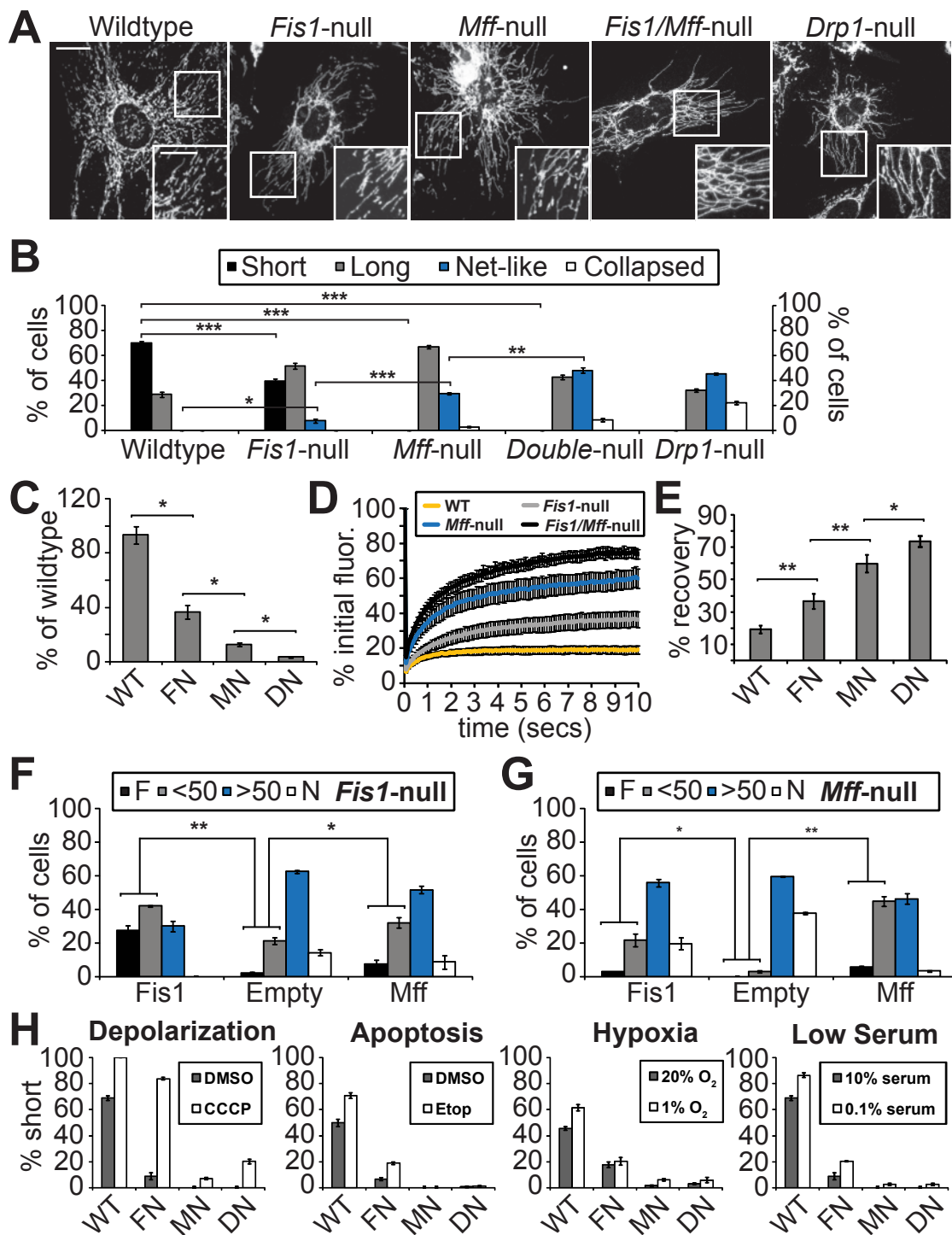


Figure 2.2

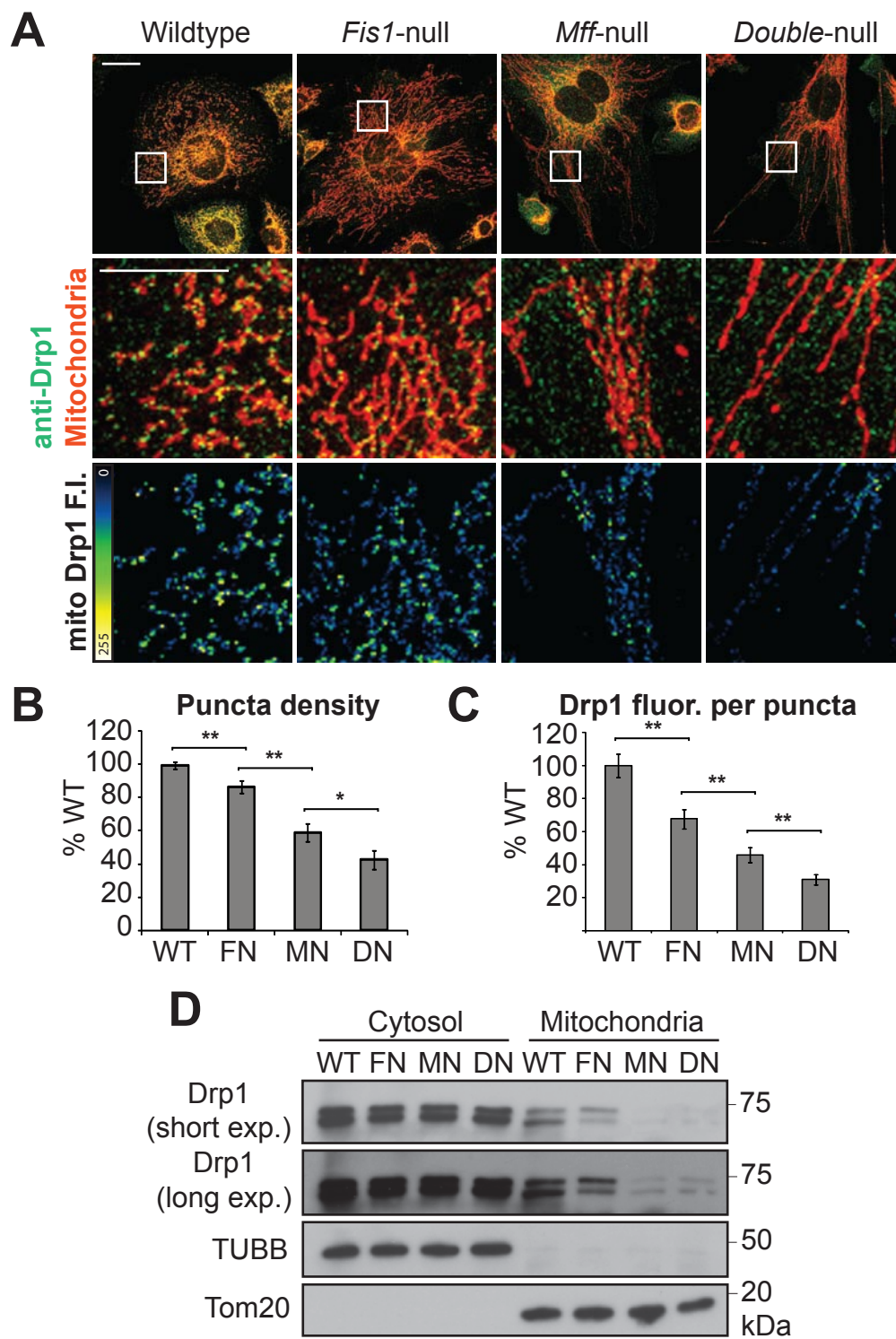


Figure 2.3

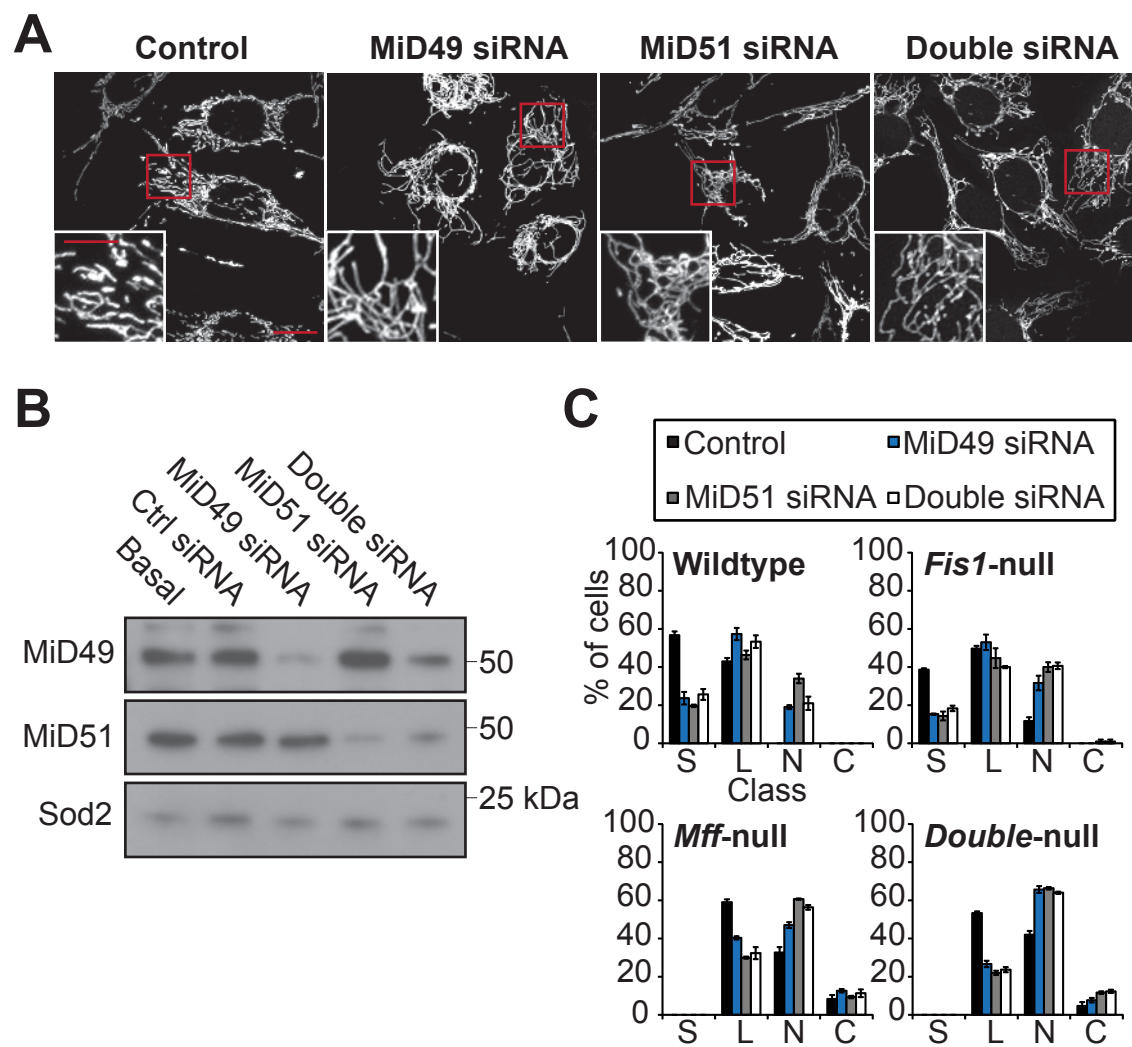


Figure 2.4

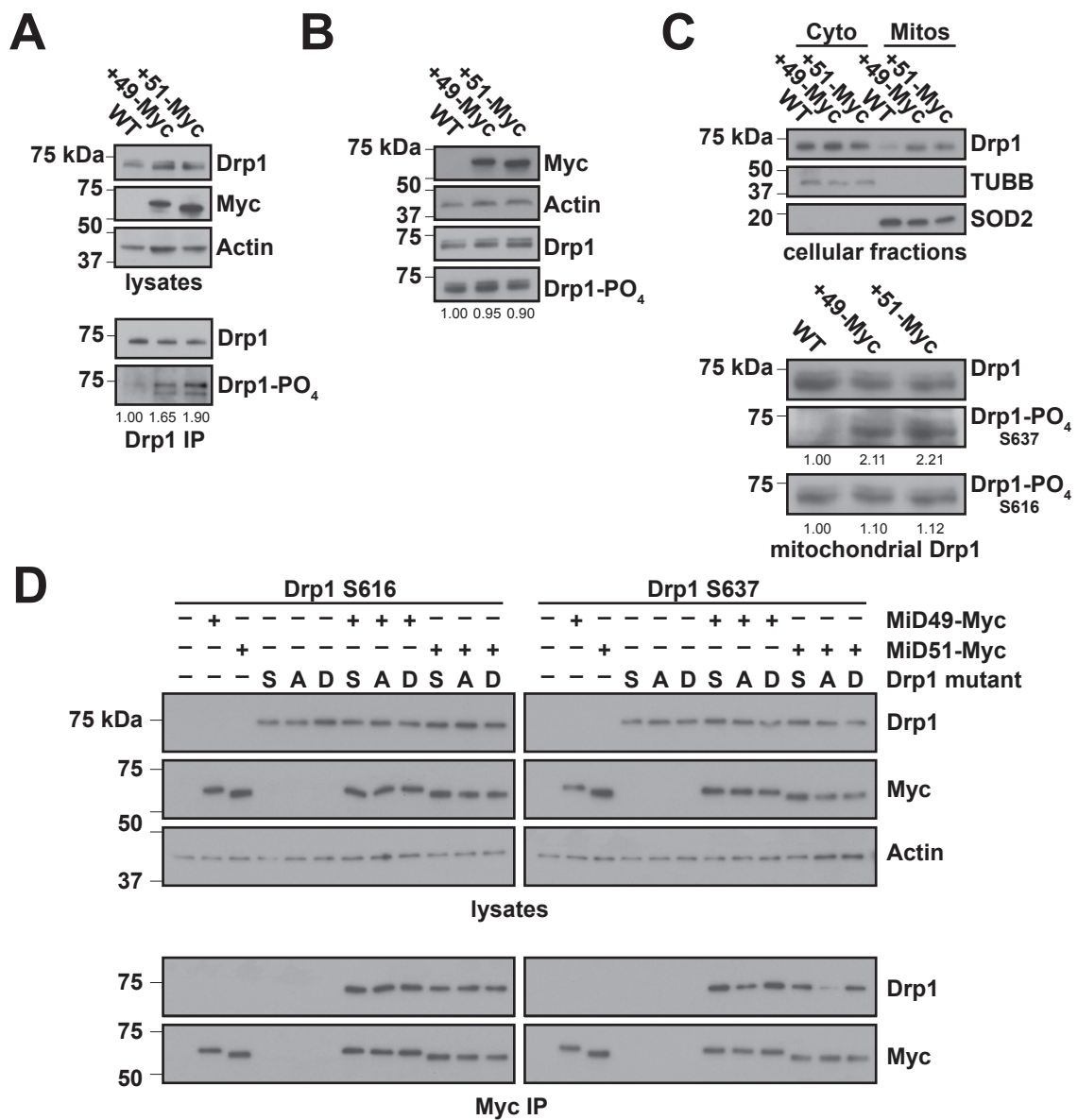


Figure 2.5

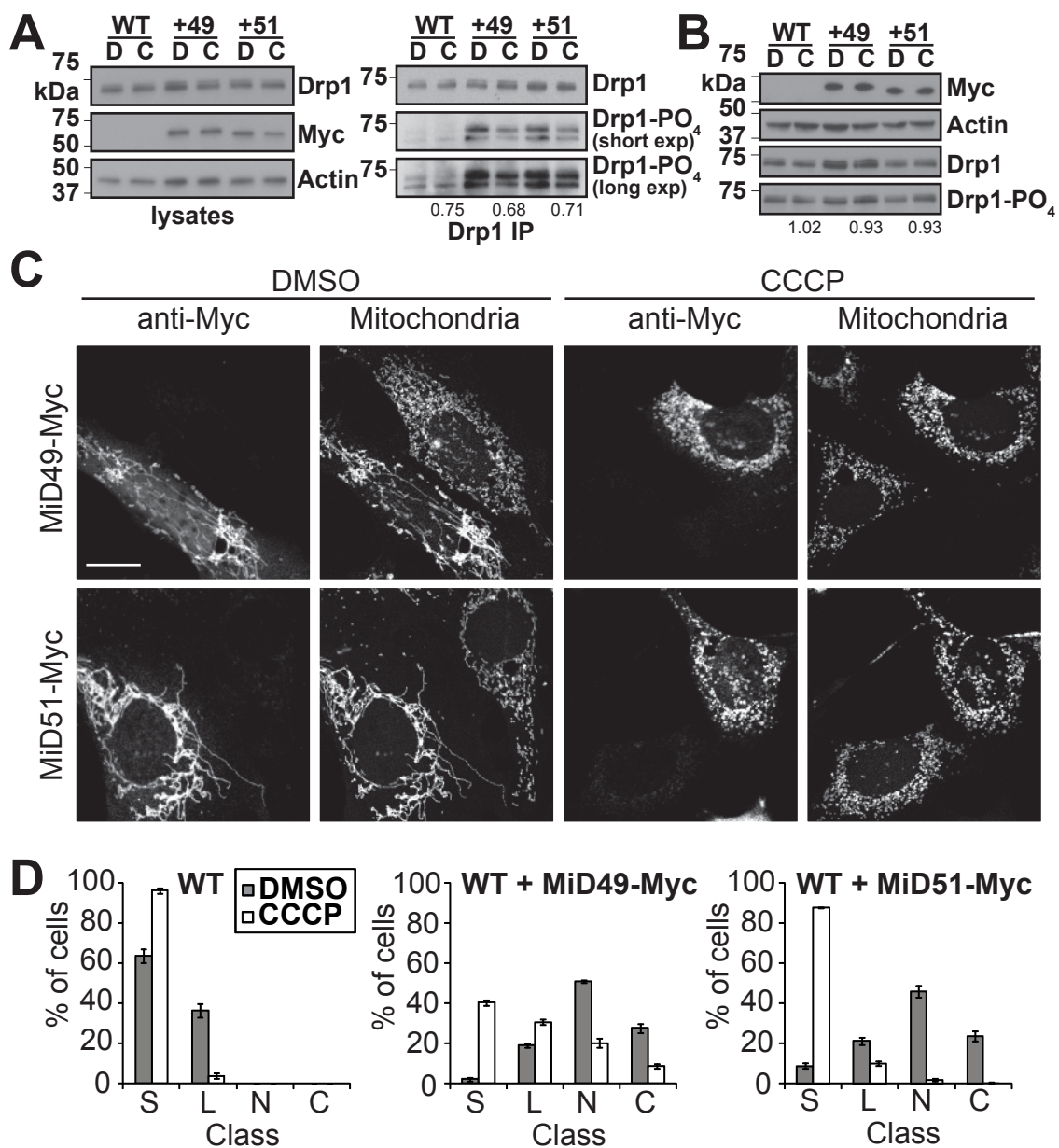
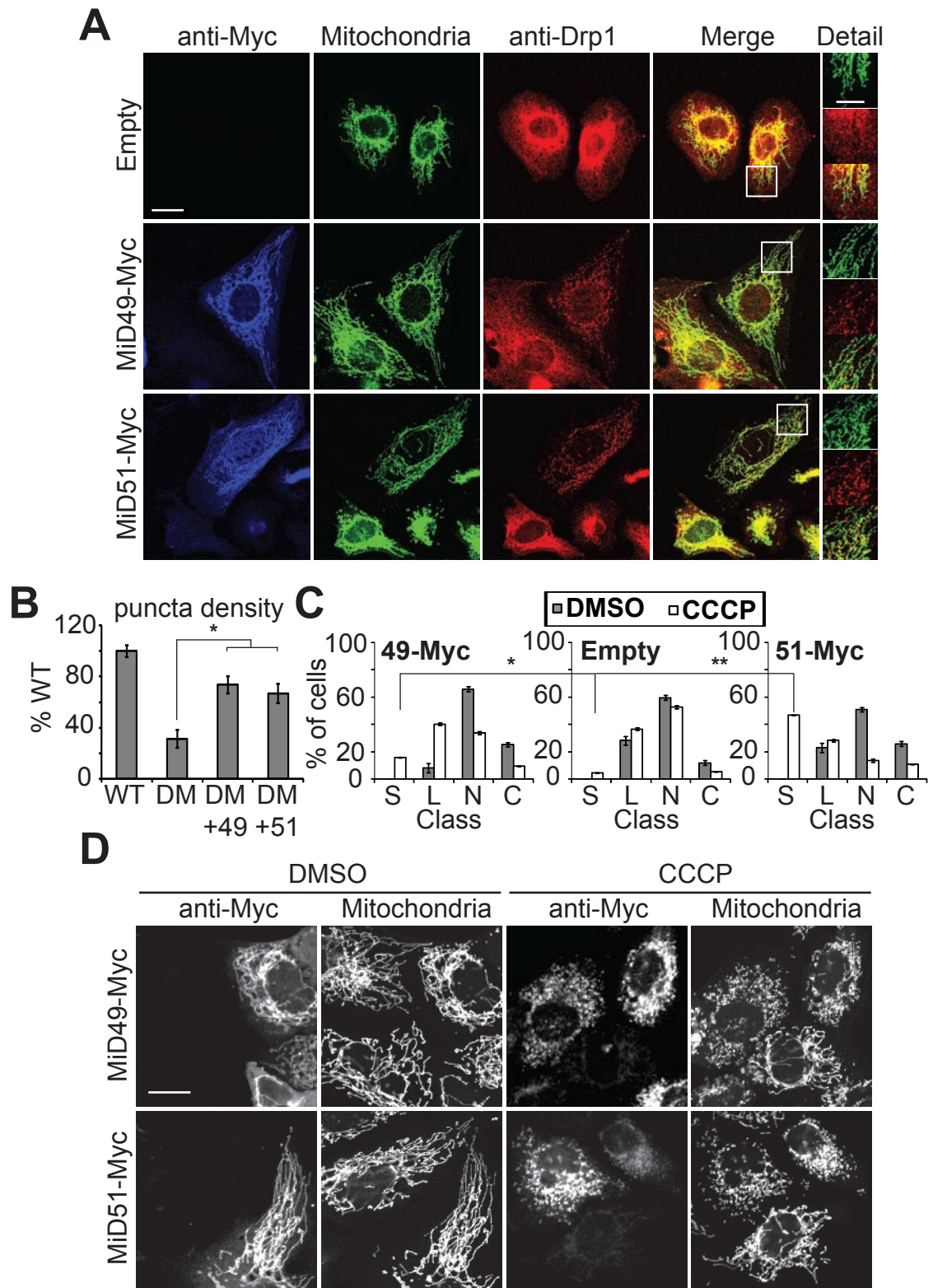


Figure 2.6



SUPPLEMENTARY FIGURE LEGENDS**Figure S2.1. Mitochondrial morphology in *Fis1*-null, *Mff*-null and *Fis1/Mff*-null MEF cells.**

(A) Western blotting of lysates from *Fis1*-null, *Mff*-null and *Fis1/Mff*-null cells. Lysates were evaluated for Fis1 and Mff, and actin is a loading control. (B) Mitochondrial morphology in two independently isolated pairs of WT and *Fis1*-null cell lines. Cells were scored into 1 of 4 morphological categories. F, fragmented; <50, less than 50% of mitochondria are long tubules; >50, greater than 50% of mitochondria are long tubules; N, net-like. Data are from three independent experiments, each with 100 cells scored. (C) Representative fluorescence micrographs of FRAP experiments corresponding to Fig. 2.1 D. The white box indicates region that was bleached. Scale bar, 2 μ m. (D) Diffusion of photoconverted Cox8-Dendra2. A region of interest was photo-converted, and the area to which the signal had spread at 2 seconds was quantified. The area ratio value is the final area divided by the initial photoconverted area of mitochondria. Data are the averages from 10-14 diffusion measurements and are normalized to *Fis1/Mff*-null. Asterisks indicates $P < 0.05$. (E) Cells from the indicated cell lines were treated with 1 μ M staurosporine for 5 hours. The percent of cells with short mitochondria is plotted. Data are from three independent experiments, each with 100 cells scored. (F) Mitochondrial Drp1 puncta size. Data are the averages from 25 ROIs from 10-12 cells per group. Data are normalized to wildtype. Asterisks indicates $P < 0.001$. All error bars indicate SEM,

and statistical testing was performed with the Student's *t* test. For panels D through F: WT, wildtype; FN, *Fis1*-null; MN, *Mff*-null; DN, *Double*-null.

Figure S2.2. Rescue of *Fis1*-null and *Mff*-null cells.

(A and B) Mitochondrial morphology and Drp1 puncta. (A) *Fis1*-null cells were transiently transfected with *Fis1*, empty vector, or *Fis1* lacking the transmembrane domain (*Fis1*ΔTMD). *Cox8*-TagRFP was co-transfected to label the mitochondria. (B) *Mff*-null cells were transduced with *Mff*, empty vector, *Mff*ΔR1, or *Mff*ΔTMD. Mitochondria were highlighted by immunofluorescence against Tom20. Scale bars in left panels, 10 μm. Center and right panels are magnified images of the boxed regions. Scale bars, 5 μm. (C and D) Rescue of mitochondrial morphology. *Fis1*-null (C) and *Mff*-null (D) cells expressing the indicated constructs were scored into 1 of 4 morphological categories. F, fragmented; <50, less than 50% of mitochondria are long tubules; >50, greater than 50% of mitochondria are long tubules; N, net-like.

Figure S2.3. Mitochondrial elongation by a second set of MiD siRNAs.

Similar to Fig. 2.3B and C, except that different siRNAs against MiD49 and MiD51 were used. (A) Western blot analysis of lysates containing single and double knockdown of MiD49 and MiD51. SOD2 is a loading control. (B) Scoring of mitochondrial network morphologies into categories S, short; L, long; N, net-like; C, collapsed.

Figure S2.4. Mitochondrial elongation and increased Drp1 S637-PO₄ caused by MiD overexpression can be reversed by CCCP or STS.

(A) Increased Drp1 S637-PO₄ in MEFs over-expressing MiD49-Myc or MiD51-Myc. In the left panel, lysates from control MEFs or MEFs expressing MiD49-Myc or MiD51-Myc were analyzed by Western blotting for Drp1 and the Myc-tagged MiD. Actin was used as a loading control. In the right panel, Drp1 was immunoprecipitated, and the levels of Drp1 S637-PO₄ were detected with a phosphospecific Drp1 antibody. Drp1 was used as a loading control for the immunoprecipitated samples. (B) Scoring of mitochondrial network morphologies for HeLa cells over-expressing MiD49-Myc or MiD51-Myc. Cells were treated with vehicle (DMSO), 50 μM CCCP for 1 hour, or 1 μM STS for 5 hours. Data are from three independent experiments, each with 100 cells scored. Error bars indicate SEM. F, fragmented; <50, less than 50% of mitochondria are long tubules; >50, greater than 50% of mitochondria are long tubules; N, netlike. (C) Drp1 recruitment to mitochondria. Cytosol and crude mitochondrial fractions were prepared from the indicated HeLa cells treated with DMSO (D) or CCCP(C), and analyzed by Western blotting for Drp1, superoxide dismutase 2 (SOD2; mitochondrial), and β-tubulin (TUBB; cytosolic). The mitochondrial lanes were loaded with 10-fold more cell equivalents compared to the cytosolic lanes.

Figure S2.1

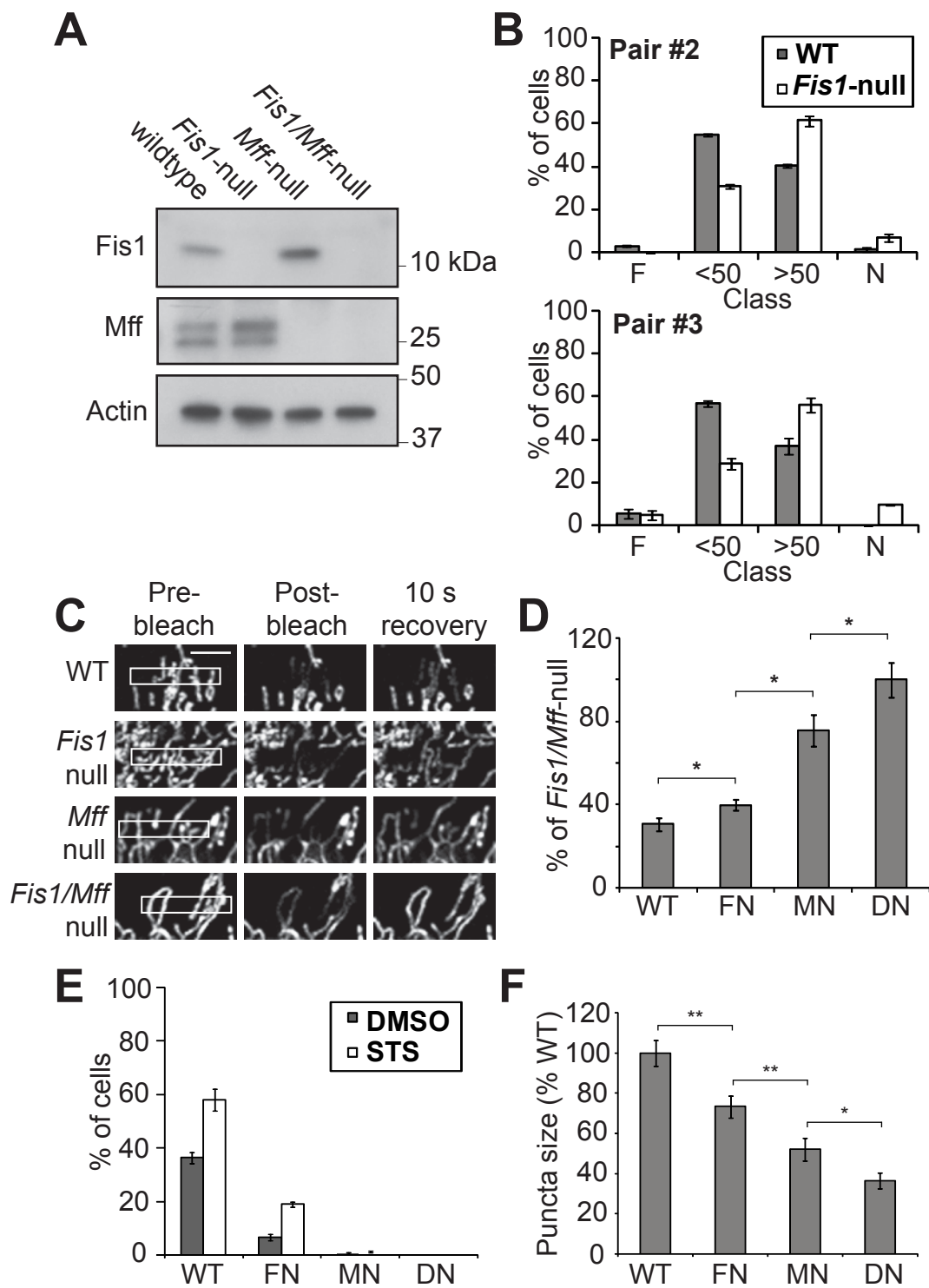


Figure S2.2

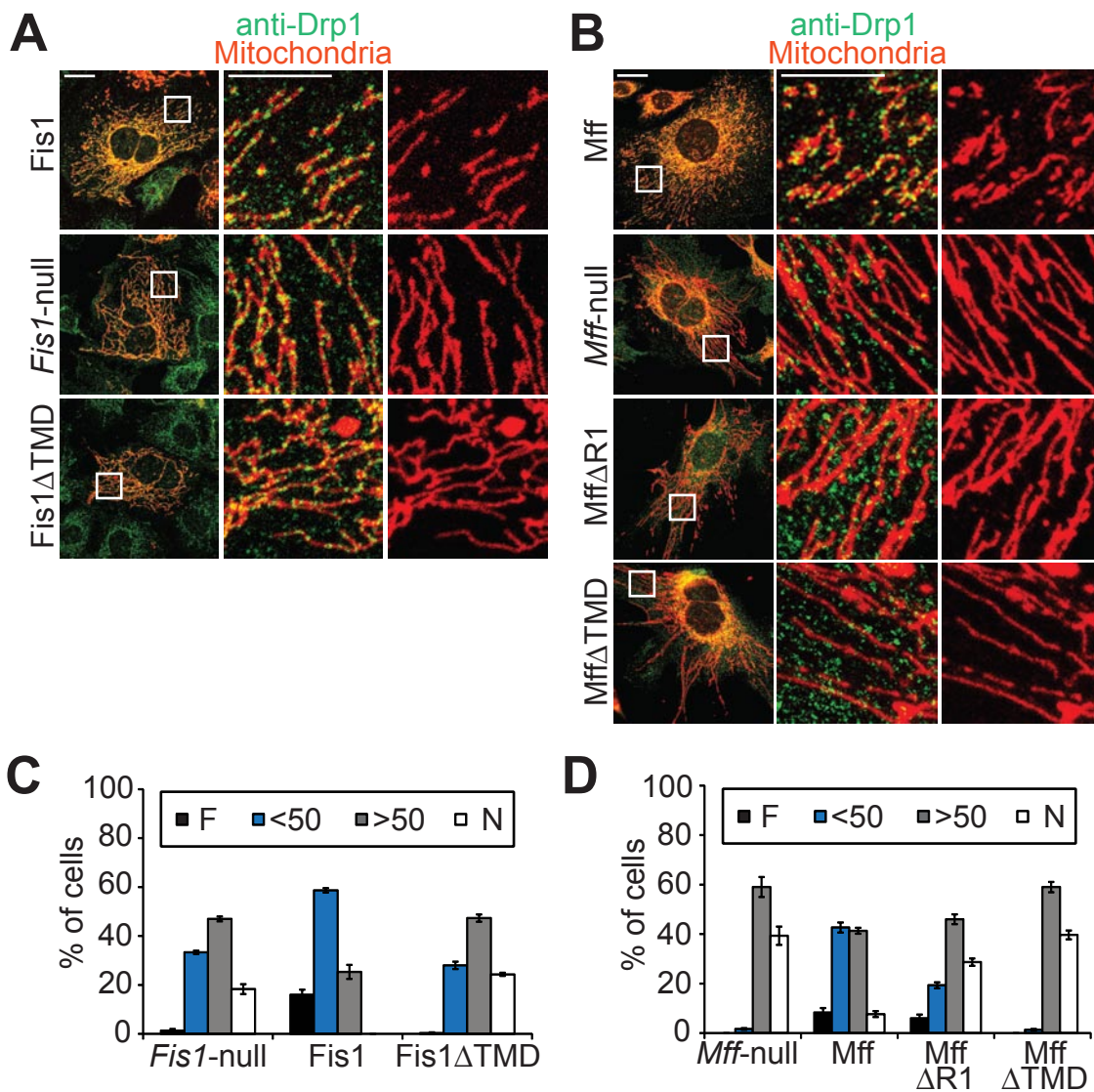


Figure S2.3

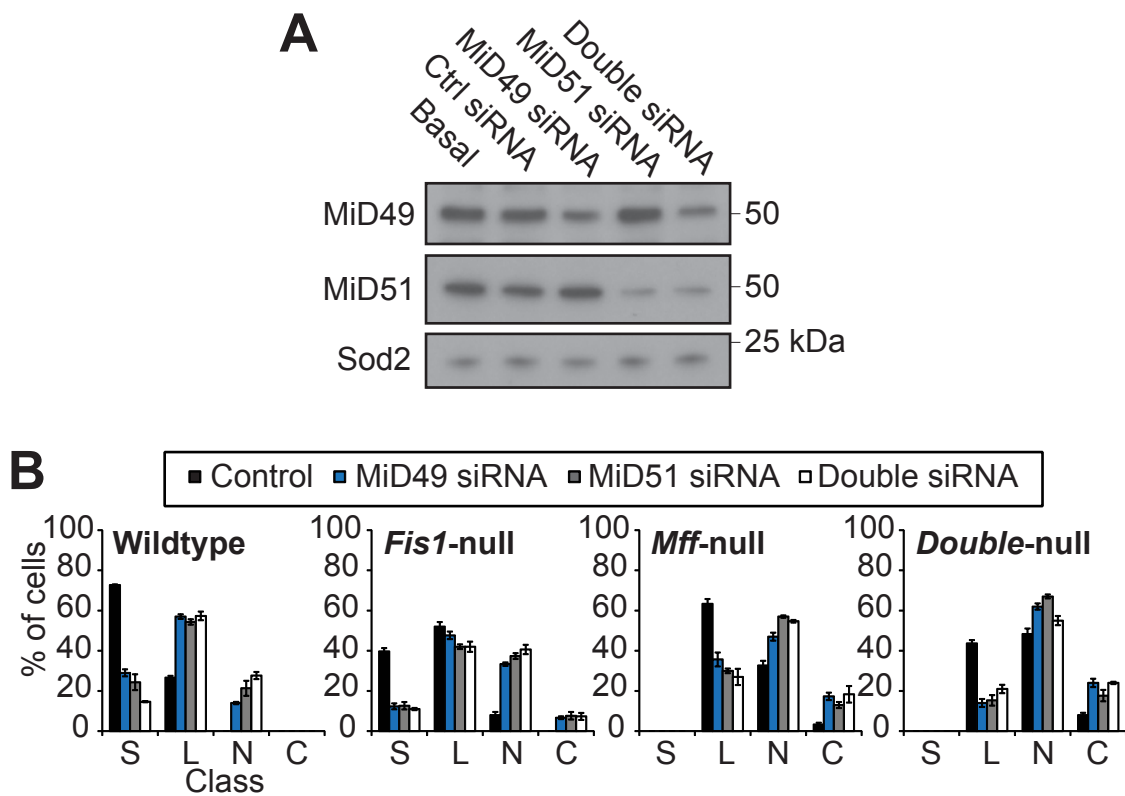
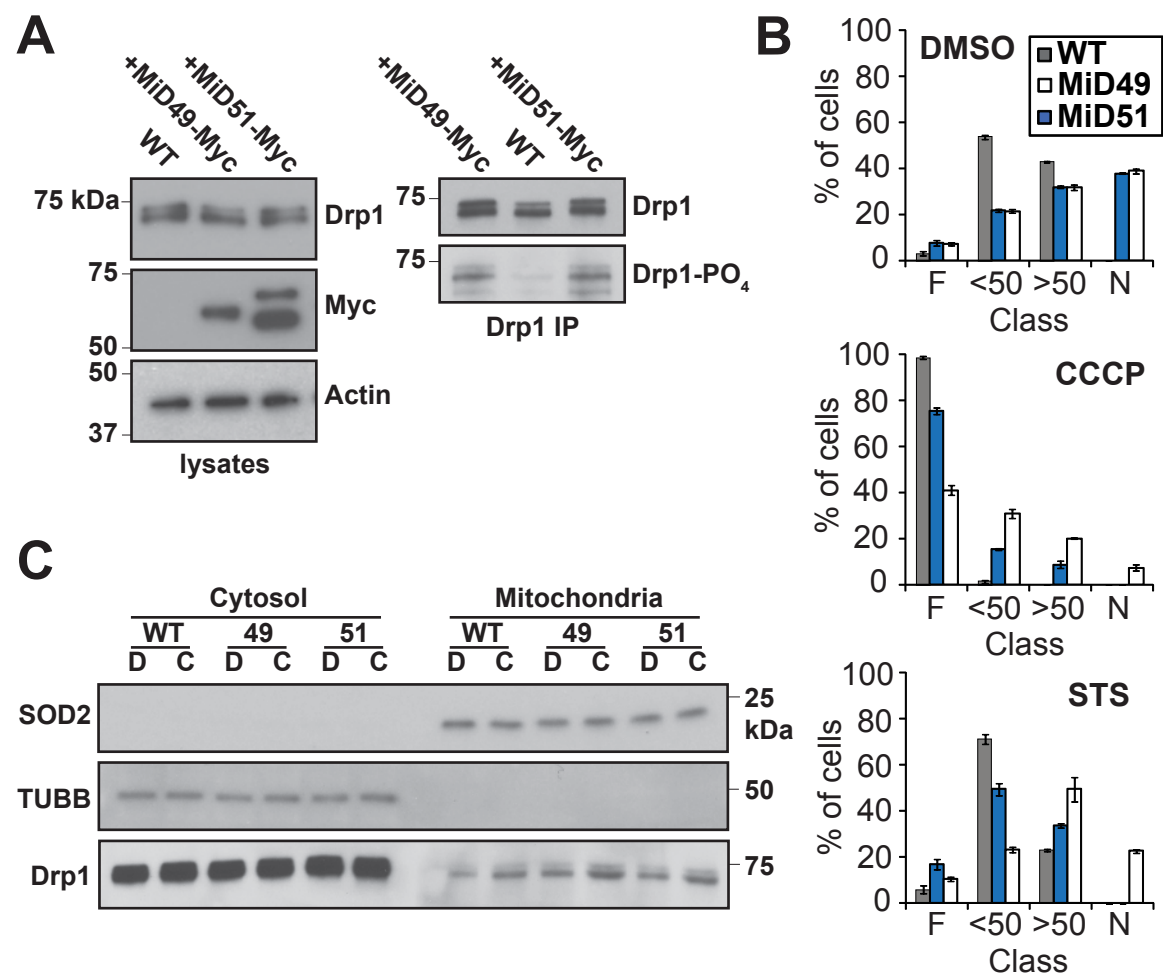


Figure S2.4



REFERENCES

- Cereghetti, G.M., Stangherlin, A., Martins de Brito, O., Chang, C.R., Blackstone, C., Bernardi, P., and Scorrano, L. (2008). Dephosphorylation by calcineurin regulates translocation of Drp1 to mitochondria. *Proceedings of the National Academy of Sciences of the United States of America* *105*, 15803-15808.
- Cervený, K.L., and Jensen, R.E. (2003). The WD-repeats of Net2p interact with Dnm1p and Fis1p to regulate division of mitochondria. *Mol Biol Cell* *14*, 4126-4139.
- Chan, D.C. (2012). Fusion and fission: interlinked processes critical for mitochondrial health. *Annu Rev Genet*, in press.
- Chang, C.R., and Blackstone, C. (2007). Cyclic AMP-dependent protein kinase phosphorylation of Drp1 regulates its GTPase activity and mitochondrial morphology. *The Journal of biological chemistry* *282*, 21583-21587.
- Chen, H., Detmer, S.A., Ewald, A.J., Griffin, E.E., Fraser, S.E., and Chan, D.C. (2003). Mitofusins Mfn1 and Mfn2 coordinately regulate mitochondrial fusion and are essential for embryonic development. *The Journal of cell biology* *160*, 189-200.
- Cribbs, J.T., and Strack, S. (2007). Reversible phosphorylation of Drp1 by cyclic AMP-dependent protein kinase and calcineurin regulates mitochondrial fission and cell death. *EMBO reports* *8*, 939-944.
- Fekkes, P., Shepard, K.A., and Yaffe, M.P. (2000). Gag3p, an outer membrane protein required for fission of mitochondrial tubules. *J Cell Biol* *151*, 333-340.
- Ferguson, S.M., and De Camilli, P. (2012). Dynamin, a membrane-remodelling GTPase. *Nature reviews Molecular cell biology* *13*, 75-88.
- Gandre-Babbe, S., and van der Bliek, A.M. (2008). The novel tail-anchored membrane protein Mff controls mitochondrial and peroxisomal fission in mammalian cells. *Molecular biology of the cell* *19*, 2402-2412.
- Griffin, E.E., Graumann, J., and Chan, D.C. (2005). The WD40 protein Caf4p is a component of the mitochondrial fission machinery and recruits Dnm1p to mitochondria. *The Journal of cell biology* *170*, 237-248.
- Kashatus, D.F., Lim, K.H., Brady, D.C., Pershing, N.L., Cox, A.D., and Counter, C.M. (2011). RALA and RALBP1 regulate mitochondrial fission at mitosis. *Nature cell biology* *13*, 1108-1115.

- Koch, A., Yoon, Y., Bonekamp, N.A., McNiven, M.A., and Schrader, M. (2005). A role for Fis1 in both mitochondrial and peroxisomal fission in mammalian cells. *Molecular biology of the cell* 16, 5077-5086.
- Lackner, L.L., Horner, J.S., and Nunnari, J. (2009). Mechanistic analysis of a dynamin effector. *Science* 325, 874-877.
- Lee, Y.J., Jeong, S.Y., Karbowski, M., Smith, C.L., and Youle, R.J. (2004). Roles of the mammalian mitochondrial fission and fusion mediators Fis1, Drp1, and Opa1 in apoptosis. *Molecular biology of the cell* 15, 5001-5011.
- Mears, J.A., Lackner, L.L., Fang, S., Ingberman, E., Nunnari, J., and Hinshaw, J.E. (2011). Conformational changes in Dnm1 support a contractile mechanism for mitochondrial fission. *Nature structural & molecular biology* 18, 20-26.
- Mozdy, A.D., McCaffery, J.M., and Shaw, J.M. (2000). Dnm1p GTPase-mediated mitochondrial fission is a multi-step process requiring the novel integral membrane component Fis1p. *The Journal of cell biology* 151, 367-380.
- Otera, H., Wang, C., Cleland, M.M., Setoguchi, K., Yokota, S., Youle, R.J., and Mihara, K. (2010). Mff is an essential factor for mitochondrial recruitment of Drp1 during mitochondrial fission in mammalian cells. *The Journal of cell biology* 191, 1141-1158.
- Palmer, C.S., Osellame, L.D., Laine, D., Koutsopoulos, O.S., Frazier, A.E., and Ryan, M.T. (2011). MiD49 and MiD51, new components of the mitochondrial fission machinery. *EMBO reports* 12, 565-573.
- Schmid, S.L., and Frolov, V.A. (2011). Dynamin: functional design of a membrane fission catalyst. *Annu Rev Cell Dev Biol* 27, 79-105.
- Stojanovski, D., Koutsopoulos, O.S., Okamoto, K., and Ryan, M.T. (2004). Levels of human Fis1 at the mitochondrial outer membrane regulate mitochondrial morphology. *Journal of cell science* 117, 1201-1210.
- Taguchi, N., Ishihara, N., Jofuku, A., Oka, T., and Mihara, K. (2007). Mitotic phosphorylation of dynamin-related GTPase Drp1 participates in mitochondrial fission. *The Journal of biological chemistry* 282, 11521-11529.
- Tieu, Q., and Nunnari, J. (2000). Mdv1p is a WD repeat protein that interacts with the dynamin-related GTPase, Dnm1p, to trigger mitochondrial division. *The Journal of cell biology* 151, 353-366.

Tieu, Q., Okreglak, V., Naylor, K., and Nunnari, J. (2002). The WD repeat protein, Mdv1p, functions as a molecular adaptor by interacting with Dnm1p and Fis1p during mitochondrial fission. *The Journal of cell biology* 158, 445-452.

Westermann, B. (2010). Mitochondrial fusion and fission in cell life and death. *Nature reviews Molecular cell biology* 11, 872-884.

Yoon, Y., Krueger, E.W., Oswald, B.J., and McNiven, M.A. (2003). The mitochondrial protein hFis1 regulates mitochondrial fission in mammalian cells through an interaction with the dynamin-like protein DLP1. *Molecular and cellular biology* 23, 5409-5420.

Youle, R.J., and van der Bliek, A.M. (2012). Mitochondrial fission, fusion, and stress. *Science* 337, 1062-1065.

Yu, T., Fox, R.J., Burwell, L.S., and Yoon, Y. (2005). Regulation of mitochondrial fission and apoptosis by the mitochondrial outer membrane protein hFis1. *Journal of cell science* 118, 4141-4151.

Zhao, J., Liu, T., Jin, S., Wang, X., Qu, M., Uhlen, P., Tomilin, N., Shupliakov, O., Lendahl, U., and Nister, M. (2011). Human MIEF1 recruits Drp1 to mitochondrial outer membranes and promotes mitochondrial fusion rather than fission. *The EMBO journal* 30, 2762-2778.

CHAPTER 3

The mitochondrial fission receptor MiD51 requires ADP as a co-factor

Oliver C. Losón¹, Raymond Liu¹, Michael E. Rome^{1,2}, Shuxia Meng^{1,3}

Jens T. Kaiser², Shu-ou Shan², and David C. Chan^{1,3}

¹From the Division of Biology and Biological Engineering

²Division of Chemistry and Chemical Engineering

³Howard Hughes Medical Institute

California Institute of Technology

Pasadena, CA 91125

This chapter was published in *Structure*.

ABSTRACT

Mitochondrial fission requires recruitment of dynamin-related protein 1 (Drp1) to the mitochondrial surface and activation of its GTP-dependent scission function. The Drp1 receptors MiD49 and MiD51 recruit Drp1 to facilitate mitochondrial fission, but their mechanism of action is poorly understood. Using X-ray crystallography, we demonstrate that MiD51 contains a nucleotidyl transferase domain that binds ADP with high affinity. MiD51 recruits Drp1 via a surface loop that functions independently of ADP binding. However, in the absence of nucleotide binding, the recruited Drp1 cannot be activated for fission. Purified MiD51 strongly inhibits Drp1 assembly and GTP hydrolysis in the absence of ADP. Addition of ADP relieves this inhibition and promotes Drp1 assembly into spirals with enhanced GTP hydrolysis. Our results reveal ADP as an essential co-factor for MiD51 during mitochondrial fission.

INTRODUCTION

Mitochondrial dynamics requires a balance between the opposing processes of fusion and fission and serves to protect mitochondrial function (Chan, 2012; Westermann, 2010; Youle and van der Bliek, 2012). Disruption of either process causes mid-gestational lethality in mice and neurological disease in humans (Chen et al., 2003; Ishihara et al., 2009; Wakabayashi et al., 2009).

Drp1, a dynamin-related GTPase, is the central player in mitochondrial fission (Bleazard et al., 1999; Labrousse et al., 1999; Sesaki and Jensen, 1999; Smirnova et al., 2001). A pool of Drp1 exists in the cytosol and can be recruited to the surface of mitochondria, where it assembles into highly ordered structures that wrap around mitochondrial tubules. Assembly of Drp1 increases its GTP hydrolysis activity, leading to conformational changes that mediate constriction and scission of the mitochondrial tubule (Ingeman et al., 2005; Mears et al., 2011). In mammals, four proteins on the mitochondrial outer membrane act as Drp1 receptors—Fis1, Mff, MiD49, and MiD51 (Gandre-Babbe and van der Bliek, 2008; Palmer et al., 2011; Stojanovski et al., 2004; Yoon et al., 2003; Zhao et al., 2011). Overexpression of Mff causes mitochondrial fragmentation (Otera et al., 2010), and depletion of Mff causes mitochondrial elongation (Gandre-Babbe and van der Bliek, 2008). Fis1 behaves similarly, but the degree of mitochondrial elongation upon depletion depends on the study (Losón et al., 2013; Otera et al., 2010; Yoon et al., 2003; Yu et al., 2005).

MiD49 and MiD51 appear to operate in a more regulated manner. As Drp1 receptors, overexpression of either causes increased recruitment of Drp1 to the

mitochondrial surface. Paradoxically, this increased recruitment is not normally accompanied by increased fission rates. The mitochondria instead dramatically elongate, indicating inhibition of the recruited Drp1 (Liu et al., 2013; Palmer et al., 2013; Palmer et al., 2011; Zhao et al., 2011). Treatment of such cells with CCCP causes rapid activation of fission and mitochondrial fragmentation, with a greater effect on MiD51 than on MiD49 (Losón et al., 2013).

To address the structural biology of MiD51 function, we used X-ray crystallography to solve the atomic structure of the cytosolic domain of MiD51. Structural and biophysical analyses indicate that MiD51 contains a variant nucleotidyl transferase fold that binds ADP with high affinity. Although ADP binding is dispensable for Drp1 recruitment, it is essential for activation of Drp1 *in vitro* and *in vivo*. These results identify ADP as an essential co-factor for MiD51 function.

RESULTS

MiD51 has a nucleotidyl transferase domain that binds ADP

Like other Drp1 receptors on mitochondria, MiD51 is an integral outer membrane protein, with most of the protein exposed to the cytosol. Initial attempts to crystallize the entire cytoplasmic portion of mouse MiD51 failed to yield promising hits. Secondary structure prediction indicated that the membrane-proximal region is likely to be disordered (Fig. 3.1A). Limited trypsin proteolysis of the cytosolic domain produced a stable product (Fig. S3.1A). N-terminal peptide sequencing combined with mass spectrometry revealed that proteolysis removed almost all the predicted unstructured region, with the C-terminus of MiD51 remaining intact (Fig. S3.1B). Using a recombinant form of this shorter polypeptide (MiD51 Δ 1-133), we readily obtained crystals that diffract to high resolution and solved the structure by multi-wavelength anomalous diffraction (MAD) analysis (Table S2.1) of a selenomethionine-substituted crystal. The native structure was solved at a resolution of 2.2 Å (Table S2.1 and Fig. 3.1B). Model building and refinement produced a final structure with excellent stereochemistry, with an R_{free} of 27.4% and an R_{work} of 21.9%.

MiD51 Δ 1-133 has a compact, globular structure consisting of two α -helical regions separated by a central β -strand region (Fig. 3.1B). To find structurally related proteins, we used the DALI server to search the MiD51 structure against structures deposited in the Protein Data Bank. Proteins belonging to the nucleotidyl transferase (NTase) family had the highest Z-scores. Cyclic GMP-AMP synthase (PDB 4K99; (Gao et al., 2013)) showed the greatest similarity,

with a Z-score of 27.7 and a root-mean-square deviation (RMSD) of 2.4 Å for backbone atoms (Fig. 3.1C). NTase proteins typically catalyze the polymerization of nucleic acids from triphosphate nucleotides. They bind nucleotide triphosphates in the cleft located between the central β -sheet and the C-terminal α -helical segment (Kristiansen et al., 2011). Intriguingly, the corresponding region of MiD51 Δ 1-133 contained additional electron density, suggesting partial occupancy by a ligand (see Experimental Procedures). Structural alignments show that residues canonically used for nucleotide binding are partially conserved in MiD51. These same residues are more divergent in MiD49 (Fig. S3.1C).

To identify potential MiD51 ligands, we used a fluorescence-based thermal shift assay to screen a broad panel of nucleotides (Fig. S3.2A-D). Contrary to what would be expected for a canonical NTase, MiD51 Δ 1-133 shows no stabilization when incubated with NTPs, except for a modest stabilization with ATP. Instead, MiD51 Δ 1-133 shows substantial stabilization with ADP (4-6 degrees) and modest stabilization with GDP. No potential ligands were identified for MiD49 (Fig. S3.2E).

Because MiD51 showed the greatest stabilization with ADP, we performed crystallization trials in the presence of ADP and determined the structure of MiD51 Δ 1-133 bound to ADP at a resolution of 2.0 Å (Table S2.1; Fig. 3.2A, B). NTases use a triad of negatively charged residues (either Asp or Glu) from the central β -sheet to coordinate two Mg^{2+} ions that buffer the negative charges of the α and β phosphate groups of NTPs (Kristiansen et al., 2011). Our structure

revealed that MiD51 uses a related triad of residues (H201, Q203 and D311) in the central β -sheet, but two of these residues (H201 and Q203) directly contact ADP and do not coordinate Mg^{2+} . H201 forms a hydrogen bond with the β phosphate group of ADP, and Q203 has hydrophobic interactions with carbons in the ribose and base rings (Fig. 3.2B). Like other NTases, a serine (S189) from the N-terminal domain and a lysine (K368) from the C-terminal domain help to coordinate the negative charge from the phosphate groups of the nucleotide. Specifically, S189 forms hydrogen bonds with both the α and β phosphates of ADP, and K368 forms a salt bridge with the β phosphate.

To measure the binding affinities of MiD51 to nucleotides, we monitored changes in the fluorescence anisotropy of 2'/3'-O-(N-Methyl-anthraniloyl) (MANT) labeled nucleotides upon incubation with MiD51 (Rome et al., 2013). MiD51 has the highest affinity for ADP (K_d of $0.5 \mu M \pm 0.008$). We found no detectable binding to ATP, despite its ability to modestly stabilize MiD51 in the thermal shift assay. MiD51 binds guanine-based nucleotides more weakly, but still exhibits a strong preference for GDP ($K_d = 8 \mu M \pm 0.9$) relative to GTP (not detectable) (Fig. 3.2C). Binding to ADP does not require Mg^{2+} . Mutation of the residues structurally implicated in nucleotide binding (H201, S189, and K368) greatly reduces the affinity of MiD51 for ADP. Mutations H201A and S189A abolish nearly all nucleotide binding, whereas K368A ($K_d = 2.6 \mu M \pm 0.4$) causes a 5-fold reduction (Fig. 3.2D). Taken together, these results show that MiD51 has a nucleotidyl transferase domain but differs substantially from other proteins with this motif. It uses a variant set of nucleotide binding residues to directly contact

ADP rather than using a Mg^{2+} co-factor to bind a nucleotide triphosphate. MiD49 does not bind ADP (Fig. 3.2D), and we have not identified an alternative ligand. With MiD51, we have not detected nucleotide transfer reactions with ATP or GTP (data not shown), suggesting that although MiD51 has an NTase fold, it may not possess enzymatic activity.

MiD51 forms a dimer through electrostatic interactions in the N-terminal α -helical segment

MiD51 Δ 1-133 crystallizes as a dimer (Fig. 3.3) using the N-terminal α -helical segments from two monomers as an interaction interface. The interface is largely composed of electrostatic interactions between charged residues from a loop, and the interface has a buried surface area of 1184.1 \AA^2 (Fig. 3.3B). Additionally, the guanidinium groups from a pair of Arg169 residues from α -helix number 2 adopt a planar stacking conformation (Neves et al., 2012), and their interaction is bridged through hydrogen bonds with a sulfate group. The interaction surface of MiD51 is distinct from that of other NTase family members known to dimerize. To determine the biological relevance of this interface, we designed a series of mutants to disrupt the dimer interface and tested their ability to self-associate in a co-immunoprecipitation assay (Fig. 3.3C). Compared to wildtype MiD51, several mutants showed a moderately reduced ability to self-associate. A mutant (hereafter refer to as the "compound dimer mutant") combining 5 substitutions in the dimer interface showed a severe ablation of self-association.

MiD51 does not undergo a significant structural change upon ADP binding or dimerization

Interestingly, the structures of MiD51 in its apo form (crystallized without added ADP) and in the ADP complex are identical (Fig. S3.3A). This observation suggests that MiD51 does not undergo a conformational change upon ADP binding. However, this interpretation is complicated by the possibility of low levels of ADP being present in our apo MiD51 crystals. To address this issue, we crystallized the MiD51 H201A mutant, which is incapable of nucleotide binding. Upon structure determination, we found that the H201A mutant has no significant structural changes compared to the ADP-bound form of MiD51 (Fig. S3.3B, D). Importantly, the H201A mutant had no apparent electron density in the putative nucleotide-binding pocket. These results indicate that although ADP stabilizes MiD51, it does not induce a conformational change. Moreover, we solved the structure of the compound dimer mutant (Fig. S3.3C) and found that this monomer is identical to the monomers within the dimeric structures of wildtype MiD51 and H201A (Fig. S3.3D).

Identification of a surface loop necessary for Drp1 binding

We tested whether ADP binding or dimerization of MiD51 is necessary for its recruitment of Drp1 to mitochondria. MiD51 mutants defective for either function are fully active in recruiting Drp1 puncta to the mitochondria (Fig. S3.4A). Furthermore, the MiD51 mutants co-immunoprecipitated with Drp1 from

cells as efficiently as wildtype (Fig. S3.4B). These results clearly indicate that Drp1 binding is independent of ADP binding or dimer formation.

To determine the Drp1 binding surface on MiD51, we designed 16 mutants, each containing a cluster of 3-4 point mutations, to systematically sample the solvent-exposed surface of MiD51 (Fig. S3.4C, D). As assessed by yeast two-hybrid analysis, mutants 6 and 8 show nearly complete loss of Drp1 binding, and mutant 7 shows substantially reduced binding (Fig. 3.4A). Remarkably, all three clusters converge onto a single exposed loop on the top surface of MiD51 (green residues, Fig. 3.4B). The residues within this loop are well-conserved between MiD51 and MiD49 (Fig. S3.1C, D). We expressed mutants 6 and 7 in 293T cells and found that neither can co-immunoprecipitate Drp1 (Fig. 3.4C). Mutant 6, but not 7, shows reduced expression. Furthermore, these mutants are defective in recruiting Drp1 puncta to mitochondria, even though they localize properly to mitochondria (Fig. 3.4D).

Inhibition of respiration stimulates mitochondrial fission by MiD51

Cells over-expressing MiD51 have severely elongated and interconnected mitochondria (Palmer et al., 2011; Zhao et al., 2011). We previously showed that over-expressed MiD51 recruits Drp1 to the mitochondrial outer membrane in an inactive form (Losón et al., 2013). Treatment of MiD51 over-expressing cells with carbonyl cyanide 3-chlorophenylhydrazone (CCCP, a proton ionophore that dissipates the mitochondrial membrane potential) activates the recruited Drp1

and promotes rapid mitochondrial fragmentation independently of Fis1 or Mff (Losón et al., 2013).

We found that treatment with antimycin A (an inhibitor of complex III of the electron transport chain) also induces rapid mitochondrial fission in MiD51 over-expressing cells (Fig. 3.5A, B). This fragmentation occurs independently of Fis1 and Mff, because it occurs in mouse embryonic fibroblasts (MEFs) deleted for Fis1 and Mff (Fig. 3.5C, D). Mitochondrial fragmentation induced by antimycin A is specific to MiD51-expressing cells and does not occur with MiD49-expressing cells (Fig. 3.5B). CCCP treatment causes enhanced processing of OPA1 (Ishihara et al., 2006), but antimycin A treatment does not (Fig. S3.5D).

These observations allowed us to use CCCP or antimycin A treatment to assess the mitochondrial fission activity of MiD51 mutants. When expressed in MEFs, MiD51 mutants defective in ADP binding or dimerization promote Drp1 recruitment (Fig. S3.4A, B) and robust elongation of mitochondria (Fig. S3.5A-C). However, upon addition of CCCP or antimycin A, all the nucleotide-binding mutants show little or no stimulation of mitochondrial fission. For the dimerization mutants, the fission defects correlate well with the dimerization defect. The Q212A/N213A mutant, which has normal dimerization, stimulates fission as well as wildtype. The compound dimer mutant has the most severe fission defect amongst the dimer mutants, and the rest have intermediate defects. Taken together, these results indicate that MiD51 mitochondrial fission activity, but not Drp1 recruitment, requires ADP binding and dimerization.

ADP binding to MiD51 stimulates Drp1 oligomerization

Like dynamin (Ferguson and De Camilli, 2012; Schmid and Frolov, 2011), Drp1 and its yeast homolog dynamin 1 (Dnm1) polymerize into ordered oligomers (Frohlich et al., 2013; Ingerman et al., 2005; Mears et al., 2011) that have enhanced GTP hydrolysis activity. To test whether MiD49 or MiD51 can regulate Drp1 oligomerization, we performed sedimentation experiments using recombinant Drp1 and either recombinant MiD49 or MiD51. In the absence of ADP, both MiD49 Δ 1-124 and MiD51 Δ 1-133 moderately stimulate Drp1 sedimentation in the presence of GTP γ S (a non-hydrolysable form of GTP). Remarkably, MiD51 Δ 1-133, but not MiD49 Δ 1-124, further stimulates Drp1 sedimentation upon addition of ADP (Fig. 3.6A). In contrast, the MiD51 nucleotide-binding mutant S189A is incapable of enhancing Drp1 sedimentation upon addition of ADP. The compound dimer mutant also does not promote any sedimentation of Drp1 in the presence of ADP (Fig. 3.6B). These results demonstrate that both MiD49 and MiD51 can basally promote Drp1 oligomerization. This function of MiD51 requires dimerization and is enhanced by ADP binding.

Binding of ADP to MiD51 stimulates assembly of Drp1 tubules and GTP hydrolysis

We used negative stain transmission electron microscopy to examine the effects of MiD51 on Drp1 oligomeric structures at high resolution. In the presence of GTP γ S, recombinant Drp1 forms tubules with a repeating spiral pattern (Fig.

3.7A). Interestingly, in samples incubated with MiD51 in the absence of ADP, these tubules are replaced with short, ring-like structures (Fig. 3.7B). In the presence of both MiD51 and ADP, Drp1 forms spiral tubules that are slightly wider than those formed from Drp1 alone. The nucleotide-binding mutant S189A is completely defective in stimulation of tubule formation by ADP. Moreover, the compound dimerization mutant prevents any Drp1 assembly with or without ADP (Fig. 3.7B). Our ultrastructural analysis demonstrates that MiD51 without ADP inhibits formation of Drp1 tubules and promotes a different form of Drp1 assembly. ADP relieves this inhibition and stimulates Drp1 tubule formation in a dimerization-dependent manner.

We further determined how the structural states of Drp1 correlate with its GTP hydrolysis activity (Fig. 3.7C). Under physiological salt concentration and saturating GTP (1 mM), recombinant Drp1 hydrolyzes approximately 1.5 molecules of GTP per minute. Like other dynamins (Praefcke and McMahon, 2004), mutation of a putative catalytic threonine (T59) abolishes GTP hydrolysis (Fig. 3.7C). Incubation of Drp1 with MiD51 Δ 1-133 causes a dramatic suppression of GTP hydrolysis. Remarkably, addition of ADP to the reaction relieves this inhibition, resulting in a 20-fold stimulation of Drp1 GTP hydrolysis between the ADP-free and the ADP-containing reactions. The S189A and compound dimer mutants similarly inhibited GTP hydrolysis in the absence of ADP, but addition of ADP had no stimulatory effect. Analogously, MiD49 Δ 1-124 inhibited the GTPase activity of Drp1 and did not respond to ADP. Thus, both apo-MiD49 and apo-

MiD51 inhibit the GTPase activity of Drp1, but in the case of MiD51, ADP binding relieves this inhibition and promotes GTP hydrolysis.

DISCUSSION

Our results indicate that MiD51 has a variant nucleotidyl transferase domain that binds ADP instead of a nucleotide triphosphate. A previous bioinformatics study using sensitive protein fold recognition algorithms greatly expanded the number of putative nucleotidyl transferase family members, suggesting that this family may have diverse functions in the cell. This study also suggested that MiD49 and MiD51 may be distant members of the NTase family (Kuchta et al., 2009). Our results raise the possibility that some non-canonical members of the NTase family may not catalyze nucleotide transfer, but instead use metabolites as co-factors. Based on their sequence similarity, MiD49 is expected to be structurally similar to MiD51. MiD49 has also been shown to stimulate Drp1 assembly (Koirala et al., 2013). However, it does not bind ADP and shows only partial conservation in the key residues used by MiD51 for nucleotide binding (Fig. S3.1C). In future studies, it will be important to determine whether MiD49 indeed binds another co-factor.

Our results identify ADP as an essential co-factor for MiD51. In the absence of ADP binding, MiD51 can still recruit Drp1 via a binding loop that we have identified by mutational analysis. In dimeric MiD51, the adjacent binding loops form an extended interface on the top surface, which would be expected to protrude furthest from the mitochondrial outer membrane (Figure 3.3A). However, when expressed in cultured cells, nucleotide-binding mutants of MiD51 are unable to activate mitochondrial fission. *In vitro*, apo-MiD51 strongly suppresses the assembly of Drp1 into spirals and its GTP hydrolysis activity.

Upon addition of ADP, this suppression is relieved. Drp1 spirals are tailored to the diameter of mitochondrial tubules and are thought to wrap around mitochondria to mediate constriction (Ingelman et al., 2005). Drp1 spirals also have enhanced GTP hydrolysis, which is critical for mitochondrial fission (Mears et al., 2011).

Rather than inducing a conformational change, ADP appears to act as a structural co-factor that stabilizes the folding of MiD51. Our results favor a model in which ADP binding is necessary to stabilize MiD51 so that Drp1 can assemble properly. Dimerization of MiD51 is also necessary for mitochondrial fission, and further work will be necessary to understand whether there is a relationship between ADP binding and dimerization. Because of the unexpected role for ADP, it will also be interesting to explore the possibility that cellular metabolism can impact MiD51 function.

EXPERIMENTAL PROCEDURES

Materials

Antibody sources: Drp1 (BD Biosciences), Tom20 (Santa Cruz), MiD51 (also known as SMCR7L; Thermo Pierce), Actin (Millipore), Myc (mouse monoclonal 9E10 from Covance, and rabbit polyclonal from Sigma-Aldrich), OPA1 (in-house mouse monoclonal). CCCP (Sigma-Aldrich) was used at 50 μ M. Antimycin A (Sigma-Aldrich) was used at 10 μ M in cell culture experiments. Cells were grown in LabTek chambered glass slides (Nunc) for fixed cell imaging. Dithiobis(succinimidyl propionate) (DSP) was purchased from Thermo-Pierce. MANT labeled nucleotides were from Jena Biosciences.

Recombinant protein production, purification and crystallization

Recombinant mouse MiD49 Δ 1-51, MiD49 Δ 1-124, MiD51 Δ 1-48, MiD51 Δ 1-133, and Drp1 variant 2 were produced in Rosetta (DE3) BL21 *E. coli* (Invitrogen). In a typical purification, one liter of terrific broth containing 100 μ g/mL ampicillin and 50 μ g/mL chloramphenicol was grown at 37°C to an OD₆₀₀ of 1.5. Cultures were cooled on ice for 30 minutes and induced with 1 mM isopropyl β -D-1-thiogalactopyranoside (IPTG) overnight at 16°C. The cells were harvested and stored at -80°C. 10 grams of cells expressing MiD proteins were lysed in 50 mL GST buffer (50 mM HEPES, 300 mM NaCl, 10% glycerol, 2 mM DTT, pH 7.4) using sonication. 10 grams of cells expressing Drp1 were lysed in 50 mL Hisx6 buffer (50 mM KH₂PO₄, 300 mM NaCl, 5 mM imidazole, 10% glycerol, pH 8.0) using sonication. Lysates were cleared by centrifugation at

43,000 *g* for 30 mins at 4°C. GST tagged MiD49 and MiD51 proteins were captured with glutathione sepharose (GE Healthcare) and washed with GST buffer. Hisx6 tagged Drp1 was captured with Ni-NTA sepharose (Qiagen) and washed with Hisx6 wash buffer (20 mM Tris, 300 mM NaCl, 40 mM imidazole, 10% sucrose, 10% glycerol, pH 8.0). Beads for MiD49 and MiD51 protein purification were exchanged into protease buffer (50 mM HEPES, 150 mM NaCl, 2 mM DTT, pH 7.4). PreScission Protease (80 units, GE Healthcare) was incubated for 20 hours at 4°C with continuous end-over-end mixing. The eluted protein was further purified by size exclusion on a Hi-Load Superdex 200 16/60 column (GE Healthcare) pre-equilibrated with GST column buffer (50 mM HEPES, 150 mM NaCl, 2 mM DTT, pH 7.4) and driven by an AKTA Purifier (Amersham). Eluted Drp1 protein was further purified by size exclusion on a Hi-load Superdex 200 16/60 column pre-equilibrated with Hisx6 column buffer (10 mM Tris, 100 mM NaCl, 2 mM DTT, 1 mM EDTA, pH 8.0) and driven by an AKTA Purifier. Drp1 protein was additionally purified by binding to a Hi-Load HiTrapQ column (GE Healthcare) pre-equilibrated with Hisx6 column buffer and driven by an AKTA Purifier. The protein was then eluted with a NaCl gradient. Peak fractions were collected and concentrated to approximately 1 mM for MiD49 and MiD51 proteins and 0.5 mM for Drp1 proteins using Amicon Ultra-15 concentrators (Millipore) with a molecular weight cutoff of 30 kDa. Proteins were flash-frozen in liquid nitrogen and stored at -80°C.

Selenomethionine-labeled MiD51 Δ 1-133 was produced by growing cells in M9 minimal media at 37°C to OD₆₀₀ of 1.0, then incubating with amino acids (lysine,

phenylalanine, threonine at 100 mg/L; isoleucine, leucine, valine at 50 mg/L; selenomethionine at 60 mg/L) for 15 minutes, cooling cells on ice for 30 mins and finally inducing with 1 mM IPTG overnight at 16°C. Protein purification was carried out as above.

Limited proteolysis of MiD51Δ1-48 was performed with 1 μg/μL recombinant protein and 0.001 μg/μL trypsin (Promega) at 4°C. Time points were taken by diluting aliquots in Laemmli buffer (25 mM Tris, 10% glycerol, 1% SDS, 0.01% Bromophenol Blue, 2% β-mercaptoethanol, pH 6.8) and boiling samples immediately.

Crystallization, data collection and structure determination

Crystallization trials by hanging drop-vapor diffusion at room temperature identified a condition [100 mM HEPES (pH 7.0), 200 mM LiSO₄, 20% PEG 3,350 (w/v),] that yielded rod-shaped crystals for wildtype, selenomethionine-substituted, and H201A mutant proteins. The compound dimer mutant crystallized in a differential condition [200 mM NaH₂PO₄, 20% PEG 3,350 (w/v)]. Diffraction data were collected from vitrified crystals on beamline 12-2 at the Stanford Synchrotron Radiation Lightsource. All data were processed with XDS (Kabsch, 2010), and merged using SCALA (Evans, 2006) as implemented in CCP4 (Bailey, 1994). Selenomethionine-substituted MiD51Δ1-133 was used for phasing. Using intensity data at 2.6 Å from three wavelengths, all four selenium sites were located by PHENIX (Adams et al., 2002). After solvent flattening and density modification in PHENIX, the map revealed clear density for the protein.

Manual model building in COOT (Emsley and Cowtan, 2004) using the 2.6 Å experimental map generated a starting model. Refinement was carried out using PHENIX, with an initial round of rigid body refinement followed by a round of simulated annealing. The selenomethionine-substituted crystal is non-isomorphous to the native crystal. However, molecular replacement in PHENIX with the 2.2 Å native data set produced an excellent map, and refinement produced density for most of the side chains. After a few rounds of manual model building and refinement with TLS obtained from the TLSMD server (Painter and Merritt, 2006), the R_{work} converged to 21.9% and the R_{free} to 27.4% for the apo structure. For the ADP bound structure, R_{work} was 17.8% and R_{free} was 22.5%. R_{work} was 17.7% and R_{free} was 21.9% for the H201A mutant structure, and R_{work} was 17.7% and R_{free} was 21.8% for the compound dimer mutant structure. After refinement of the native model, significant density was present in the binding cleft. ADP was fitted into this density, and the final model and refinement statistics were produced with ADP in the binding cleft. With the exception of a stretch of 3 prolines (residues 290-291), the final models include residues 134–463 of MiD51 and have excellent stereochemistry with no/few Ramachandran outliers, as assessed by MOLPROBITY (Davis et al., 2007). To determine the structure of the MiD51-ADP complex, MiD51 Δ 1-133 was mixed with 10 mM ADP and 5 mM MgCl₂, and incubated on ice for 1 hour before setting crystallization trials. Molecular replacement in PHENIX for a 2.0 Å MiD51-ADP complex data set produced an excellent map, and refinement produced clear density for the nucleoside and phosphate groups of ADP.

Fluorescence anisotropy and determination of K_d values

Fluorescence measurements were performed using a Fluorolog-3–22 spectrofluorometer (Jobin Yvon) at 25°C (50 mM HEPES, 150 mM NaCl, 10 mM MgCl₂, 2 mM DTT, pH 7.5). Samples were excited at 355 nm, and fluorescence emission was monitored at 448 nm. For titrations, MANT-nucleotide was held constant at 300 nM and the protein concentration was varied as indicated. To determine K_d values, observed anisotropy values (A_{obsd}) were plotted as a function of MiD concentration and fit to Eq. 1,

$$A = A_0 + (A_1 - A_0) \left\{ \frac{c_0 + [\text{MiD}]_{\text{max}/2} + K_d - \sqrt{(c_0 + [\text{MiD}]_{\text{max}/2} + K_d)^2 - 4c_0[\text{MiD}]_{\text{max}/2}}{2c_0} \right\} \quad [1]$$

in which A_0 is the anisotropy value of free MANT-nucleotide, A_1 is the anisotropy when MANT-nucleotide is bound to protein, c_0 is the concentration of total MANT-nucleotide, and K_d is the equilibrium dissociation constant of MiD for MANT-nucleotide.

Immunofluorescence and imaging

For immunofluorescence, cells were fixed in 4% formaldehyde for 10 min at 37°C, permeabilized with 0.1% Triton-X100 at room temperature, and incubated with antibodies in 5% fetal calf serum in phosphate buffered saline. Bound antibody was visualized with Alex Fluor conjugated secondary antibodies (Life Technologies). Scoring of mitochondrial network morphology was performed

blind to genotype and treatment. All quantifications were done in triplicate, and 100 cells were scored per experiment.

All fluorescence imaging was performed using a Plan-Apochromat 63X/1.4 oil objective on a Zeiss LSM 710 confocal microscope driven by Zen 2009 software (Carl Zeiss). Image cropping and global adjustments to brightness and contrast were performed using Photoshop (Adobe).

Cell culture

All cell lines were cultured in Dulbecco's modified Eagle's medium (DMEM) containing 10% FBS and supplemented with 100 U/mL penicillin and 100 μ g/mL streptomycin. Treatment with 50 μ M CCCP occurred for 1 hour, and treatment with 10 μ M Antimycin A occurred for 2 hours.

Cloning and transfection

MiD49, *MiD51*, and *Drp1* variant 2 transcripts were amplified from a MEF cDNA library using PCR. *MiD49* and *MiD51* were cloned into the XhoI and BamHI sites of a pcDNA3.1(-) plasmid containing a C-terminal 4xMyc tag and were also cloned into the XhoI and BamHI sites of pEGFP-N2 (Invitrogen) for C-terminal GFP tagging. For the generation of an MiD51-Myc constitutively expressing cell line, *MiD51* was cloned into the NotI and EcoRI sites of the retroviral vector pQCXIP (Invitrogen). The entire open reading frames were confirmed by DNA sequencing. For recombinant protein expression in bacteria, mouse MiD49 Δ 1-51, MiD49 Δ 1-124, MiD51 Δ 1-48, and MiD51 Δ 1-133 were cloned

into the BamHI and XhoI sites of plasmid pGEX6P1 (GE Healthcare). Mouse *Drp1* variant 2 was cloned into the NdeI and BamHI sites of a modified pET21b vector (Novagen). All mutants for MiD51 and Drp1 were constructed by PCR using oligonucleotides encoding mutations.

Plasmids were transfected using Lipofectamine 2000 (Invitrogen). Cells transfected with plasmids were assessed 24 hours post transfection. MiD49/51-Myc positive cells were visualized with Myc immunofluorescence, and mitochondria were visualized with Tom20 immunofluorescence.

Immunoprecipitation

To assess MiD51 dimerization or MiD51 interaction with Drp1, mouse MiD51-Myc was co-transfected with either mouse MiD51-GFP or mouse Drp1 into 293T cells growing in 35 mm plates. 24 hours post-transfection, cells were trypsinized, washed once with PBS, and crosslinked with 250 μ M DSP in PBS for 20 minutes at room temperature. Crosslinker was quenched by the addition of Tris pH 7.4 to 100 mM final, and cells were washed once with PBS containing 100 mM Tris pH 7.4. Cells were lysed in IP buffer (1% Triton X100, 150 mM NaCl, 25 mM Tris-HCl, 1 mM EDTA, pH 7.4) and lysates were cleared with a 21,000 *g* spin at 4°C for 10 minutes. Immunoprecipitations were performed in IP buffer, and immune complexes were captured with protein A/G agarose (Thermo-Pierce). Beads were washed with IP buffer, and crosslinker reversed by boiling samples in Laemmli buffer containing 5% β -mercaptoethanol.

Drp1 sedimentation assay

5 μ M Drp1 was incubated in sedimentation assay buffer (10 mM HEPES, 110 mM NaCl, 2 mM MgCl₂, 1 mM GTP γ S, pH 7.0) for 30 minutes at 25°C. Where indicated, MiD49 or MiD51 protein was added to 10 μ M and ADP to 100 μ M. The reactions were centrifuged at 100,000 g (TLA100.3 rotor) in a Beckman Optima MAX Ultracentrifuge for 20 minutes at 4°C. Supernatants were removed, and pellet fractions were resuspended in an equal volume of buffer. Supernatant and pellet fractions were resolved on gradient (4-20%) SDS/PAGE gels and stained with Coomassie Brilliant Blue dye.

GTPase assay

All reactions were performed in GTPase assay buffer (10 mM HEPES, 150 mM NaCl, 2 mM MgCl₂, 1 mM GTP, pH 7.0) at 37°C with 50 nM [γ -³²P]-GTP (MP Biomedicals). Drp1 proteins were used at 3 μ M, and MiD49 and MiD51 proteins were used at 15 μ M. Where indicated, ADP was added to 100 μ M. Reactions were quenched in 0.75 M potassium phosphate (pH 3.3), resolved by polyethylenimine cellulose thin layer chromatography in 1 M formic acid/ 0.5 M LiCl, and quantified by autoradiography. Initial rates were derived from a linear fit to the initial stage of reactions, in which <40% [γ -³²P]-GTP had been hydrolyzed.

Electron microscopy

For negative-stain EM, carbon-coated copper grids were glow discharged for 60 seconds. 3 μ L of sample was added to the surface, blotted, and stained

with 2% uranyl acetate. Images were acquired using an FEI Tecnai T12 electron microscope equipped with a LaB6 filament and operated at 120 kV. Magnifications of 15,000 and 42,000x were recorded on a Gatan CCD. Samples for EM were prepared by incubating 2.5 μ M Drp1 alone or with 12.5 μ M MiD51 in reaction buffer (10 mM HEPES, 150 mM NaCl, 2 mM MgCl₂, 1 mM GTP γ S, pH 7.0) for 2 hours at 25°C. Where indicated, ADP was added to 100 μ M. Samples were diluted 5-fold in reaction buffer before application to grids.

Thermal shift assay

Sypro Orange (Sigma-Aldrich) was used at 1x to report protein unfolding. Fluorescence measurements were taken in a Bio-Rad CFX96 thermal cycler using the FRET mode and performed in assay buffer (50 mM HEPES, 150 mM NaCl, 1 mM DTT, 2 mM MgCl₂, pH 7.5). MiD49 Δ 1-51 and MiD51 Δ 1-133 were used at 1 μ M.

ACKNOWLEDGEMENTS

We are grateful to Meera Rao for assistance with the GTPase assay, and Alasdair McDowell for guidance with electron microscopy. We thank the Beckman Foundation at Caltech for support of the EM resource, and the Gordon and Betty Moore Foundation and Augoron Institute for support of the Grant Jensen lab microscopy center. We acknowledge the Gordon and Betty Moore Foundation, the Beckman Institute, and the Sanofi-Aventis Bioengineering Research Program at Caltech for their generous support of the Molecular Observatory at Caltech. Operations at SSRL are supported by the US DOE and NIH. This work was supported by the National Institutes of Health (GM062967). OCL was supported by a R. L. Kirschstein National Research Service Award (5F31GM089327) and an American Physiological Society William Townsend Porter Pre-doctoral fellowship.

FIGURE LEGENDS

Figure 3.1. The cytosolic region of MiD51 has a nucleotidyl transferase domain. (A) Schematic of MiD51. The region determined by X-ray crystallography is indicated and color-coded as in (B). The red squiggle indicates a region predicted to have low probability of regular secondary structure. Boxes highlight residues important for nucleotide binding and the dimer interface. TMD, transmembrane domain. Cylinders, α -helical segments; triangles, strand segments. α -helices and β -strands from the crystallized segment are numbered. (B) Ribbon representation of mouse MiD51 Δ 1-133. Orange, N-terminal domain; gray, inter-domain linker; blue, C-terminal domain. α -helices and strands are numbered according to (A). Dashed lines denote residues missing from the model. N and C denote the N and C termini. The circle indicates the predicted nucleotide-binding pocket. (C) Structural overlay of MiD51 (colored as in panel B) and cyclic GMP-AMP synthase (cGAS) (green).

Figure 3.2. MiD51 binds ADP with high affinity. (A) Ribbon representation of mouse MiD51 Δ 1-133 bound to ADP. (B) Details of the nucleotide-binding pocket. The 2 Fo-Fc map for ADP (red) is contoured at 1.2 σ . Key residues are depicted, and interactions with the ADP are denoted with black dashed lines. (C) Binding of MiD51 to ADP. Equilibrium titrations were performed with MANT-labeled nucleotides to determine the affinity of MiD51 Δ 1-133 for MANT-ATP (no binding), MANT-GTP (no binding), MANT-ADP ($K_d=0.5 \mu\text{M} \pm 0.008$), and MANT-GDP ($8.0 \mu\text{M} \pm 0.9$). (D) Mutational analysis of residues structurally implicated in ADP

binding. Note that MiD51 S189A, H201A, and MiD49 do not bind MANT-ADP. MiD51 K368A has a K_d of $2.6 \mu\text{M} \pm 0.4$.

Figure 3.3. MiD51 forms a dimer through electrostatic interactions. (A) MiD51 Δ 1-133 crystallizes as a dimer through an interface found in the N-terminal domain. The two molecules are differentially colored gray (left) and as in Fig. 3.1B (right). In the bottom figure, the dimer has been rotated to view the interface from the top. The right panels are a 2-fold axis rotation. Red arrows indicate the α -helix and loop shown in (B). Drp1 binding residues are colored green. (B) Detailed view of residues important for the dimer interface. Interactions are indicated with dashed lines. The color scheme is the same as in panel A. Electrostatic interactions were determined using the PDBePISA server. R169 self-associates by hydrogen bonding with a sulfate ion (not depicted). (C) Mutational analysis of dimer formation. MiD51-GFP mutants were co-transfected with either empty vector or Myc tagged MiD51 constructs. For each reaction, the same mutant was used for both the GFP and Myc tagged constructs. Cells were treated with a reversible crosslinker and solubilized before immunoprecipitation against the Myc epitope. Top, expression of MiD51-GFP and MiD51-Myc in cell lysates. Actin is a loading control. Bottom, anti-Myc immunoprecipitates analyzed for MiD51-GFP. Comp Mut, compound dimerization mutant.

Figure 3.4. MiD51 uses a surface loop to bind Drp1. (A) A yeast two-hybrid screen to identify MiD51 regions necessary for Drp1 binding. The top panel

shows the diploid selection plate, and the bottom panel shows the interaction selection plate. Three mutational clusters (6, 7, 8) perturb MiD51 binding to Drp1. (B) The three clusters localize to a loop at the top surface of MiD51. Mutated residues are colored green and depicted as sticks. (C) Analysis of MiD51-Drp1 binding in 293T cells. Wildtype or mutant MiD51-Myc was co-expressed and Myc-immunoprecipitates were analyzed for Drp1. Top, expression of MiD51-Myc and Drp1 in cell lysates. Actin is a loading control. Bottom, anti-Myc immunoprecipitate analyzed for Drp1 levels. Loading of immunoprecipitates was normalized to Myc levels. (D) MiD51 cluster mutants 6 and 7 fail to rescue mitochondrial Drp1 recruitment in *Fis1/Mff*-null cells. Drp1 was visualized with anti-Drp1 immunofluorescence, and transfected cells were Myc-positive. *Fis1/Mff*-null cells are used because they have severely reduced recruitment of Drp1 to mitochondria, allowing the recruitment activity of MiD51 to be readily assessed (Losón et al., 2013).

Figure 3.5. ADP binding and dimerization are required for the fission activity of MiD51. (A) ADP and dimerization mutants localize to mitochondria but are defective for mitochondrial fission. Wildtype MEFs were transfected with empty vector or MiD51-Myc constructs and treated with antimycin A. NM, nucleotide-binding site mutant (S189A); DM, compound dimer mutant. (B) Quantification of results in (A). Mitochondrial morphologies were scored as described previously (Losón et al., 2013). (C) Mitochondrial morphology in *Fis1/Mff*-null MEFs transfected with empty vector or MiD51-Myc and treated with

vehicle (DMSO) or antimycin A. Effects are quantified in (D). Transfected cells were visualized with anti-Myc immunofluorescence, and mitochondria were highlighted with anti-Tom20 immunofluorescence. Data are averages from three independent experiments \pm standard deviation. Mitochondrial morphology scoring: S, short; L, long; N, net-like; C, collapsed. Scale bars, 10 μ m. Regions within the white boxes are shown in greater magnification below.

Figure 3.6. ADP promotes Drp1 oligomerization by MiD51. (A) Effect of MiD51 and ADP on Drp1 sedimentation. Recombinant mouse MiD49 Δ 1-124 or MiD51 Δ 1-133 was incubated with recombinant mouse Drp1 in the presence of GTP γ S with or without ADP. Reactions were incubated for 30 mins, and Drp1 oligomers were sedimented at 100,000 g. Equivalent volumes of the supernatant (S) and pellet (P) were loaded and resolved by SDS-PAGE. Dashed boxes indicate key comparison groups. (B) Analysis of MiD51 mutants on Drp1 sedimentation. The MiD51 nucleotide binding mutant (NM, S189A) and the compound dimer mutant (DM) were assessed for their ability to facilitate Drp1 sedimentation in the presence of GTP γ S and ADP.

Figure 3.7. MiD51 and ADP promote Drp1 spiral assembly and GTP hydrolysis. (A and B) Negative stain transmission electron microscopy of Drp1 oligomers. Images are representative of three independent experiments. (A) Recombinant mouse Drp1 forms regular spiral-tubular structures in the presence of a non-hydrolysable analog of GTP, GTP γ S. White arrow highlights the thin

edge of spiral-tubular structures. (B) Effects on Drp1 spiral-tubular formation upon addition of MiD51 proteins with and without ADP. GTP γ S was present in all reactions. Dashed boxes indicate inset boundaries. Scale bar, 100 nm; inset scale bar, 50 nm. (C) Effect of MiD51 and ADP on GTP hydrolysis by Drp1. Initial GTP hydrolysis rates were measured with the indicated proteins, with or without ADP. Reactions were performed at saturating GTP (1 mM) with 150 mM NaCl. NM, nucleotide-binding site mutant (S189A); DM, compound dimer mutant. T59A is a Drp1 catalytic mutant. Results are the average of three independent experiments \pm standard deviation.

Figure 3.1

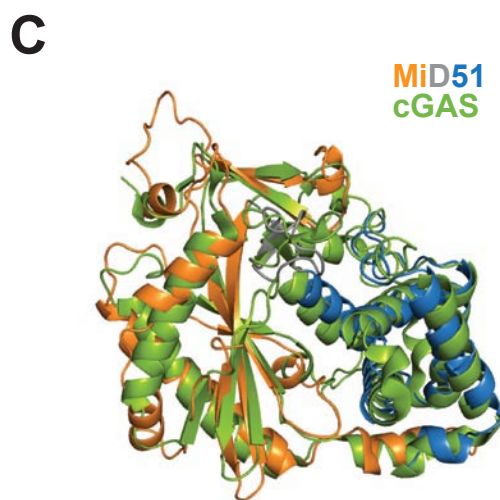
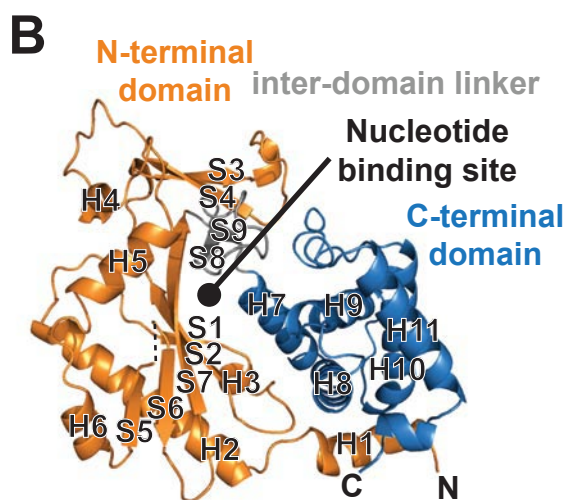
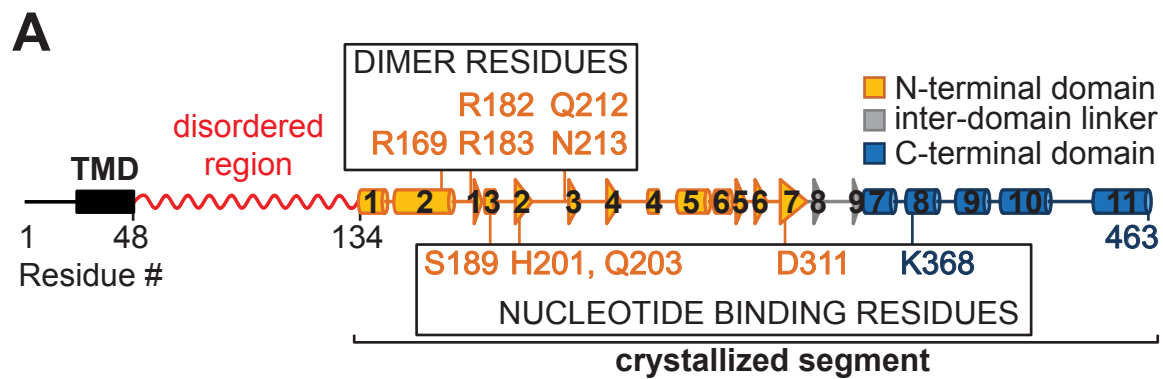


Figure 3.2

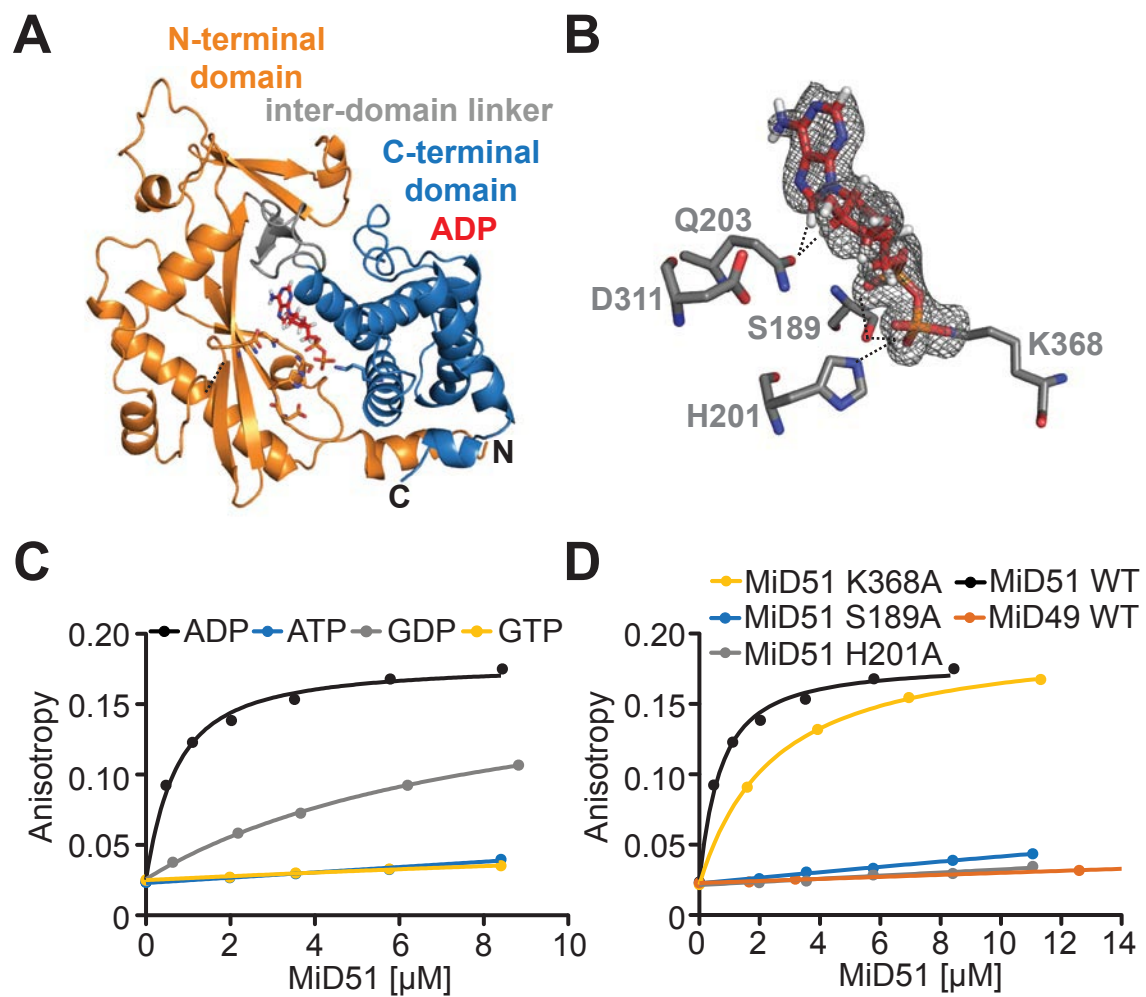


Figure 3.3

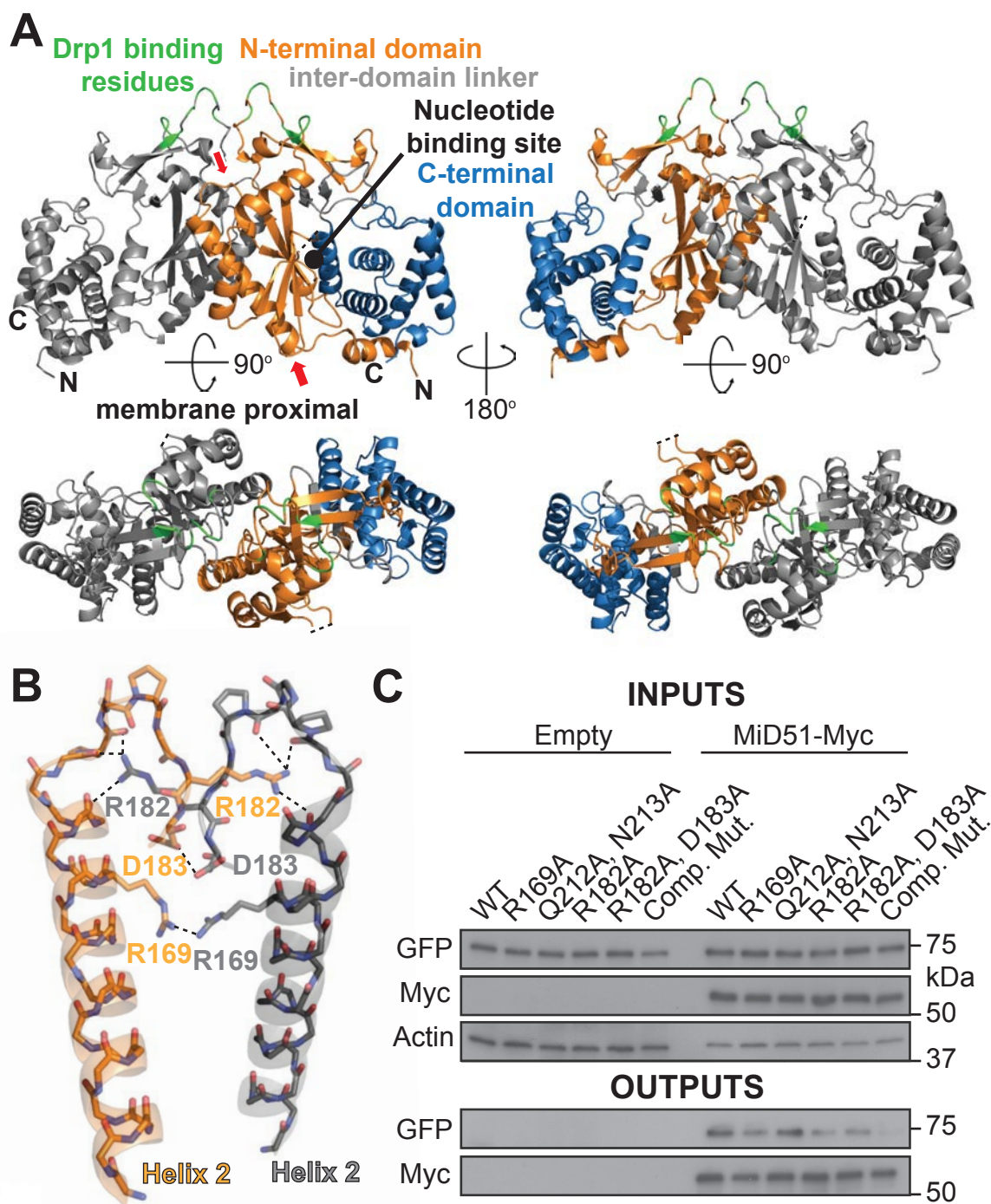


Figure 3.4

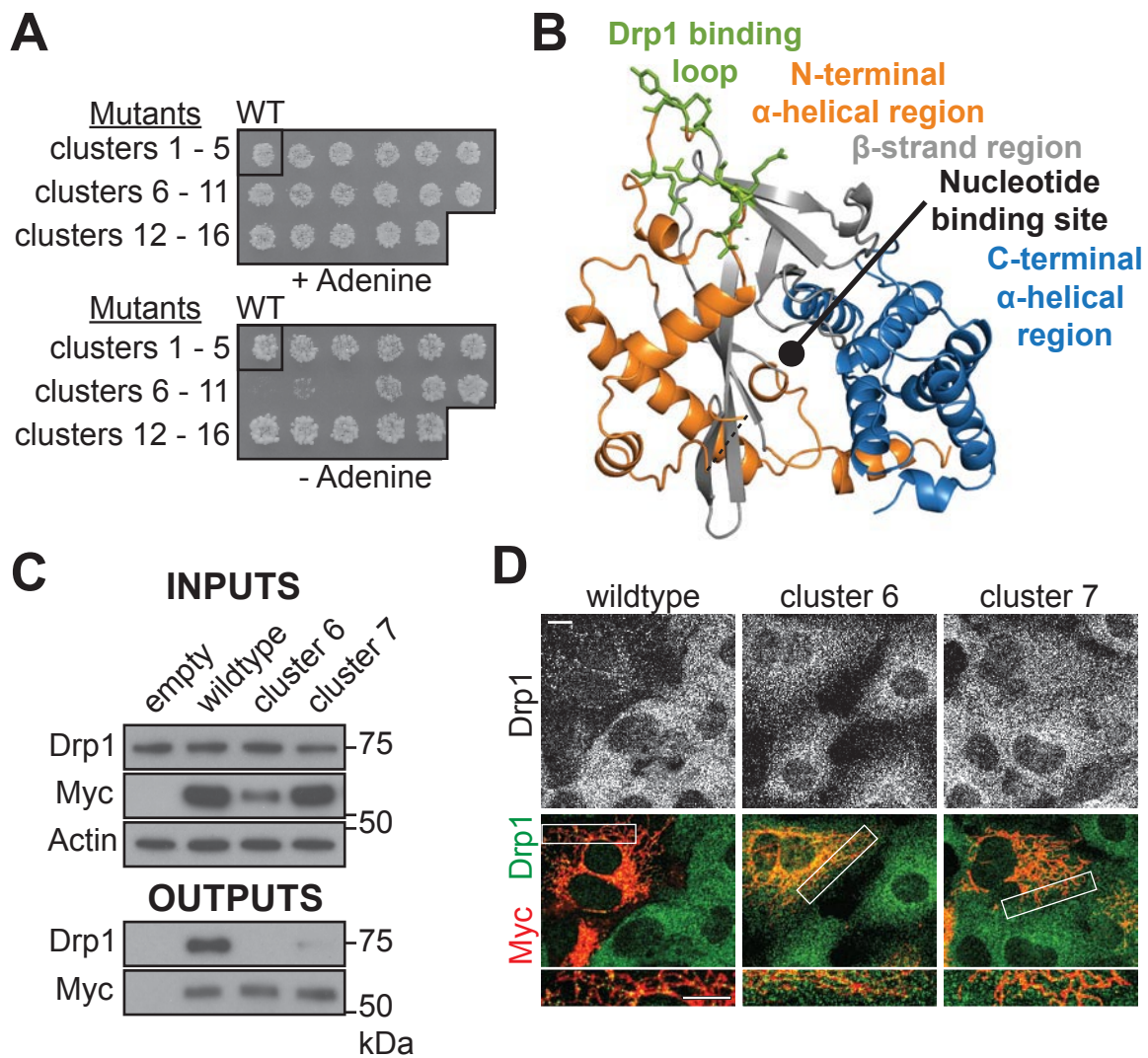


Figure 3.5

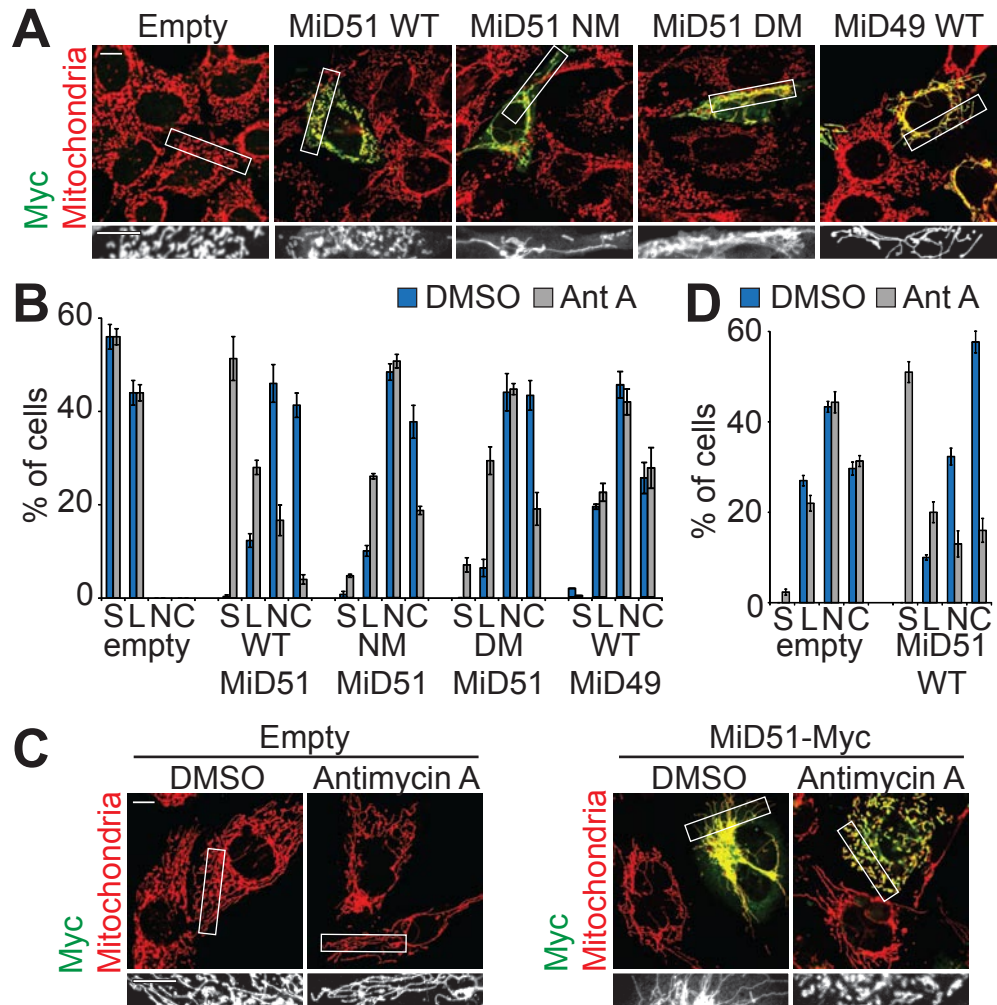


Figure 3.6

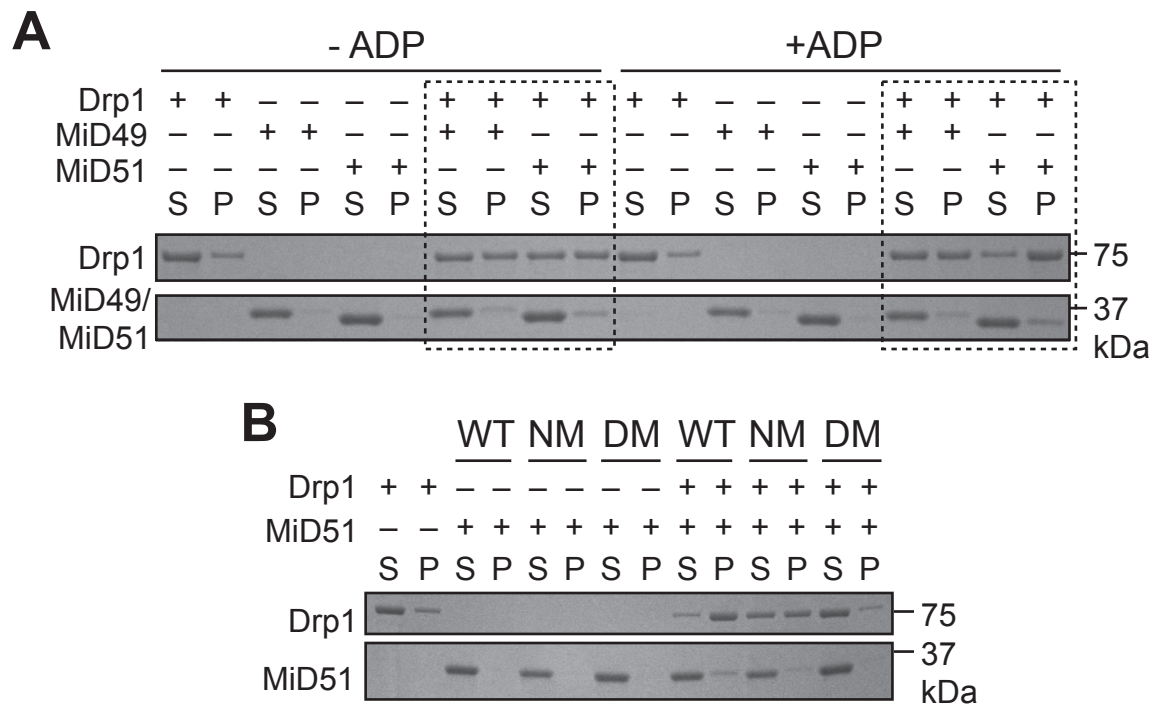
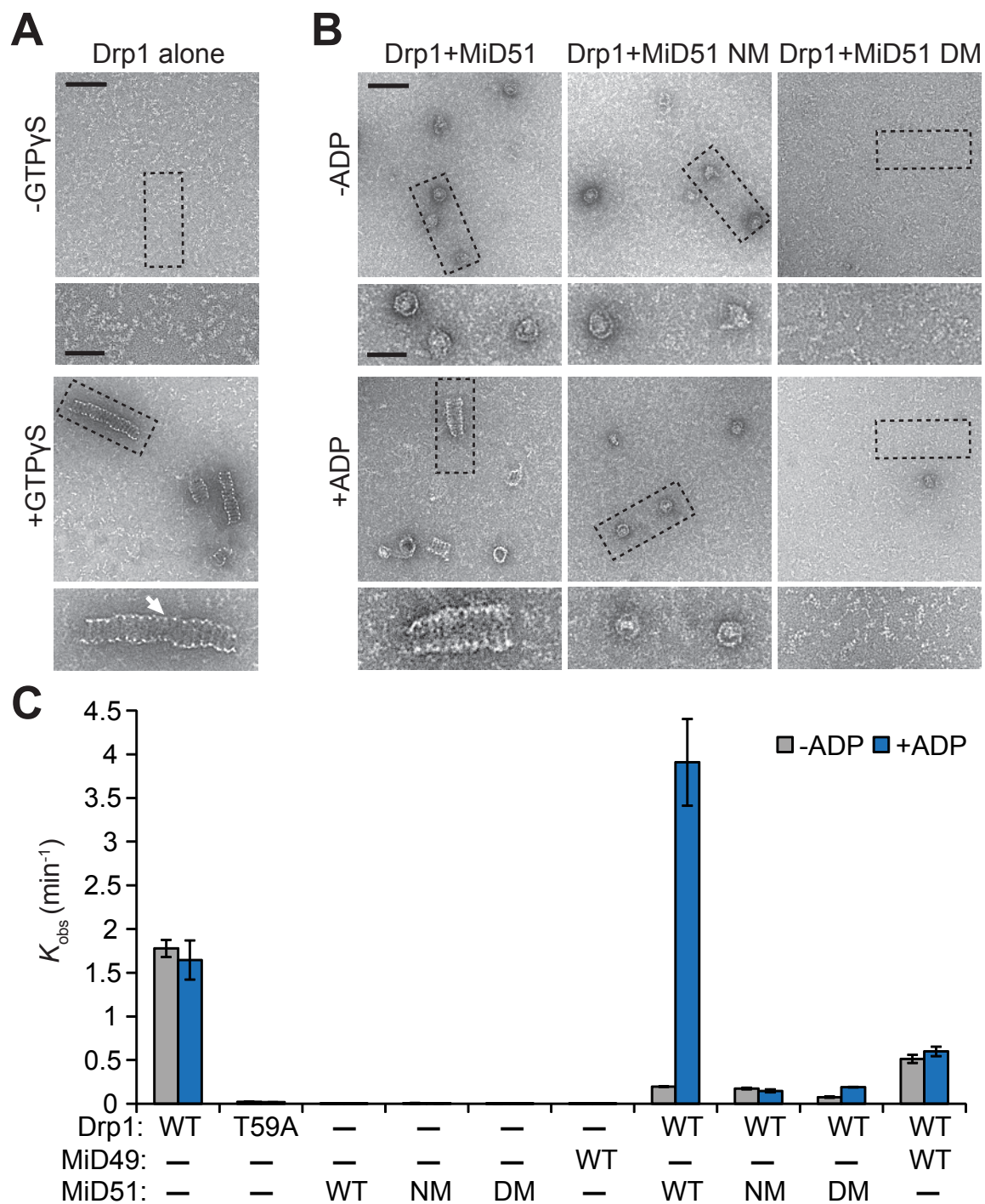


Figure 3.7



SUPPLEMENTAL FIGURE LEGENDS

Figure S3.1. Related to Figure 3.1. (A, B) Identification of a stable MiD51 domain. (A) Limited trypsin proteolysis of MiD51 Δ 1-48 produces a stable fragment that is resistant to proteolysis over 2 days. Proteolysis products were analyzed by SDS-PAGE. (B) Details of the stable domain. The sequence of MiD51 protein at the C-terminal end of the non-regular secondary structure (NRSS) segment is shown. NRSS sequence is depicted in red, and the black arrow indicates the trypsin site. N-terminal sequencing identified the underlined residues. The orange shading denotes the N-terminal sequence of the crystallized segment. (C) Protein sequence alignment for *Mus musculus* MiD49 and MiD51. The dashed boxes highlight residues in MiD51 involved in nucleotide binding. The green boxes highlight conserved residues for Drp1 binding. Residue chemistries are depicted by their color. Red, small and/or hydrophobic; blue, acidic; magenta, basic; green, sulfhydryl, hydroxyl or amine containing, and glycine. Sequence similarity symbols: asterisk, fully conserved; colon, highly conserved; period, weakly conserved. Protein secondary structure topology from the MiD51 model is depicted above the sequence. α -helix and strand numbering and coloring are done as in Fig. 3.1A. (D) Surface representation of mouse MiD51 Δ 1-133 with MiD49 conserved residues depicted in red. Yellow residues are MiD49 conserved residues that are important for Drp1 binding. Green residues are residues important for Drp1 binding that are not conserved.

Figure S3.2. Related to Figure 3.2. Screening for potential MiD51 ligands. (A-D) In the thermal shift assay, thermal denaturation of MiD51 causes dequenching of Sypro Orange. As a result, increases in Sypro Orange fluorescence report protein unfolding. (A) Raw fluorescence traces from representative groups. (B) The protein melting temperature is determined by calculating the first derivative for each fluorescence trace. (C) MiD51 Δ 1-133 melting temperatures in the presence of the indicated nucleotides without Mg²⁺. (D) MiD51 Δ 1-133 melting temperatures in the presence of the indicated nucleotides with Mg²⁺. (E) MiD49 Δ 1-124 melting temperatures in the presence of the indicated nucleotides with Mg²⁺. Melting temperatures in (C) through (E) are averages from three independent experiments \pm standard deviation.

Figure S3.3. Related to Figure 3.3. (A) Structural alignment of native MiD51 Δ 1-133 and ADP-bound dimers. The native (apo) dimer is colored as in Fig. 3.3, and the ADP-bound dimer is colored green. (B) Ribbon representation of MiD51 Δ 1-133 H201A (nucleotide-binding mutant). (C) Ribbon representation of compound dimer mutant of MiD51 Δ 1-133. Models in (B) and (C) are colored as in Fig. 3.1B. (D) Superimposition of MiD51 Δ 1-133 wildtype (gray), H201A (blue) and compound dimer mutant (CDM, red).

Figure S3.4, related to Figure 3.4. Identification of the Drp1 binding site on MiD51. (A) Effect of MiD51 nucleotide-binding and dimerization mutations on Drp1 recruitment to mitochondria. *Fis1/Mff*-null MEFs were transfected with the

indicated MiD51-Myc construct, and Drp1 localization was visualized by immunostaining. Transfected cells were determined by an anti-Myc antibody. MiD51 Δ 1-48 lacks the transmembrane domain and does not localize to mitochondria. Scale bars, 10 μ m. White boxes delineate bottom inset boundaries. NM, nucleotide-binding site mutant (S189A); DM, compound dimer mutant. (B) Co-immunoprecipitation of MiD51 mutants with Drp1. Drp1 was co-transfected with either empty vector or Myc-tagged MiD51 mutant constructs. Cells were treated with a reversible crosslinker and solubilized before immunoprecipitation. The output panels show Drp1 association with the anti-Myc immunoprecipitates. The top panels show expression of MiD51-Myc and Drp1 in the cell lysates. Actin is a loading control. Green, dimer mutants; orange, nucleotide binding mutants. (C) A tabulation of the 16 cluster mutants. Cluster mutants that perturb Drp1 binding are indicated with asterisks. (D) Structural depiction of the cluster mutants. The mutants were designed to systematically probe the solvent-exposed surface of MiD51. Three clusters showed significant loss of Drp1 binding (6, 7, and 8).

Figure S3.5, related to Figure 3.5. MiD51 nucleotide-binding site and dimerization mutants are defective in CCCP-induced mitochondrial fragmentation. (A) Fission activity of MiD51 variants. MEFs were transfected with empty vector or the indicated MiD51 construct and treated with vehicle or CCCP. Transfected cells were identified with an anti-Myc antibody, and mitochondria were highlighted with an anti-Tom20 antibody. (B) Quantification of mitochondrial

morphology for nucleotide-binding site mutants. (C) Quantification of mitochondrial morphology for dimerization mutants. Comp Mut, compound mutant containing 5 substitutions at the dimer interface. Data in (B) and (C) are averages from three independent experiments \pm standard deviation. Mitochondrial morphology scoring: S, short; L, long; N, net-like; C, collapsed. Scale bars, 10 μ m. The regions within the white boxes are shown at higher magnification below. (D) Proteolytic processing of OPA1 analyzed by Western blotting of cell lysates. Loss of membrane potential during CCCP treatment causes activation of Oma1 mediated cleavage at site 1 (S1) in both isoforms 1 and 7 (Ehses et al., 2009; Head et al., 2009). Cleavage at S2 is mediated by Yme1 and is insensitive to loss of membrane potential (Griparic et al., 2007; Song et al., 2007). CCCP treatment causes increased processing of OPA1, but antimycin A treatment does not. Actin is a loading control.

Figure S3.1

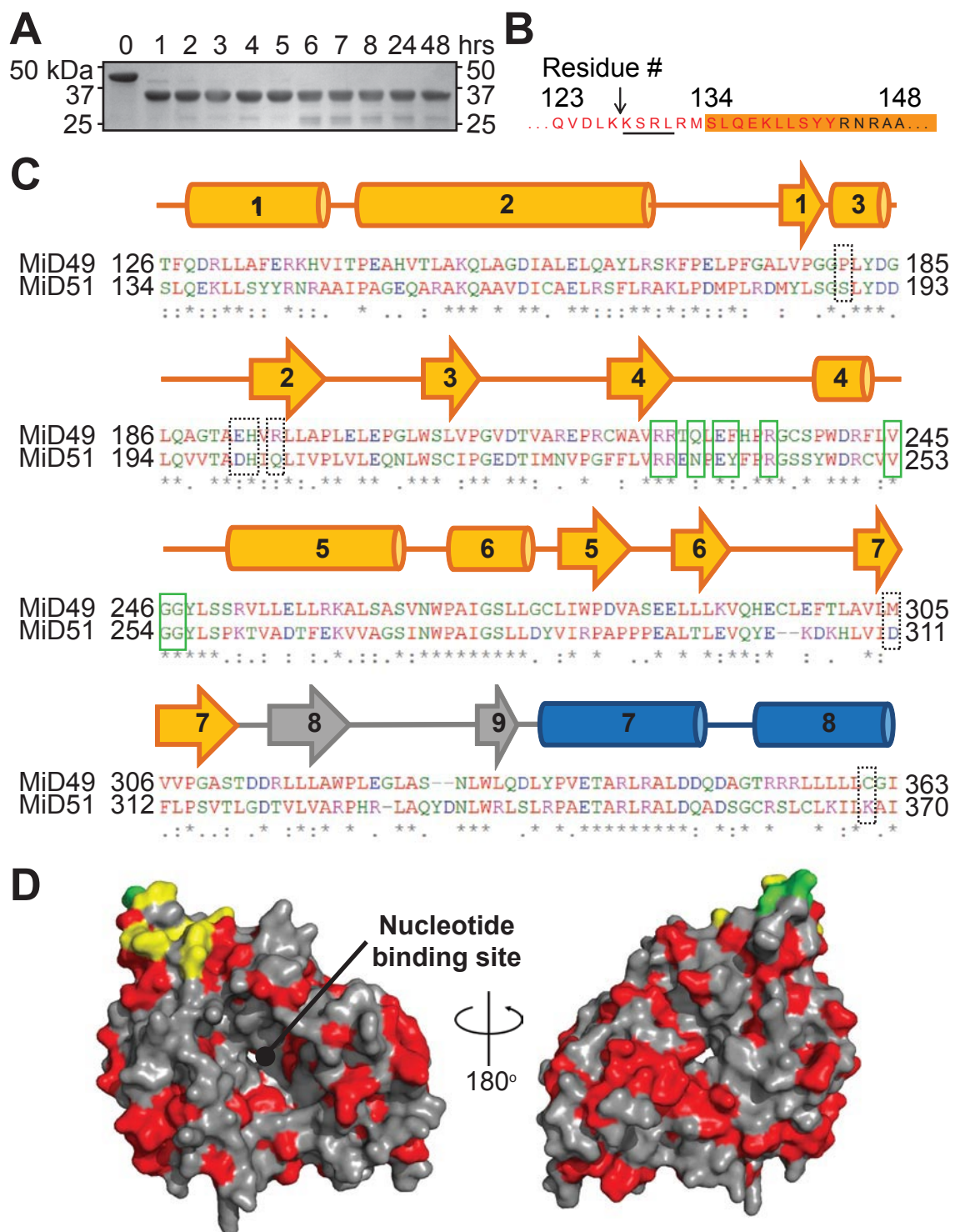


Figure S3.2

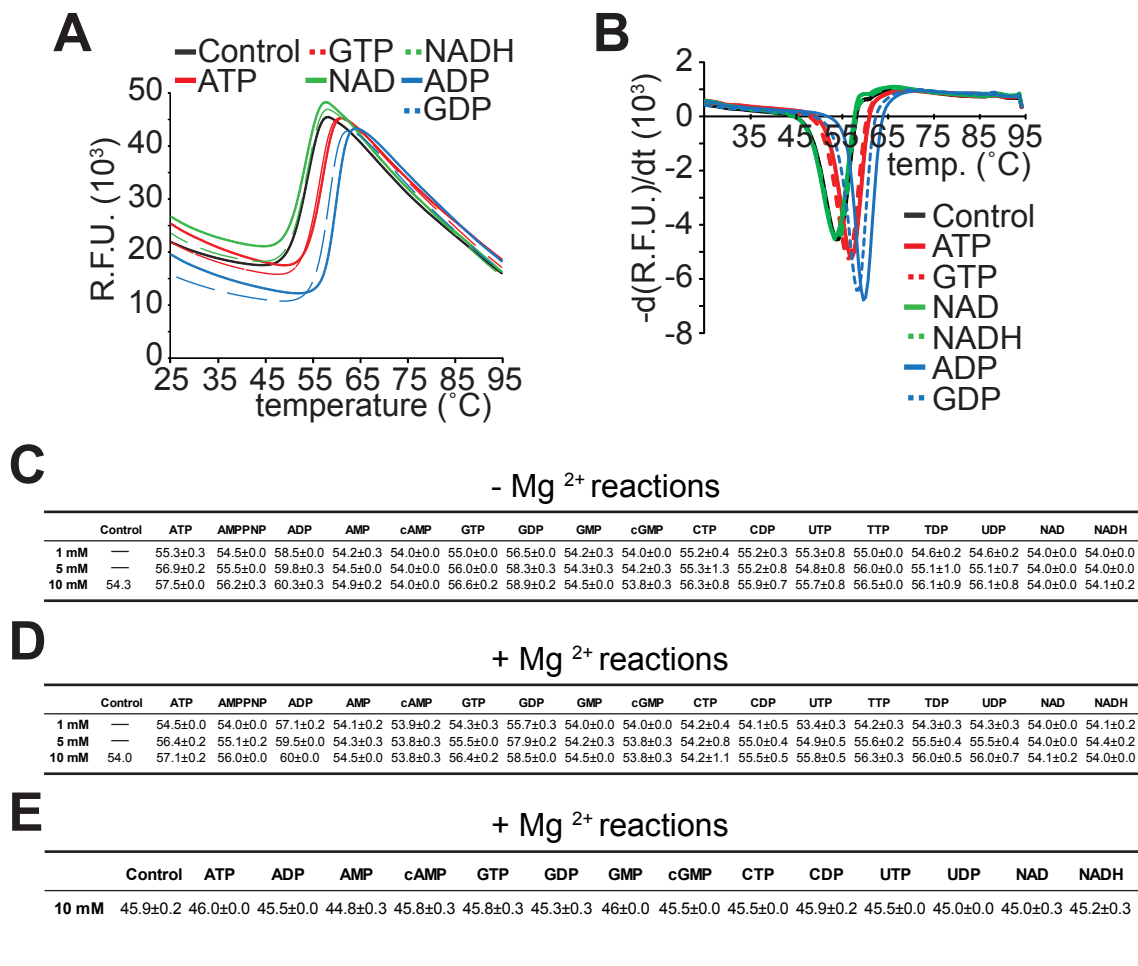


Figure S3.3

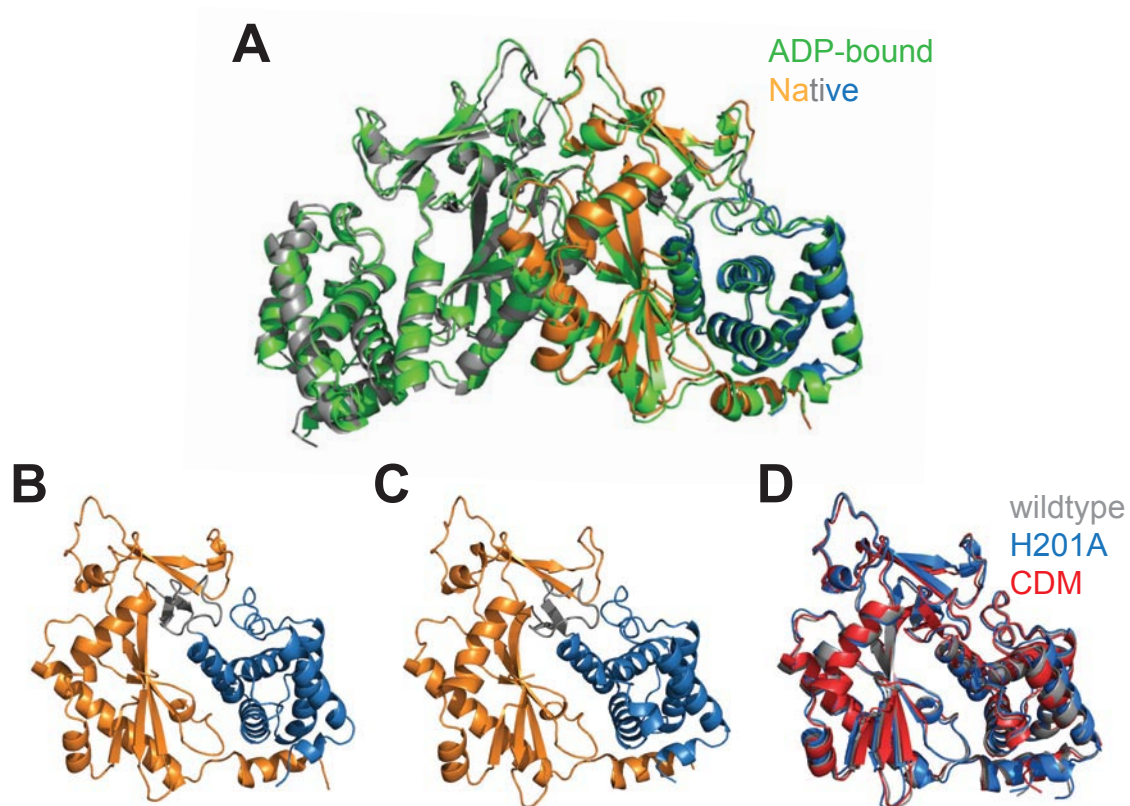


Figure S3.4

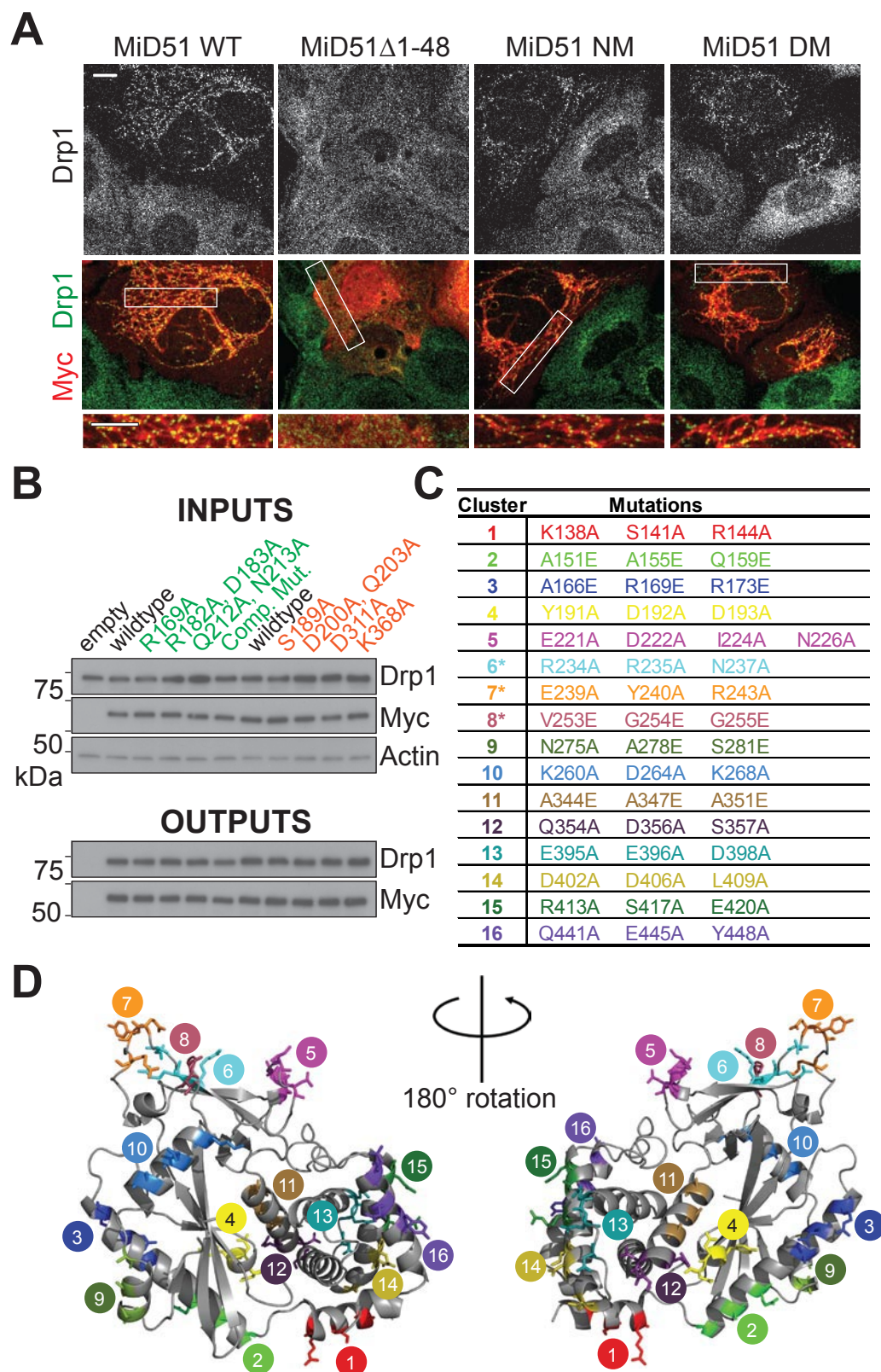


Table S3.1. Data Collection and Refinement Statistics

Data	Se-Met	Native	ADP-bound	H201A mutant	CDM mutant
Space group	P 1 21 1	P 21 21 21			
Unit cell (Å, °)	81.42, 79.22, 103.17, 90, 97.86, 90	91.07, 78.59, 102.31, 90, 96.61, 90	62.07, 80.81, 65.38, 90, 105.74, 90	82.43, 79.15, 103.45, 90, 98.04, 90	63.68, 67.1, 79.41, 90, 90, 90
Number of molecules in ASU	4	4	2	4	1
Resolution (Å)	39.4 – 2.6 (2.74 – 2.60) ^a	39.3 – 2.2 (2.32 – 2.2)	38.43 – 2.0 (2.11 – 2.0)	39.58 – 2.0 (2.11 – 2.0)	34.17 – 2.0 (2.11 – 2.0)
R _{merge} (%) ^b	7.9 (60.5)	7.2 (64.0)	5.7 (37.1)	6.2 (51.5)	7.3 (65.2)
Completeness (%)	95.8 (95.9)	96.1 (95.4)	97.7 (97.4)	98.1 (98.7)	98 (99.8)
Mean I/σ	16.4 (3.4)	10.5 (2.3)	16.6 (3.4)	12.8 (2.4)	17.1 (2.8)
Number of measured reflections	272,481 (39,317)	200,830 (28,326)	141,942 (20,295)	282,928 (41,589)	116,233 (17,069)
Number of unique reflections	38,509 (5,598)	70,056 (10,157)	41,061 (5,957)	87,318 (12,772)	23,493 (3,379)
Redundancy	7.1 (7.0)	2.9 (2.8)	3.5 (3.4)	3.2 (3.3)	4.9 (5.1)
R _{work} (%) ^c	20.2	21.9	17.8	17.7	17.7
R _{free} (%)	25.7	27.4	22.5	21.9	21.8
Average B-factor (Å ²)	44.8	56.4	30.4	31.0	26.1
Rmsd from ideal values					
Bonds (Å)	0.010	0.009	0.009	0.009	0.008
Angle (°)	1.37	1.39	1.312	1.289	1.155
Ramachandran statistics (%)					
Favored	97.7	97.3	96.9	97.8	97.2
Allowed	2.1	2.5	3.1	2.1	2.8
Outliers	0.2	0.2	0	0.1	0

^a Values in parentheses are for the highest resolution shell

^b $R_{\text{merge}} = \frac{\sum_i |I_i - \langle I \rangle|}{\sum_i \langle I \rangle}$, where $\langle I \rangle$ is the mean intensity of N reflections with intensities I_i and common indices h, k , and l .

^c $R_{\text{work}} = \frac{\sum_{hkl} |F_{\text{obs}}| - k|F_{\text{cal}}|}{\sum_{hkl} |F_{\text{obs}}|}$, where F_{obs} and F_{cal} are the observed and calculated structure factors, respectively.

REFERENCES

- Adams, P.D., Grosse-Kunstleve, R.W., Hung, L.W., Ioerger, T.R., McCoy, A.J., Moriarty, N.W., Read, R.J., Sacchettini, J.C., Sauter, N.K., and Terwilliger, T.C. (2002). PHENIX: building new software for automated crystallographic structure determination. *Acta Crystallogr D* 58, 1948-1954.
- Bailey, S. (1994). The Ccp4 Suite - Programs for Protein Crystallography. *Acta Crystallogr D* 50, 760-763.
- Bleazard, W., McCaffery, J.M., King, E.J., Bale, S., Mozdy, A., Tieu, Q., Nunnari, J., and Shaw, J.M. (1999). The dynamin-related GTPase Dnm1 regulates mitochondrial fission in yeast. *Nat Cell Biol* 1, 298-304.
- Chan, D.C. (2012). Fusion and fission: interlinked processes critical for mitochondrial health. *Annu Rev Genet*, in press.
- Chen, H., Detmer, S.A., Ewald, A.J., Griffin, E.E., Fraser, S.E., and Chan, D.C. (2003). Mitofusins Mfn1 and Mfn2 coordinately regulate mitochondrial fusion and are essential for embryonic development. *The Journal of cell biology* 160, 189-200.
- Davis, I.W., Leaver-Fay, A., Chen, V.B., Block, J.N., Kapral, G.J., Wang, X., Murray, L.W., Arendall, W.B., Snoeyink, J., Richardson, J.S., *et al.* (2007). MolProbity: all-atom contacts and structure validation for proteins and nucleic acids. *Nucleic acids research* 35, W375-W383.
- Ehse, S., Raschke, I., Mancuso, G., Bernacchia, A., Geimer, S., Tondera, D., Martinou, J.C., Westermann, B., Rugarli, E.I., and Langer, T. (2009). Regulation of OPA1 processing and mitochondrial fusion by m-AAA protease isoenzymes and OMA1. *The Journal of cell biology* 187, 1023-1036.
- Emsley, P., and Cowtan, K. (2004). Coot: model-building tools for molecular graphics. *Acta Crystallogr D* 60, 2126-2132.
- Evans, P. (2006). Scaling and assessment of data quality. *Acta crystallographica Section D, Biological crystallography* 62, 72-82.
- Ferguson, S.M., and De Camilli, P. (2012). Dynamin, a membrane-remodelling GTPase. *Nature reviews Molecular cell biology* 13, 75-88.
- Frohlich, C., Grabiger, S., Schwefel, D., Faelber, K., Rosenbaum, E., Mears, J., Rocks, O., and Daumke, O. (2013). Structural insights into oligomerization and mitochondrial remodelling of dynamin 1-like protein. *Embo J* 32, 1280-1292.

Gandre-Babbe, S., and van der Bliet, A.M. (2008). The novel tail-anchored membrane protein Mff controls mitochondrial and peroxisomal fission in mammalian cells. *Molecular biology of the cell* 19, 2402-2412.

Gao, P., Ascano, M., Wu, Y., Barchet, W., Gaffney, B.L., Zillinger, T., Serganov, A.A., Liu, Y., Jones, R.A., Hartmann, G., *et al.* (2013). Cyclic [G(2',5')pA(3',5')p] is the metazoan second messenger produced by DNA-activated cyclic GMP-AMP synthase. *Cell* 153, 1094-1107.

Griparic, L., Kanazawa, T., and van der Bliet, A.M. (2007). Regulation of the mitochondrial dynamin-like protein Opa1 by proteolytic cleavage. *J Cell Biol* 178, 757-764.

Head, B., Griparic, L., Amiri, M., Gandre-Babbe, S., and van der Bliet, A.M. (2009). Inducible proteolytic inactivation of OPA1 mediated by the OMA1 protease in mammalian cells. *The Journal of cell biology* 187, 959-966.

Ingerman, E., Perkins, E.M., Marino, M., Mears, J.A., McCaffery, J.M., Hinshaw, J.E., and Nunnari, J. (2005). Dnm1 forms spirals that are structurally tailored to fit mitochondria. *The Journal of cell biology* 170, 1021-1027.

Ishihara, N., Fujita, Y., Oka, T., and Mihara, K. (2006). Regulation of mitochondrial morphology through proteolytic cleavage of OPA1. *The EMBO journal* 25, 2966-2977.

Ishihara, N., Nomura, M., Jofuku, A., Kato, H., Suzuki, S.O., Masuda, K., Otera, H., Nakanishi, Y., Nonaka, I., Goto, Y., *et al.* (2009). Mitochondrial fission factor Drp1 is essential for embryonic development and synapse formation in mice. *Nature cell biology* 11, 958-966.

Kabsch, W. (2010). Xds. *Acta Crystallogr D* 66, 125-132.

Koirala, S., Guo, Q., Kalia, R., Bui, H.T., Eckert, D.M., Frost, A., and Shaw, J.M. (2013). Interchangeable adaptors regulate mitochondrial dynamin assembly for membrane scission. *Proceedings of the National Academy of Sciences of the United States of America* 110, E1342-1351.

Kristiansen, H., Gad, H.H., Eskildsen-Larsen, S., Despres, P., and Hartmann, R. (2011). The oligoadenylate synthetase family: an ancient protein family with multiple antiviral activities. *Journal of interferon & cytokine research : the official journal of the International Society for Interferon and Cytokine Research* 31, 41-47.

Kuchta, K., Knizewski, L., Wyrwicz, L.S., Rychlewski, L., and Ginalski, K. (2009). Comprehensive classification of nucleotidyltransferase fold proteins: identification of novel families and their representatives in human. *Nucleic acids research* *37*, 7701-7714.

Labrousse, A.M., Zappaterra, M.D., Rube, D.A., and van der Bliek, A.M. (1999). *C. elegans* dynamin-related protein DRP-1 controls severing of the mitochondrial outer membrane. *Molecular cell* *4*, 815-826.

Liu, T., Yu, R., Jin, S.B., Han, L., Lendahl, U., Zhao, J., and Nister, M. (2013). The mitochondrial elongation factors MIEF1 and MIEF2 exert partially distinct functions in mitochondrial dynamics. *Experimental cell research*.

Losón, O.C., Song, Z.Y., Chen, H.C., and Chan, D.C. (2013). Fis1, Mff, MiD49, and MiD51 mediate Drp1 recruitment in mitochondrial fission. *Mol Biol Cell* *24*, 659-667.

Mears, J.A., Lackner, L.L., Fang, S., Ingberman, E., Nunnari, J., and Hinshaw, J.E. (2011). Conformational changes in Dnm1 support a contractile mechanism for mitochondrial fission. *Nature structural & molecular biology* *18*, 20-26.

Neves, M.A., Yeager, M., and Abagyan, R. (2012). Unusual arginine formations in protein function and assembly: rings, strings, and stacks. *The journal of physical chemistry B* *116*, 7006-7013.

Otera, H., Wang, C., Cleland, M.M., Setoguchi, K., Yokota, S., Youle, R.J., and Mihara, K. (2010). Mff is an essential factor for mitochondrial recruitment of Drp1 during mitochondrial fission in mammalian cells. *The Journal of cell biology* *191*, 1141-1158.

Painter, J., and Merritt, E.A. (2006). TLSMD web server for the generation of multi-group TLS models. *J Appl Crystallogr* *39*, 109-111.

Palmer, C.S., Elgass, K.D., Parton, R.G., Osellame, L.D., Stojanovski, D., and Ryan, M.T. (2013). Adaptor proteins MiD49 and MiD51 can act independently of Mff and Fis1 in Drp1 recruitment and are specific for mitochondrial fission. *The Journal of biological chemistry* *288*, 27584-27593.

Palmer, C.S., Osellame, L.D., Laine, D., Koutsopoulos, O.S., Frazier, A.E., and Ryan, M.T. (2011). MiD49 and MiD51, new components of the mitochondrial fission machinery. *Embo Rep* *12*, 565-573.

Praefcke, G.J., and McMahon, H.T. (2004). The dynamin superfamily: universal membrane tubulation and fission molecules? *Nature reviews Molecular cell biology* 5, 133-147.

Rome, M.E., Rao, M., Clemons, W.M., and Shan, S.O. (2013). Precise timing of ATPase activation drives targeting of tail-anchored proteins. *Proceedings of the National Academy of Sciences of the United States of America* 110, 7666-7671.

Schmid, S.L., and Frolov, V.A. (2011). Dynamin: functional design of a membrane fission catalyst. *Annu Rev Cell Dev Biol* 27, 79-105.

Sesaki, H., and Jensen, R.E. (1999). Division versus fusion: Dnm1p and Fzo1p antagonistically regulate mitochondrial shape. *The Journal of cell biology* 147, 699-706.

Smirnova, E., Griparic, L., Shurland, D.L., and van der Bliek, A.M. (2001). Dynamin-related protein Drp1 is required for mitochondrial division in mammalian cells. *Molecular biology of the cell* 12, 2245-2256.

Song, Z., Chen, H., Fiket, M., Alexander, C., and Chan, D.C. (2007). OPA1 processing controls mitochondrial fusion and is regulated by mRNA splicing, membrane potential, and Yme1L. *The Journal of cell biology* 178, 749-755.

Stojanovski, D., Koutsopoulos, O.S., Okamoto, K., and Ryan, M.T. (2004). Levels of human Fis1 at the mitochondrial outer membrane regulate mitochondrial morphology. *Journal of cell science* 117, 1201-1210.

Wakabayashi, J., Zhang, Z., Wakabayashi, N., Tamura, Y., Fukaya, M., Kensler, T.W., Iijima, M., and Sesaki, H. (2009). The dynamin-related GTPase Drp1 is required for embryonic and brain development in mice. *The Journal of cell biology* 186, 805-816.

Westermann, B. (2010). Mitochondrial fusion and fission in cell life and death. *Nature reviews Molecular cell biology* 11, 872-884.

Yoon, Y., Krueger, E.W., Oswald, B.J., and McNiven, M.A. (2003). The mitochondrial protein hFis1 regulates mitochondrial fission in mammalian cells through an interaction with the dynamin-like protein DLP1. *Molecular and cellular biology* 23, 5409-5420.

Youle, R.J., and van der Bliek, A.M. (2012). Mitochondrial fission, fusion, and stress. *Science* 337, 1062-1065.

Yu, T., Fox, R.J., Burwell, L.S., and Yoon, Y. (2005). Regulation of mitochondrial fission and apoptosis by the mitochondrial outer membrane protein hFis1. *Journal of cell science* 118, 4141-4151.

Zhao, J., Liu, T., Jin, S.B., Wang, X.M., Qu, M.Q., Uhlen, P., Tomilin, N., Shupliakov, O., Lendahl, U., and Nister, M. (2011). Human MIEF1 recruits Drp1 to mitochondrial outer membranes and promotes mitochondrial fusion rather than fission. *Embo J* 30, 2762-2778.

CHAPTER 4

STRUCTURE-FUNCTION ANALYSIS OF MiD49

Oliver C. Losón¹, Shuxia Meng¹, Raymond Liu¹, and David C. Chan^{1,2}

¹From the Division of Biology and Biological Engineering

²Howard Hughes Medical Institute

California Institute of Technology

Pasadena, CA 91125

INTRODUCTION

Mitochondrial shape is regulated by the opposing forces of fusion and division (Chan, 2012; Westermann, 2010; Youle and van der Bliek, 2012). The balance between these forces is critical for mitochondrial function and physiology. Disruption of either process causes disease in humans and midgestational lethality in mouse models (Alexander et al., 2000; Chen et al., 2003; Ishihara et al., 2009; Wakabayashi et al., 2009; Zuchner et al., 2004).

In mammals, mitochondrial fission (division) requires the recruitment of a dynamin related protein called Drp1 to the mitochondrial surface. Recombinant Drp1 can form ordered oligomers *in vitro* and deform liposomes (Koirala et al., 2013; Loson et al., 2014). This oligomerization is critical to its GTP hydrolysis efficiency (Frohlich et al., 2013). Like dynamin on the neck of endocytic vesicles, Drp1 is believed to oligomerize around the circumference of the mitochondrion, and its GTPase activity is thought to power membrane scission (Mears et al., 2011).

Drp1 recruitment to mitochondria is regulated by four integral outer membrane proteins called Fission 1 (Fis1), Mitochondrial Fission Factor (Mff), and Mitochondrial Dynamics proteins of 49 and 51 kDa (MiD49 and MiD51). Early studies demonstrated that Fis1 was important for fission (Koch et al., 2005; Lee et al., 2004; Yoon et al., 2003; Yu et al., 2005), but a recent study that ablated *Fis1* in several cell lines found that Fis1 is dispensable for fission (Otera et al., 2010). Recently, we demonstrated that ablation of *Fis1* in mouse embryonic fibroblasts (MEFs) caused significant mitochondrial elongation but

little change in Drp1 recruitment, suggesting Fis1 plays a minor role for Drp1 recruitment, but an important role in fission (Loson et al., 2013). The study of Mff has shown that it is critical for the recruitment of Drp1 and regulation of mitochondrial morphology in several different cell types (Gandre-Babbe and van der Blik, 2008; Loson et al., 2013; Otera et al., 2010). The MiD proteins also regulate Drp1 recruitment, but their role for fission is debated. In every study, overexpression of these proteins causes dramatic elongation of mitochondria, because fission is inhibited and fusion is unopposed (Liu et al., 2013; Palmer et al., 2013; Palmer et al., 2011; Zhao et al., 2011). Paradoxically, overexpression of either protein also causes robust recruitment of Drp1. Our work demonstrated that Drp1 recruited by MiD51 overexpression can be activated to execute fission during treatment with carbonyl cyanide m-chlorophenyl hydrazine, which causes loss of mitochondrial membrane potential (Loson et al., 2013). Drp1 recruited by MiD49 overexpression can also be activated for fission by this treatment, but to a lesser degree. Furthermore, regulation of recruited Drp1 by MiD49 and MiD51 differs, as treatment with the respiration inhibitor antimycin A robustly activates fission in MiD51 overexpressing cells but not MiD49 cells (Loson et al., 2014).

In order to better understand the functional differences between MiD49 and MiD51, we are working to determine the crystal structure for the cytosolic domain of recombinant MiD49. Wildtype mouse MiD49 Δ 1-125 can be readily produced in bacteria, but fails to crystallize. We created a library of surface entropy reduction (SER) mutants of mouse MiD49 Δ 1-125 using a predicted structure derived using the atomic model of MiD51 Δ 1-133. One of these mutants

yielded crystals, but data collected from these crystals has not been satisfactory for determining the structure of MiD49 through molecular replacement. Here, I describe our continued efforts for determining the MiD49 structure, and also present data describing the Drp1 binding motif on MiD49.

RESULTS AND DISCUSSION

Recombinant MiD49 Δ 1-125 has not crystallized

Limited trypsin proteolysis of recombinant MiD49 Δ 1-51 produced a stable fragment similar in size to limited trypsin proteolysis of MiD51 Δ 1-48 (Fig. S3.1). Intact mass spectrometry and N-terminal sequencing demonstrated that cleavage occurred after residue 130, but did not affect the C-terminal portion of the stable peptide. Like MiD51, this cleavage removes the N-terminal segment predicted to lack secondary structure. We generated recombinant protein constructs with varying N-terminal truncations, and found that constructs with deletions up to threonine 126 retained solubility, but not those with deletions beyond threonine 126. Crystallization trials were performed with MiD49 Δ 1-124, MiD49 Δ 1-125, and MiD49 Δ 1-126 using the following screens: Hampton Research Index, Crystal Screen I and II, PEGRx I and II, SaltRx I and II, and Emerald Biosciences Wizard I, II, III, and IV. No crystalline hit was obtained in these screens.

Determining SER mutants

The cytosolic segments of MiD49 and MiD51 share 42% sequence homology. Both proteins were predicted to adopt a nucleotidyl transferase (NTase) fold by a bioinformatics approach (Kuchta et al., 2009). Because of their similarities in predicted structure, sequence, and function, we assumed that MiD49 should adopt a structure similar to that of MiD51. Hence, MiD49 should have the capacity to crystallize, but may not be able to because of a particular

sequence dissimilarity from MiD51. Residues with side groups that have high flexibility and polarity found on the surface of globular proteins can impede crystallization because they inhibit the necessary intermolecular interactions (Derewenda, 2004). We created a predicted structure of MiD49 Δ 1-124 using the I-TASSER server and structural restraints from the MiD51 Δ 1-133 model as a template (Fig. 4.1). As expected, the predicted structure is very similar to that of MiD51, with some loop segments showing variability.

We inspected the surface of the predicted structure for residues having sidechains believed to cause high entropy; these residues include arginine, lysine, glutamine, and glutamate (Baud and Karlin, 1999; Lo Conte et al., 1999). After the initial inspection, the suspect residues and neighboring sequences were compared against that of homologous segments in MiD51. Residues and surrounding sequences showing little chemical conservation were considered prime targets for mutagenesis. Polar residues with no neighboring moiety to coordinate their charge were also highly considered. Additionally, we included residues with large sidechains conspicuously protruding from the surface. Selected residues were grouped into clusters (Fig. 4.2A and B), and mutant MiD49 Δ 1-125 constructs were made (Table 4.1).

Screening SER mutants for solubility and crystallization

All SER mutants were first expressed in small cultures. Their solubility was assessed by lysing bacterial pellets after overnight expression, pelleting cellular debris at 43,000 *g*, and assessing whether any recombinant protein was found in

the supernatant (Fig. 4.3A). The relative level of each in the supernatant was compared to that of wildtype and scored (Table 4.1). Surprisingly, some mutants showed enhanced solubility. Mutants showing solubility comparable to wildtype were grown in large scale for purification and crystal trials. The solubility of some mutants did not scale-up and were not used for crystal trials.

Initially, purified mutants were evaluated for an ability to crystallize by using the Hampton Research Index screen. Of the five mutants tested, one (R218A) produced crystals and spherulites in this initial screen (Fig. 4.3B). Additional screens were performed with R218A and include Hampton Research Crystal Screen I and II, PEGRx I and II, SaltRx I and II, Natrix I and II, and Emerald Biosciences Wizard I, II, III, and IV. Several other crystalline hits were obtained. A list of these hits is presented in Table 4.2. SDS-PAGE analysis of crystals from two different conditions confirms that the crystals obtained are composed of MiD49 protein (Fig. 4.3C).

MiD49 Δ 1-125 R218A crystals diffract but are unsatisfactory for structure determination

Several x-ray diffraction data sets were collected from four different crystallization conditions (Table 4.2, bolded). Summaries of three representative data collections are presented in Table 4.3. MiD49 Δ 1-125 R218A crystallized in the same space group (C222) for the majority of the analyzed crystals, and sometimes in another (I222). All crystals had a diffraction limit of about 3.5 Å. Molecular replacement was attempted for these data sets using the structure of

MiD51 Δ 1-133 as a search model, but a replacement was not found for any of them. Also, statistical analysis of spot densities and intensities suggests that these crystals may have merohedral twinning. It is not clear what crystal pathology is impeding molecular replacement success.

Future directions for MiD49 crystallography

The crystallization space for MiD49 Δ 1-125 R218A has been thoroughly explored using both salts and polymers as precipitants. Thus, our focus for the R218A mutant is centered on trying to enhance the crystals we have obtained, specifically the limit to which they diffract. The merohedral twinning analysis suggests that these crystals may be growing too quickly. Twinning can occur when growths from multiple nucleation events amalgamate and produce a heterogeneous crystal. The crystals used for data collection grew quickly, requiring about 10-12 hours to reach their final size. Furthermore, these crystals grow at a high density. To reduce the rate of crystal growth, we are performing seeding experiments using the same conditions, but lower concentrations of protein.

We are also testing new mutants of mouse MiD49 Δ 1-125, and homologous constructs of *Danio rerio* (zebrafish) and *Xenopus laevis* (African clawed frog) for crystallization as an additional strategy to overcome the current ambiguous crystal pathology. Of the SER mutants tested, only R218A allows crystallization. Thus, we are combining this mutation with other SER mutations in the hope that these proteins will behave differentially during crystallization. The

use of homologous proteins from other species is a commonly used strategy for proteins recalcitrant to crystallization (Campbell et al., 1972; Dale et al., 2003). Zebrafish and frog MiD49 share about 42% sequence homology with that of mouse. This sequence variability may provide permissive substitutions in comparison to mouse that allows crystallization.

Characterizing the Drp1-binding motif on MiD49

We previously characterized a Drp1-binding loop motif on MiD51 by testing a library of surface residue mutation clusters in a yeast two-hybrid screen (Loson et al., 2014). MiD49 and MiD51 have high sequence homology in this segment (Fig. 4.5A). MiD49 cannot be used in the yeast two-hybrid screen due to auto-activation. We instead mutated homologous residues in MiD49 and tested their importance for interaction with Drp1 in a co-immunoprecipitation assay (Fig. 4.5B). Mutation of Arg227 caused a dramatic decrease in Drp1 interaction. The homologous residue in MiD51, Arg235, is part of a loop segment not found in other NTase proteins. This residue forms a salt bridge with Asp249 that is critical for the stability of this loop segment (Richter et al., 2014). Single and double point mutations of other residues in the loop segment did not appreciably affect Drp1 interaction. A compound mutant containing several of these mutations did affect Drp1 interaction (Fig. 4.5C), suggesting that these residues function together to bind Drp1. Furthermore, the mutant V245E, G246E also reduced MiD49-Drp1 binding. These residues are not part of the loop segment, but are

found in a proximal region. These residues provide an additional surface for Drp1 binding, as is the case for MiD51.

Our directed mutagenesis of MiD49 suggests a segment similar to that of MiD51 is used for Drp1 binding. The predicted structure of MiD49 suggests that this segment also adopts a loop structure, and although similar, it does have some variability. Determining the structure of MiD49 will help confirm the importance of these residues for Drp1 binding, and will also be critical for understanding the functional differences between MiD49 and MiD51.

EXPERIMENTAL PROCEDURES

Materials

Antibody sources: Drp1 (BD Biosciences), Tom20 (Santa Cruz), Actin (Millipore), Myc (mouse monoclonal 9E10 from Covance, and rabbit polyclonal from Sigma-Aldrich). Cells were grown in LabTek chambered glass slides (Nunc) for fixed cell imaging. Dithiobis(succinimidyl propionate) (DSP) was purchased from Thermo-Pierce. Crystallization screens were from Hampton Research and Emerald Biosciences.

Protein structure prediction

The I-TASSER server builds 3D models of proteins based on multiple-threading alignments using the local meta-threading-server (LOMETS) and iterative template fragment assembly simulations (<http://zhanglab.ccmb.med.umich.edu/I-TASSER/>). Chain A from Protein Data Bank model 4OAF (native MiD51 Δ 1-133) was used as a template to guide I-TASSER modeling of MiD49 Δ 1-124. Similar results were obtained using the structures of cyclic GMP-AMP synthase or human MiD51 as templates.

Recombinant protein production and purification

Recombinant proteins were produced in Rosetta (DE3) BL21 *E. coli* (Invitrogen). One liter of terrific broth (TB) containing 100 μ g/mL ampicillin and 50

$\mu\text{g/mL}$ chloramphenicol was grown at 37°C to an OD_{600} of 1.5. Cultures were cooled on ice for 30 minutes and induced with 1 mM isopropyl β -D-1-thiogalactopyranoside (IPTG) overnight at 16°C . The cells were harvested and stored at -80°C . Pilot cultures were grown in 50 mL TB to an OD_{600} of 1.5. For a typical purification, 10 grams of cells expressing MiD49 protein were lysed in 50 mL GST buffer (50 mM HEPES, 300 mM NaCl, 10% glycerol, 2 mM DTT, pH 7.4) using sonication. Lysates were cleared by centrifugation at $43,000\ g$ for 30 mins at 4°C . GST tagged MiD49 proteins were captured with glutathione sepharose (GE Healthcare) and washed with GST buffer. The beads were then exchanged into protease buffer (50 mM HEPES, 150 mM NaCl, 2 mM DTT, pH 7.4). PreScission Protease (80 units, GE Healthcare) was incubated for 20 hours at 4°C with continuous end-over-end mixing. The eluted protein was further purified by size exclusion on a Hi-Load Superdex 200 16/60 column (GE Healthcare) pre-equilibrated with GST column buffer (20 mM HEPES, 150 mM NaCl, 2 mM DTT, pH 7.4) and driven by an AKTA Purifier (Amersham). Peak fractions were collected and concentrated to approximately 2 mM using Amicon Ultra-15 concentrators (Millipore) with a molecular weight cutoff of 10 kDa. Proteins were flash-frozen in liquid nitrogen and stored at -80°C .

Crystallization and data collection

Crystallization trials were performed using the hanging drop-vapor diffusion method at room temperature. $1\ \mu\text{L}$ of 1 or 0.5 mM protein was mixed with $1\ \mu\text{L}$ mother liquor for screens. Diffraction data were collected from vitrified

crystals on beamline 12-2 at the Stanford Synchrotron Radiation Lightsource. All data were processed with XDS (Kabsch, 2010), and merged using SCALA (Evans, 2006) as implemented in CCP4 (Bailey, 1994). Diffraction data statistics were processed in CCP4.

Immunofluorescence and imaging

For immunofluorescence, cells were fixed in 4% formaldehyde for 10 min at 37°C, permeabilized with 0.1% Triton-X100 at room temperature, and incubated with antibodies in 5% fetal calf serum in phosphate buffered saline. Bound antibody was visualized with Alex Fluor conjugated secondary antibodies (Life Technologies).

All fluorescence imaging was performed using a Plan-Apochromat 63X/1.4 oil objective on a Zeiss LSM 710 confocal microscope driven by Zen 2009 software (Carl Zeiss). Image cropping and global adjustments to brightness and contrast were performed using Photoshop (Adobe).

Cell culture

All cell lines were cultured in Dulbecco's modified Eagle's medium (DMEM) containing 10% FBS and supplemented with 100 U/mL penicillin and 100 µg/mL streptomycin.

Cloning and transfection

MiD49 transcripts were amplified from a MEF, a zebrafish (*Danio rerio*), and a frog egg (*Xenopus laevis*) cDNA library using PCR. Mouse and zebrafish *MiD49* were cloned into the XhoI and BamHI sites of a pcDNA3.1(-) plasmid containing a C-terminal 4xMyc tag, and frog *MiD49* was cloned into the XhoI and EcoRI sites. The entire open reading frames were confirmed by DNA sequencing. For recombinant protein expression in bacteria, mouse MiD49 Δ 1-125 and zebrafish MiD49 Δ 1-132 were cloned into the BamHI and XhoI sites of pGEX6P1 (GE Healthcare), and frog MiD49 Δ 1-132 was cloned into the EcoRI and XhoI sites. All mutants for MiD49 were constructed by PCR using oligonucleotides encoding mutations.

Plasmids were transfected using Lipofectamine 2000 (Invitrogen). Cells transfected with plasmids were assessed 24 hours post transfection. MiD49-Myc positive cells were visualized with Myc immunofluorescence and mitochondria were visualized with Tom20 immunofluorescence.

Immunoprecipitation

To assess MiD49 interaction with Drp1, mouse MiD49-Myc was co-transfected with mouse Drp1 into 293T cells growing in 35 mm plates. 24 hours post-transfection, cells were trypsinized, washed once with PBS, and crosslinked

with 250 μ M DSP in PBS for 20 minutes at room temperature. Crosslinker was quenched by the addition of Tris pH 7.4 to 100 mM final, and cells were washed once with PBS containing 100 mM Tris pH 7.4. Cells were lysed in IP buffer (1% Triton X100, 150 mM NaCl, 25 mM Tris-HCl, 1 mM EDTA, pH 7.4) and lysates were cleared with a 21,000 *g* spin at 4°C for 10 minutes. Immunoprecipitations were performed in IP buffer, and immune complexes were captured with protein A/G agarose (Thermo-Pierce). Beads were washed with IP buffer, and crosslinker reversed by boiling samples in Laemmli buffer containing 5% β -mercaptoethanol.

FIGURE LEGENDS

Figure 4.1. Predicted structure of MiD49 Δ 1-124. The structure was derived using the I-TASSER prediction server and restraints from the structure of MiD51 Δ 1-133.

Figure 4.2. Candidate surface entropy reduction residues. The surface of the predicted MiD49 structure was inspected for high entropy residues and clusters of suspected residues were designated based on proximity. (A and B) The clusters are color coded and numbered, and the respective residues are presented in a table.

Figure 4.3. Piloting surface entropy reduction mutants. Alanine mutants were made for suspected residues and/or clusters. (A) Constructs were screened for solubility in small-scale cultures. 50 mL TB cultures were induced overnight and bacterial pellets were lysed the next day. Supernatants were taken after clearing lysates by centrifuging at 43,000 *g*. Numbers refer to the SER mutants listed in table 4.1. The red rectangle denotes the 63 kDa band corresponding to the GST tagged MiD49 Δ 1-125 mutants. Note the absence of the band in the empty vector control. E, empty vector; WT, wildtype. (B) Crystals of MiD49 Δ 1-125 R218A in 0.1 M HEPES pH 7.5, 0.02 M MgCl₂, and 22% Polyacrylic acid 5,100. Crystals of similar quality obtained with different mother liquors had a similar morphology. (C) Confirming crystals are derived from MiD49 Δ 1-125 R218A. Droplets

containing crystals were recovered and diluted 1:10 in mother liquor. Crystals were pelleted at 10,000 *g* and washed two times with an equivalent volume of mother liquor. A sample of supernatant was taken before the first wash. Equivalent volumes of supernatant and pellet were loaded. Expected, total amount of protein expected.

Figure 4.4. Drp1-binding motif on MiD49. Residues homologous to the Drp1-binding loop of MiD51 were mutated in MiD49. (A) Sequence alignment of Drp1-binding segment. Red, MiD51 residues previously found to be critical for Drp1 binding (See Fig. 2.4). Sequence similarity symbols: asterisk, fully conserved; colon, highly conserved; period, weakly conserved. (B) Analysis of MiD49-Drp1 binding in 293T cells. Wildtype or mutant MiD49-Myc was co-expressed and Myc-immunoprecipitates were analyzed for Drp1. Top, expression of MiD49-Myc and Drp1 in cell lysates. Actin is a loading control. Bottom, anti-Myc immunoprecipitates analyzed for Drp1 levels. Loading of immunoprecipitates was normalized to Myc levels. (C) MiD49 mutants fail to rescue mitochondrial Drp1 recruitment in *Fis1/Mff*-null cells. Drp1 was visualized with anti-Drp1 immunofluorescence, and transfected cells were Myc-positive. *Fis1/Mff*-null cells are used because they have severely reduced recruitment of Drp1 to mitochondria, allowing the recruitment activity of MiD49 to be readily assessed (Loson et al., 2013).

Figure 4.1

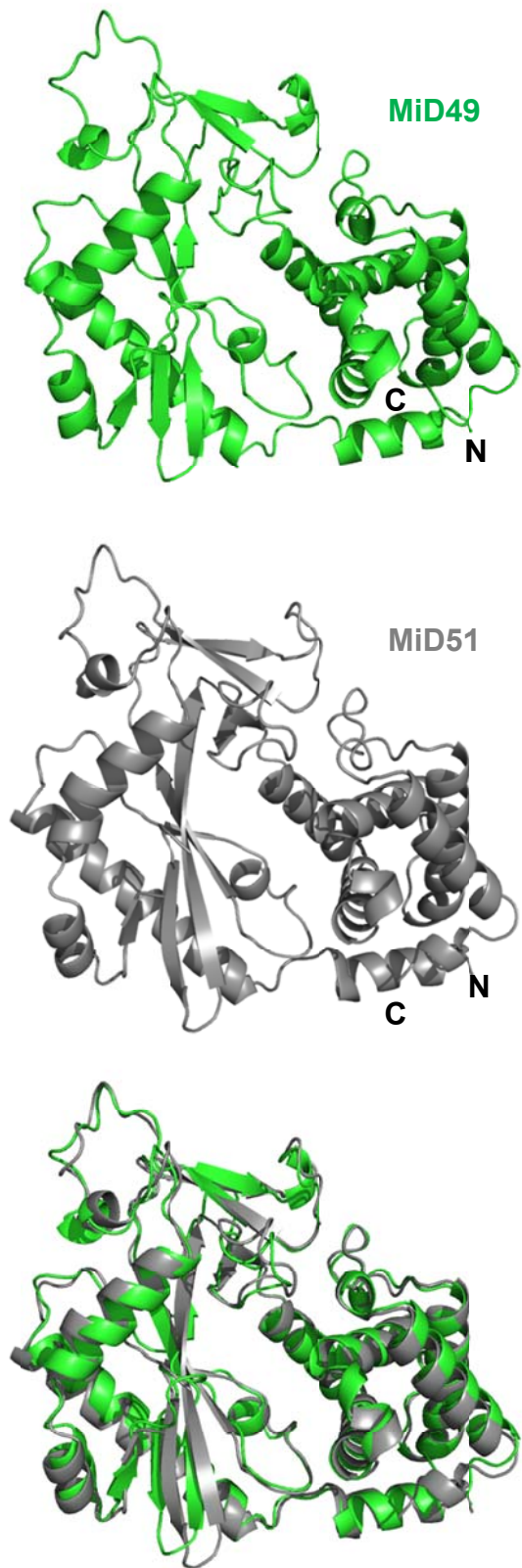
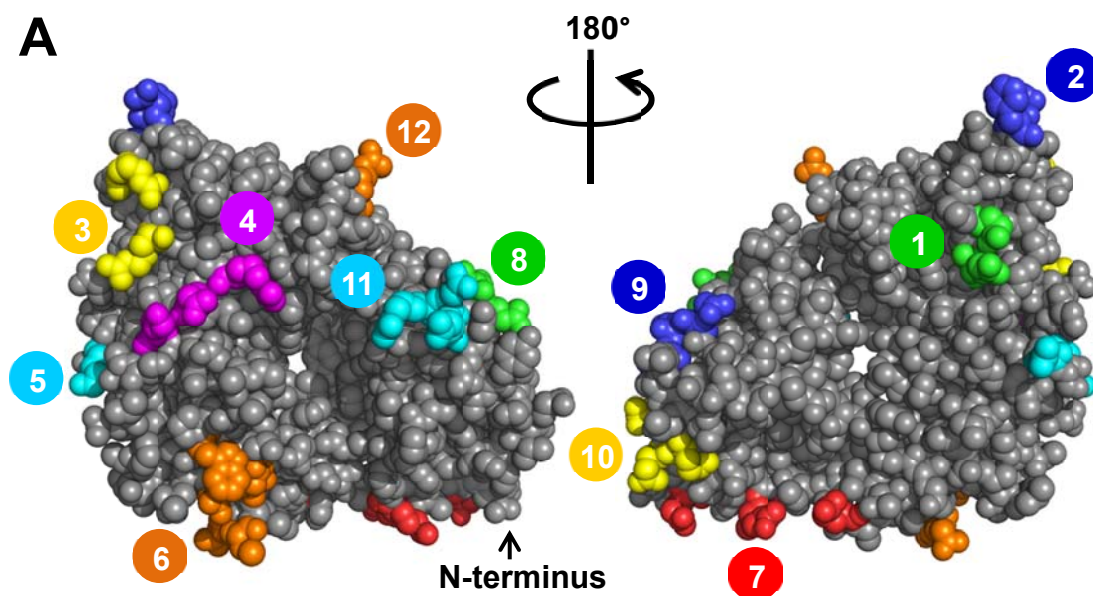


Figure 4.2

**B**

SER CLUSTER	RESIDUES
1	E201, E203
2	E231, F232
3	R235, R242
4	R252, E256, K260
5	R165, K167
6	Q293, E295, C296, E298
7	E129, R136, K137
8	E406, E413, Q414
9	E387, E388, E389
10	E394, E395, E399
11	R432, E433, E434
12	R218

Figure 4.3

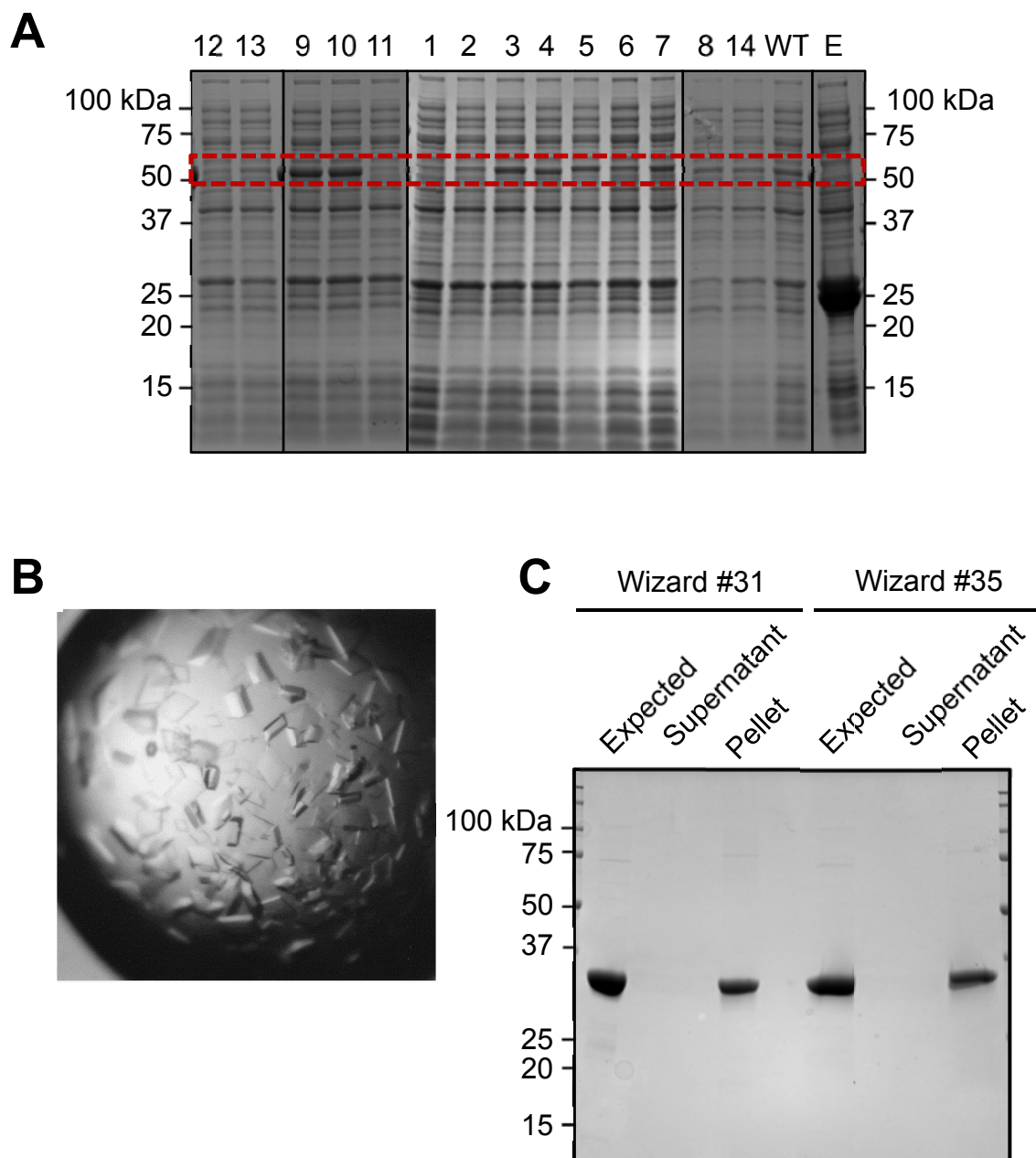


Figure 4.4

A

MiD49 225 VRRTQLEFHPRGCSPWDRFLVGGYLS 250
 MiD51 233 VRRENPEYFPRGSSYWDRCVVGGYLS 258
 *** : * : . *** . * *** : *****

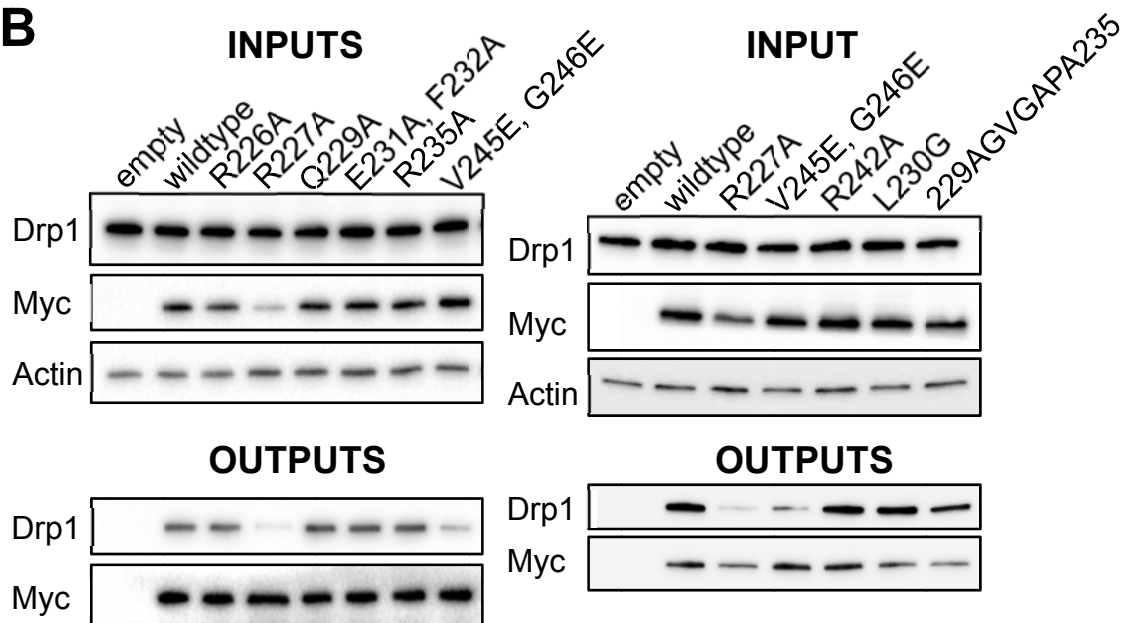
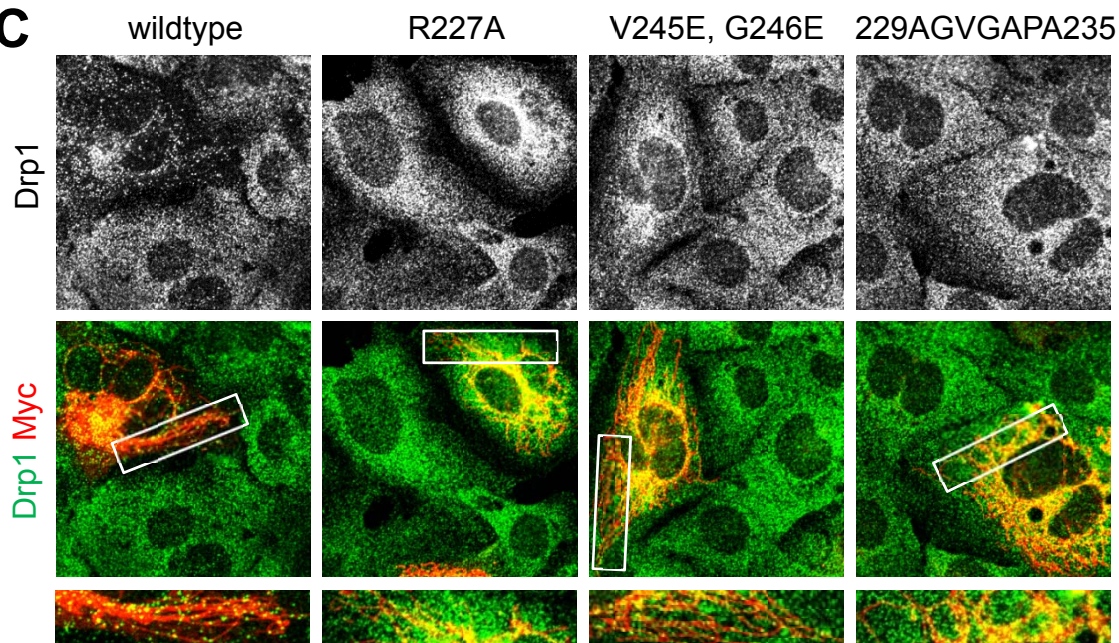
B**C**

Table 4.1. MiD49Δ1-125 SER Mutants Piloting

SER MUTANT	MUTATION	SMALL SCALE ^b		LARGE SCALE ^c	
		EXPRESSION?	SOLUBLE?	SOLUBLE?	CRYSTALLIZE?
1	E201A, E203A	Yes	*	—	—
2	K260 A	Yes	*	—	—
3	E406A	Yes	***	No	—
4	E394A, E395A	Yes	***	No	—
5	R432A, E433A, E434A	Yes	***	Yes	No
6	R218A	Yes	***	Yes	Yes
7	E387A, E388A, E389A	Yes	**** ^a	No	—
8	R235A	Yes	****	Yes	No
9	E231A, F232A	Yes	*****	Yes	No
10	R165A, K167A	Yes	*****	Yes	No
11	E394A, E395A, E399A	Yes	*	—	—
12	E256A, K260A	Yes	*	—	—
13	E129A	Yes	**	—	—
14	E413A, Q414A	Yes	**	No	—
15	R218A, R432A, E433A, E434A	Yes	***	Yes	Yes
16	R218A, R235A	Yes	***	Yes	in progress
17	R218A, R165A, K167A	Yes	*****	Yes	Yes
18	R218A, E413A, Q414A	Yes	***	No	—

^a**** = wildtype solubility

^bsmall scale = 50 mL growth

^clarge scale = 1,000 mL growth

Table 4.2. MiD49Δ1-125 R218A Crystallization Screen Hits

SCREEN	FORMULATION #	CRYSTALLINE SPECIES
HR^a Index	11	crystals
HR Index	59	crystals
HR Index	22	plate/rod clusters
HR Crystal Screen I	29	plate/rod clusters
EB ^b Wizard I	18	plates
EB Wizard II	37	needle clusters
EB Wizard II	42	small rods
EB Wizard IV	13	plate/rod clusters
EB Wizard IV	31	crystals
EB Wizard IV	35	crystals
EB Wizard IV	36	crystals
HR SaltRx I	19	shower of needles
HR SaltRx I	20	rod/needle clusters
HR SaltRx I	28	needle clusters
HR SaltRx II	11	plate stacks
HR SaltRx II	12	needle clusters
HR SaltRx II	20	needle clusters
HR PEGRx II	33	crystals

^aHR = Hampton Research

^bEB = Emerald Biosciences

Table 4.3. MiD49Δ1-125 R218A X-Ray Diffraction Data

Crystal identifier: 140221208G6			
Crystallization condition:	Hampton Research Index #59		
Average unit cell:	97.75 157.61 60.72		
	90.00 90.00 90.00		
Space group:	C 2 2 2		
	Overall	Inner	Outer
Low resolution limit	39.40	39.40	3.90
High resolution limit	3.70	11.70	3.70
R_{merge}^a	0.040	0.012	0.483
Total number of observations	17020	563	2295
Total number unique	5145	180	712
Mean((I)/σ)	19.0	70.7	2.6
Completeness	97.9	94.3	96.3
Multiplicity	3.3	3.1	3.2
Crystal identifier: 140306210C8			
Crystallization condition:	Emerald Biosciences Wizard IV #35		
Average unit cell:	95.89 158.65 60.41		
	90.00 90.00 90.00		
Space group:	C 2 2 2		
	Overall	Inner	Outer
Low resolution limit	37.56	37.56	4.01
High resolution limit	3.80	12.02	3.80
R_{merge}	0.037	0.012	0.635
Total number of observations	17958	586	2730
Total number unique	4715	164	675
Mean((I)/σ)	17.7	66.5	2.5
Completeness	98.7	94.3	99.4
Multiplicity	3.8	3.6	4.0
Crystal identifier: 140312297A3			
Crystallization condition:	Hampton Research Index #11		
Average unit cell:	84.81 93.43 147.49		
	90.00 90.00 90.00		
Space group:	I 2 2 2		
	Overall	Inner	Outer
Low resolution limit	39.46	39.46	3.16
High resolution limit	3.00	9.49	3.00
R_{merge}	0.041	0.013	0.727
Total number of observations	48392	1646	6917
Total number unique	11745	404	1706
Mean((I)/σ)	22.5	90.0	1.6
Completeness	97.7	95.4	98.6
Multiplicity	4.1	4.1	4.1

^aR_{merge} = $\sum_i |I_i - \langle I \rangle| / \sum \langle I \rangle$, where $\langle I \rangle$ is the mean intensity of N reflections with intensities I_i and common indices $h, k, \text{ and } l$.

REFERENCES

- Alexander, C., Votruba, M., Pesch, U.E., Thiselton, D.L., Mayer, S., Moore, A., Rodriguez, M., Kellner, U., Leo-Kottler, B., Auburger, G., *et al.* (2000). OPA1, encoding a dynamin-related GTPase, is mutated in autosomal dominant optic atrophy linked to chromosome 3q28. *Nature genetics* 26, 211-215.
- Bailey, S. (1994). The Ccp4 Suite - Programs for Protein Crystallography. *Acta Crystallogr D* 50, 760-763.
- Baud, F., and Karlin, S. (1999). Measures of residue density in protein structures. *Proceedings of the National Academy of Sciences of the United States of America* 96, 12494-12499.
- Campbell, J.W., Duee, E., Hodgson, G., Mercer, W.D., Stammers, D.K., Wendell, P.L., Muirhead, H., and Watson, H.C. (1972). X-ray diffraction studies on enzymes in the glycolytic pathway. *Cold Spring Harbor symposia on quantitative biology* 36, 165-170.
- Chan, D.C. (2012). Fusion and fission: interlinked processes critical for mitochondrial health. *Annual review of genetics* 46, 265-287.
- Chen, H., Detmer, S.A., Ewald, A.J., Griffin, E.E., Fraser, S.E., and Chan, D.C. (2003). Mitofusins Mfn1 and Mfn2 coordinately regulate mitochondrial fusion and are essential for embryonic development. *The Journal of cell biology* 160, 189-200.
- Dale, G.E., Oefner, C., and D'Arcy, A. (2003). The protein as a variable in protein crystallization. *Journal of structural biology* 142, 88-97.
- Derewenda, Z.S. (2004). Rational protein crystallization by mutational surface engineering. *Structure* 12, 529-535.
- Evans, P. (2006). Scaling and assessment of data quality. *Acta crystallographica Section D, Biological crystallography* 62, 72-82.
- Frohlich, C., Grabiger, S., Schwefel, D., Faelber, K., Rosenbaum, E., Mears, J., Rocks, O., and Daumke, O. (2013). Structural insights into oligomerization and mitochondrial remodelling of dynamin 1-like protein. *The EMBO journal* 32, 1280-1292.
- Gandre-Babbe, S., and van der Bliek, A.M. (2008). The novel tail-anchored membrane protein Mff controls mitochondrial and peroxisomal fission in mammalian cells. *Molecular biology of the cell* 19, 2402-2412.

- Ishihara, N., Nomura, M., Jofuku, A., Kato, H., Suzuki, S.O., Masuda, K., Otera, H., Nakanishi, Y., Nonaka, I., Goto, Y., *et al.* (2009). Mitochondrial fission factor Drp1 is essential for embryonic development and synapse formation in mice. *Nature cell biology* 11, 958-966.
- Kabsch, W. (2010). Xds. *Acta Crystallogr D* 66, 125-132.
- Koch, A., Yoon, Y., Bonekamp, N.A., McNiven, M.A., and Schrader, M. (2005). A role for Fis1 in both mitochondrial and peroxisomal fission in mammalian cells. *Molecular biology of the cell* 16, 5077-5086.
- Koirala, S., Guo, Q., Kalia, R., Bui, H.T., Eckert, D.M., Frost, A., and Shaw, J.M. (2013). Interchangeable adaptors regulate mitochondrial dynamin assembly for membrane scission. *Proceedings of the National Academy of Sciences of the United States of America* 110, E1342-1351.
- Kuchta, K., Knizewski, L., Wyrwicz, L.S., Rychlewski, L., and Ginalski, K. (2009). Comprehensive classification of nucleotidyltransferase fold proteins: identification of novel families and their representatives in human. *Nucleic acids research* 37, 7701-7714.
- Lee, Y.J., Jeong, S.Y., Karbowski, M., Smith, C.L., and Youle, R.J. (2004). Roles of the mammalian mitochondrial fission and fusion mediators Fis1, Drp1, and Opa1 in apoptosis. *Molecular biology of the cell* 15, 5001-5011.
- Liu, T., Yu, R., Jin, S.B., Han, L., Lendahl, U., Zhao, J., and Nister, M. (2013). The mitochondrial elongation factors MIEF1 and MIEF2 exert partially distinct functions in mitochondrial dynamics. *Experimental cell research* 319, 2893-2904.
- Lo Conte, L., Chothia, C., and Janin, J. (1999). The atomic structure of protein-protein recognition sites. *Journal of molecular biology* 285, 2177-2198.
- Loson, O.C., Liu, R., Rome, M.E., Meng, S., Kaiser, J.T., Shan, S.O., and Chan, D.C. (2014). The Mitochondrial Fission Receptor MiD51 Requires ADP as a Cofactor. *Structure* 22, 367-377.
- Loson, O.C., Song, Z., Chen, H., and Chan, D.C. (2013). Fis1, Mff, MiD49, and MiD51 mediate Drp1 recruitment in mitochondrial fission. *Molecular biology of the cell* 24, 659-667.
- Mears, J.A., Lackner, L.L., Fang, S., Ingberman, E., Nunnari, J., and Hinshaw, J.E. (2011). Conformational changes in Dnm1 support a contractile mechanism for mitochondrial fission. *Nature structural & molecular biology* 18, 20-26.

Otera, H., Wang, C., Cleland, M.M., Setoguchi, K., Yokota, S., Youle, R.J., and Mihara, K. (2010). Mff is an essential factor for mitochondrial recruitment of Drp1 during mitochondrial fission in mammalian cells. *The Journal of cell biology* 191, 1141-1158.

Palmer, C.S., Elgass, K.D., Parton, R.G., Osellame, L.D., Stojanovski, D., and Ryan, M.T. (2013). Adaptor proteins MiD49 and MiD51 can act independently of Mff and Fis1 in Drp1 recruitment and are specific for mitochondrial fission. *The Journal of biological chemistry* 288, 27584-27593.

Palmer, C.S., Osellame, L.D., Laine, D., Koutsopoulos, O.S., Frazier, A.E., and Ryan, M.T. (2011). MiD49 and MiD51, new components of the mitochondrial fission machinery. *EMBO reports* 12, 565-573.

Richter, V., Palmer, C.S., Osellame, L.D., Singh, A.P., Elgass, K., Stroud, D.A., Sesaki, H., Kvensakul, M., and Ryan, M.T. (2014). Structural and functional analysis of MiD51, a dynamin receptor required for mitochondrial fission. *The Journal of cell biology* 204, 477-486.

Wakabayashi, J., Zhang, Z., Wakabayashi, N., Tamura, Y., Fukaya, M., Kensler, T.W., Iijima, M., and Sesaki, H. (2009). The dynamin-related GTPase Drp1 is required for embryonic and brain development in mice. *The Journal of cell biology* 186, 805-816.

Westermann, B. (2010). Mitochondrial fusion and fission in cell life and death. *Nature reviews Molecular cell biology* 11, 872-884.

Yoon, Y., Krueger, E.W., Oswald, B.J., and McNiven, M.A. (2003). The mitochondrial protein hFis1 regulates mitochondrial fission in mammalian cells through an interaction with the dynamin-like protein DLP1. *Molecular and cellular biology* 23, 5409-5420.

Youle, R.J., and van der Bliek, A.M. (2012). Mitochondrial fission, fusion, and stress. *Science* 337, 1062-1065.

Yu, T., Fox, R.J., Burwell, L.S., and Yoon, Y. (2005). Regulation of mitochondrial fission and apoptosis by the mitochondrial outer membrane protein hFis1. *Journal of cell science* 118, 4141-4151.

Zhao, J., Liu, T., Jin, S., Wang, X., Qu, M., Uhlen, P., Tomilin, N., Shupliakov, O., Lendahl, U., and Nister, M. (2011). Human MIEF1 recruits Drp1 to mitochondrial outer membranes and promotes mitochondrial fusion rather than fission. *The EMBO journal* 30, 2762-2778.

Zuchner, S., Mersiyanova, I.V., Muglia, M., Bissar-Tadmouri, N., Rochelle, J., Dadali, E.L., Zappia, M., Nelis, E., Patitucci, A., Senderek, J., *et al.* (2004). Mutations in the mitochondrial GTPase mitofusin 2 cause Charcot-Marie-Tooth neuropathy type 2A. *Nature genetics* 36, 449-451.

CHAPTER 5

CONCLUSIONS AND FUTURE DIRECTIONS

Early study of mitochondrial fission was conducted in *Saccharomyces cerevisiae* and largely informed our molecular understanding of fission. In general, the mammalian fission mechanism parallels that of yeast. In both systems, a dynamin related protein must be recruited to the mitochondrial surface and organized, and both systems are regulated by the inter-organelle associations of mitochondria and ER. Nonetheless, recent research of the mammalian fission apparatus has demonstrated that it differs substantially from that of yeast. The study of these differences has helped reveal new molecular aspects about mammalian fission. I will summarize key findings from our research that have contributed to this new understanding, and highlight areas of study that will help advance our understanding of mammalian mitochondrial fission.

Fis1 and mammalian fission

Fis1 is critical for Dnm1 recruitment in yeast, and it was anticipated that its mammalian homolog would have similar importance. Early studies implicated Fis1 as a regulator of mammalian fission but not for Drp1 recruitment (Koch et al., 2005; Lee et al., 2004; Stojanovski et al., 2004; Yoon et al., 2003; Yu et al., 2005). A later study challenged the importance of Fis1 in the mammalian system,

showing that a *Fis1*-null human carcinoma cell line had no defect in mitochondrial morphology or Drp1 recruitment (Otera et al., 2010). The discovery of other Drp1 receptors in mammals has cast additional doubt on the importance of Fis1 for mammalian fission. We generated a *Fis1*-null MEF cell line and also found that Fis1 was dispensable for Drp1 recruitment. Yet careful analysis of mitochondrial Drp1 structures in *Fis1*-null MEFs revealed subtle abnormalities in their composition, suggesting that Fis1 may be important for Drp1 organization post-recruitment. Additionally, these cells had significantly longer and more interconnected mitochondria. One explanation for the discrepancy in results among these studies is the use of differing cell lines. These cell lines are derived from differing tissues, and Fis1 may have been adapted to regulate fission in a tissue-specific manner in multicellular organisms. Alternatively, Fis1 may only play a minor role in regulating mammalian fission because the other Drp1 receptors more efficiently recruit Drp1 and promote fission. Nonetheless, this minor role, which could be the organization of Drp1 polymers at the mitochondrial membrane, is important for fission, as ablation of *Fis1* in some cell lines causes mitochondrial elongation.

In yeast, Fis1 interacts with the adaptor Mdv1 or Caf4 to recruit and regulate Dnm1 GTPase activity. Homologs for these proteins are not known to exist in the mammalian system, yet one interaction partner for mammalian Fis1, called TBC1D15, has been discovered and like Mdv1/Caf4, it is recruited from the cytosol to mitochondria by Fis1. TBC1D15 strongly interacts with Fis1 in HeLa cell lysates, and this interaction can be recapitulated *in vitro* with

recombinant proteins, much like the interaction of yeast Fis1 and Caf4/Mdv1 (Onoue et al., 2013). TBC1D15 is a member of the TBC (Tre2/Bub2/Cdc16)-domain-containing protein family, which is a domain conserved in the GTPase-activating protein (GAP) for small GTPase Rab family proteins (Barr and Lambright, 2010; Fukuda, 2011). Interestingly, knockdown of TBC1D15 causes mitochondrial elongation in HeLa cells. This phenotype may partially explain the minor phenotypes observed for Fis1 depleted cells. Perhaps TBC1D15 can continue to influence fission in the absence of Fis1 through an alternative mode of mitochondrial recruitment, causing only a partial effect on mitochondrial morphology in Fis1 depleted cells. A better understanding of TBC1D15 function during fission would be valuable, particularly the involvement of TBC1D15 GAP activity or the identification of its partner Rab GTPase. Perhaps like Mdv1, TBC1D15 and its unknown partner, Rab GTPase may modulate Drp1 GTP hydrolysis. Understanding the molecular function of TBC1D15 would help to contextualize the role of Fis1.

Fis1 contains a variant tetratricopeptide repeat motif (Dohm et al., 2004; Zhang and Chan, 2007). This motif is an important mediator of protein interactions in many systems, and proteins with this motif often have multiple binding partners (Blatch and Lassle, 1999; Lapouge et al., 2000). Although Onoue et al. did not discover additional Fis1 binding partners besides TCB1D15, it is possible that others could exist (2013). For example, Zhao et al. found that Fis1 can also interact with MiD51, although this interaction is weak and crosslinker is required to capture it (2011). Nonetheless, Fis1 may influence

fission by modulating the function of the other mammalian Drp1 receptors. Such a function could also explain the partial defect seen in Fis1 depleted cells.

Differential regulation of fission by the MiDs

Unlike Fis1 and Mff, exogenous expression of either MiD49 or MiD51 causes inhibition of fission (Liu et al., 2013; Palmer et al., 2013; Palmer et al., 2011; Zhao et al., 2011). Paradoxically, both proteins robustly recruit Drp1 to mitochondria, but in an inactive form. Our work showed that Drp1 S637-PO₄ is enhanced during exogenous expression of either MiD, and this phosphorylation is partially reversed by CCCP treatment. Surprisingly, CCCP treatment of MiD51 expressing cells caused robust activation of fission and fragmentation of mitochondria. MiD49 expressing cells showed some propensity for fission, but to a much lesser extent. This fission did not require Fis1 or Mff. These results suggest that the MiDs promote Drp1 activity during mitochondrial stress, but how the MiDs are activated by stress is unclear. We found that the addition of the MiD51 cofactor ADP releases MiD51 inhibition of Drp1 GTPase activity *in vitro*. Perhaps CCCP and antimycin A cause changes in the local levels of ADP by inhibiting respiration, and thus affect MiD51 regulation of Drp1. MiD49 does not bind ADP and may explain why its promotion of fission during loss of respiration is less robust. MiD49 is predicted to also adopt a nucleotidyl transferase fold and may bind a yet unknown co-factor, which could be related to other forms of mitochondrial stress. It is important to note that the MiDs also function for constitutive fission, as their knockdown in *Fis1/Mff*-null MEFs causes enhanced

elongation of mitochondria. A better understanding of Drp1 regulation by these proteins *in vivo* during mitochondrial stress will help clarify their role in fission. Specifically, discovering the activation signal and/or regulatory mechanism for each MiD during mitochondrial stress as well as a better understanding of the role of Drp1 phospho-regulation, will be important.

Are the mammalian fission receptors redundant?

Mff and the MiDs were recently discovered to regulate mammalian mitochondrial fission (Gandre-Babbe and van der Blik, 2008; Liu et al., 2013; Otera et al., 2010; Palmer et al., 2013; Palmer et al., 2011; Zhao et al., 2011). Given that Fis1 plays a minor role for Drp1 recruitment, the existence of another receptor was not unexpected. But why more than one additional receptor would exist is not clear. Studies examining the effects of knockdown and exogenous expression of these fission receptors have given some insight.

Knockdown of Mff causes a severe depletion in mitochondrial Drp1 and elongation of mitochondria, as does ablation of the *Mff* locus (Gandre-Babbe and van der Blik, 2008; Loson et al., 2013; Otera et al., 2010). Knockdown of the MiDs also causes mitochondrial elongation (Loson et al., 2013; Palmer et al., 2011). We found that the mitochondrial elongation phenotype in *Fis1*-null and *Mff*-null cells was enhanced in *Fis1/Mff*-null cells, suggesting that Fis1 and Mff influence fission independently. Furthermore, knockdown of either MiD in *Fis1/Mff*-null cells enhances the elongation phenotype, suggesting that there is residual, MiD-dependent fission in these cells. These knockout and knockdown

cell studies support a hypothesis where Fis1, Mff, and the MiDs function independently to regulate fission.

Exogenous expression of the MiDs causes enhanced recruitment of Drp1, even in the absence of Fis1 or Mff (Loson et al., 2013; Palmer et al., 2013). Paradoxically, exogenous expression inhibits fission and mitochondria elongate. In contrast, expression of Fis1 or Mff causes shortening, because they promote fission. The differential effect on Drp1 recruitment and activity from exogenous expression of these proteins suggests that they regulate fission differentially. Their effects may reflect a need for functional context. Indeed, exogenous expression of the MiDs can activate fission during mitochondrial stress. Perhaps the effect on fission from the various receptors may also differ between cell types due to differential cellular physiology or the presence/absence of additional factors. Future study should focus on understanding the importance of these receptors for mitochondrial morphology in differing cell types and/or under differential physiological states.

The role of fission receptors in physiology

Only one documented case of a pathological mutation in a fission gene has been reported (Waterham et al., 2007). The patient had a heterozygous mutation in Drp1 (A395D) that caused multisystem abnormalities. There are no known hereditary diseases caused by mutations in fission genes, which may indicate the critical nature of fission for human physiology, making loss-of-function mutations intolerable. The generation of *Drp1*-null mouse models

demonstrated the importance of fission for development and the health of the nervous system (Ishihara et al., 2009; Wakabayashi et al., 2009). Ablation of Drp1 was critical to understanding the physiological importance of fission, and mouse models carrying null alleles for the fission receptors will be equally important. Generating *Mff*, *Fis1*, and *MiD49/51*-null mice will help clarify their roles for fission and for mammalian physiology. These models may help clarify if these receptors have tissue specific functions, or if they have similar roles throughout development and the organism. A *Fis1*-null animal would help resolve the debated importance of *Fis1* and help reveal its functional context.

REFERENCES

- Barr, F., and Lambright, D.G. (2010). Rab GEFs and GAPs. *Current opinion in cell biology* 22, 461-470.
- Blatch, G.L., and Lassar, M. (1999). The tetratricopeptide repeat: a structural motif mediating protein-protein interactions. *BioEssays : news and reviews in molecular, cellular and developmental biology* 21, 932-939.
- Dohm, J.A., Lee, S.J., Hardwick, J.M., Hill, R.B., and Gittis, A.G. (2004). Cytosolic domain of the human mitochondrial fission protein fis1 adopts a TPR fold. *Proteins* 54, 153-156.
- Fukuda, M. (2011). TBC proteins: GAPs for mammalian small GTPase Rab? *Bioscience reports* 31, 159-168.
- Gandre-Babbe, S., and van der Bliek, A.M. (2008). The novel tail-anchored membrane protein Mff controls mitochondrial and peroxisomal fission in mammalian cells. *Molecular biology of the cell* 19, 2402-2412.
- Ishihara, N., Nomura, M., Jofuku, A., Kato, H., Suzuki, S.O., Masuda, K., Otera, H., Nakanishi, Y., Nonaka, I., Goto, Y., *et al.* (2009). Mitochondrial fission factor Drp1 is essential for embryonic development and synapse formation in mice. *Nature cell biology* 11, 958-966.
- Koch, A., Yoon, Y., Bonekamp, N.A., McNiven, M.A., and Schrader, M. (2005). A role for Fis1 in both mitochondrial and peroxisomal fission in mammalian cells. *Molecular biology of the cell* 16, 5077-5086.
- Lapouge, K., Smith, S.J., Walker, P.A., Gamblin, S.J., Smerdon, S.J., and Rittinger, K. (2000). Structure of the TPR domain of p67phox in complex with Rac.GTP. *Molecular cell* 6, 899-907.
- Lee, Y.J., Jeong, S.Y., Karbowski, M., Smith, C.L., and Youle, R.J. (2004). Roles of the mammalian mitochondrial fission and fusion mediators Fis1, Drp1, and Opa1 in apoptosis. *Molecular biology of the cell* 15, 5001-5011.

Liu, T., Yu, R., Jin, S.B., Han, L., Lendahl, U., Zhao, J., and Nister, M. (2013). The mitochondrial elongation factors MIEF1 and MIEF2 exert partially distinct functions in mitochondrial dynamics. *Experimental cell research* 319, 2893-2904.

Loson, O.C., Song, Z., Chen, H., and Chan, D.C. (2013). Fis1, Mff, MiD49, and MiD51 mediate Drp1 recruitment in mitochondrial fission. *Molecular biology of the cell* 24, 659-667.

Onoue, K., Jofuku, A., Ban-Ishihara, R., Ishihara, T., Maeda, M., Koshihara, T., Itoh, T., Fukuda, M., Otera, H., Oka, T., *et al.* (2013). Fis1 acts as a mitochondrial recruitment factor for TBC1D15 that is involved in regulation of mitochondrial morphology. *Journal of cell science* 126, 176-185.

Otera, H., Wang, C., Cleland, M.M., Setoguchi, K., Yokota, S., Youle, R.J., and Mihara, K. (2010). Mff is an essential factor for mitochondrial recruitment of Drp1 during mitochondrial fission in mammalian cells. *The Journal of cell biology* 191, 1141-1158.

Palmer, C.S., Elgass, K.D., Parton, R.G., Osellame, L.D., Stojanovski, D., and Ryan, M.T. (2013). Adaptor proteins MiD49 and MiD51 can act independently of Mff and Fis1 in Drp1 recruitment and are specific for mitochondrial fission. *The Journal of biological chemistry* 288, 27584-27593.

Palmer, C.S., Osellame, L.D., Laine, D., Koutsopoulos, O.S., Frazier, A.E., and Ryan, M.T. (2011). MiD49 and MiD51, new components of the mitochondrial fission machinery. *EMBO reports* 12, 565-573.

Stojanovski, D., Koutsopoulos, O.S., Okamoto, K., and Ryan, M.T. (2004). Levels of human Fis1 at the mitochondrial outer membrane regulate mitochondrial morphology. *Journal of cell science* 117, 1201-1210.

Wakabayashi, J., Zhang, Z., Wakabayashi, N., Tamura, Y., Fukaya, M., Kensler, T.W., Iijima, M., and Sesaki, H. (2009). The dynamin-related GTPase Drp1 is required for embryonic and brain development in mice. *The Journal of cell biology* 186, 805-816.

Waterham, H.R., Koster, J., van Roermund, C.W., Mooyer, P.A., Wanders, R.J., and Leonard, J.V. (2007). A lethal defect of mitochondrial and peroxisomal fission. *The New England journal of medicine* 356, 1736-1741.

Yoon, Y., Krueger, E.W., Oswald, B.J., and McNiven, M.A. (2003). The mitochondrial protein hFis1 regulates mitochondrial fission in mammalian cells through an interaction with the dynamin-like protein DLP1. *Molecular and cellular biology* 23, 5409-5420.

Yu, T., Fox, R.J., Burwell, L.S., and Yoon, Y. (2005). Regulation of mitochondrial fission and apoptosis by the mitochondrial outer membrane protein hFis1. *Journal of cell science* 118, 4141-4151.

Zhang, Y., and Chan, D.C. (2007). Structural basis for recruitment of mitochondrial fission complexes by Fis1. *Proceedings of the National Academy of Sciences of the United States of America* 104, 18526-18530.

Zhao, J., Liu, T., Jin, S., Wang, X., Qu, M., Uhlen, P., Tomilin, N., Shupliakov, O., Lendahl, U., and Nister, M. (2011). Human MIEF1 recruits Drp1 to mitochondrial outer membranes and promotes mitochondrial fusion rather than fission. *The EMBO journal* 30, 2762-2778.